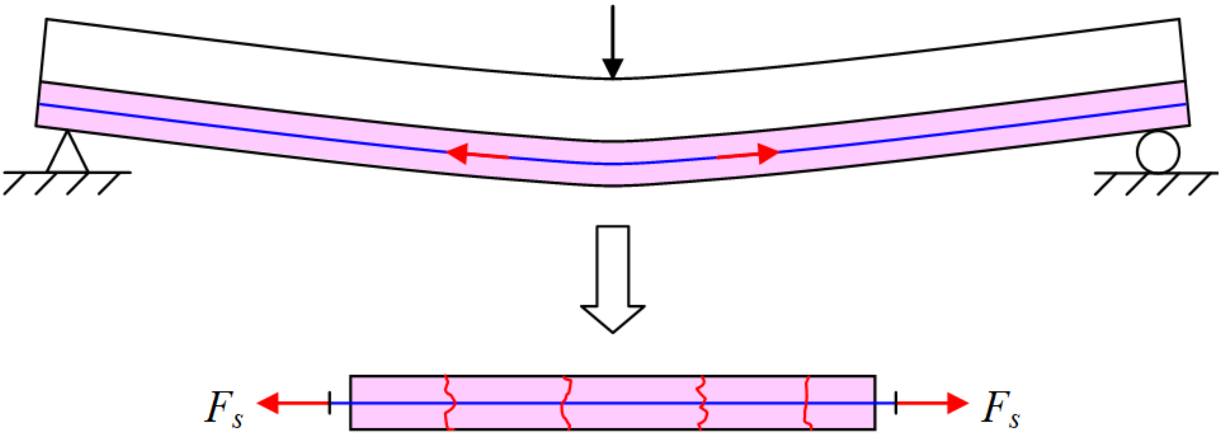

Average reinforcement strain in reinforced concrete structures loaded until failure

Bachelor's thesis in the Civil & Environmental Engineering program

EMIL KÖSEOĞLU

DEPARTMENT OF ARCHITECTURE AND CIVIL ENGINEERING
DIVISION OF STRUCTURAL ENGINEERING

CHALMERS UNIVERSITY OF TECHNOLOGY
Gothenburg, Sweden 2020
www.chalmers.se

DEPARTMENT OF ARCHITECTURE AND CIVIL ENGINEERING
DIVISION OF STRUCTURAL ENGINEERING
CHALMERS UNIVERSITY OF TECHNOLOGY
Gothenburg, Sweden 2020
www.chalmers.se

BACHELOR'S THESIS ACEX20

Average reinforcement strain in reinforced concrete structures loaded until failure

EMIL KÖSEOĞLU

Experimental study of the parameters that affect average strain in reinforced concrete prisms

Bachelor's thesis in the Civil & Environmental Engineering program

EMIL KÖSEOĞLU

© EMIL KÖSEOĞLU 2020

Bachelor's thesis ACEX20
Department of Architecture and Civil Engineering
Chalmers University of Technology 2020

Department of Architecture and Civil Engineering
Division of Structural Engineering
Chalmers University of Technology
421 96 Gothenburg, Sweden
Telephone: (+46) 031-772 10 00

Cover:
Schematic illustration of force action in the bottom of a reinforced concrete beam subjected to bending and simplified description using tensile loading of a reinforced concrete prism.

Department of Architecture and Civil Engineering
Gothenburg, Sweden 2020

Average reinforcement strain in reinforced concrete structures loaded until failure

Experimental study of the parameters that affect average strain in reinforced concrete structures

Bachelor's thesis in the bachelor's program Civil & Environmental Engineering

EMIL KÖSEOĞLU

Department of Architecture and Civil Engineering
Division of Structural Engineering
Concrete Structures
Chalmers University of Technology

ABSTRACT

Reinforced concrete's versatility and strong structural performance make it one of the most prevalent materials used in civil engineering. The effects of impulse loads on reinforced concrete structures and the structural response that follows is of ever-growing interest amongst engineers. The purpose of this thesis is to better understand the impacts of altered parameters on the average strain in reinforced concrete prisms subjected to tensile loading. This average strain is of importance as it is correlated to the structure's plastic deformation- and energy absorption capacity.

Experiments were conducted on reinforced concrete prisms in which the prisms were subjected to static tensile loading until failure. Varying reinforcement diameters along with segments of PVC tubing around the steel reinforcement were implemented in prisms resulting in varying average strains. Digital Image Correlation (DIC) was used to analyze and document the testing and subsequent responses. Strain fields, crack widths, and total displacement for each prism were studied using the processed DIC data and then plotted using Microsoft Excel.

Plastic deformation capacities were predicted to be higher amongst prisms with PVC due to the advantageous decrease in bond between the materials. Interpretation of the results, however, showed an inverse effect from the PVC tubing, i.e. lower strain values and total displacements. However, these results are difficult to apply to the study of full-scale beams as this thesis was limited to reinforced concrete prisms. Beams, with a more complex steel reinforcement configuration, may be influenced more by the PVC tubing resulting in higher average strain values. Further research on this subject is desired as protective concrete structures are of great interest amongst public agencies and engineers in the civil engineering field.

Key words: digital image correlation (DIC), impulse-loading, plastic deformation capacity, prisms, PVC tubing, reinforced concrete, reinforcement, strain

Medeltöjning av armering i armerade betongkonstruktioner belastade till brott

Försöksstudie på parametrar som påverkar medeltöjningen hos armeringen i armerade betongkonstruktioner

Examensarbete inom högskoleingenjörsprogrammet Samhällsbyggnadsteknik

EMIL KÖSEOĞLU

Institutionen för arkitektur och samhällsbyggnadsteknik
Avdelningen för konstruktionsteknik
Betongkonstruktioner
Chalmers tekniska högskola

SAMMANFATTNING

Egenskaperna hos armerad betong gör det till ett av de vanligaste materialen som används inom samhällsbyggnadsteknik. Effekterna av impulsbelastningar på armerade betongkonstruktioner i form av följande strukturella respons är av växande intresse bland ingenjörer. Syftet med detta examensarbete är att få en bättre förståelse för vilka parametrar som påverkar medeltöjningen i dragbelastade armerade betongprismor. Medeltöjningen hos dessa betongprismor är av betydelse eftersom den relaterar till den plastiska deformations- och energiupptagningsförmågan.

Experiment utfördes på armerade betongprismor där prismorna utsattes för dragbelastningar till brott. Olika armeringsdiametrar samt delar av PVC-plaströr placerades runt armeringen vilket resulterade i varierande medeltöjningar. Försöken filmades med kameror och sedan användes digital image correlation (DIC) för att kunna analysera och dokumentera responsen. Töjningsfält, sprickbredder samt förskjutningar studeras utifrån försöksdata och plottades sedan med hjälp av Microsoft Excel.

Den plastiska deformationsförmågan bland prismor med PVC-plast förväntades vara högre på grund av den minskade vidhäftningen mellan armeringen och betongen. Analysen visade, mot förvänta dvs. lägre töjningar och förskjutningar. Dessa resultat är dock svåra att tillämpa på verkliga betongkonstruktioner eftersom experimentet var begränsat till en studie av armerade betongprismor och inte balkar. En balk med en komplex armeringsutformning skulle eventuellt påverkas mer av PVC-plasten vilket i sin tur skulle resultera i en ökad medeltöjning. Ytterligare forskning inom detta ämne är nödvändigt eftersom skyddande betongkonstruktioner är av stort intresse av myndigheter och ingenjörer inom samhällsbyggnadsteknik.

Nyckelord: armerad betong, armering, digital image correlation (DIC), impulslast, plastisk deformationsförmåga, prismor, PVC plast, töjning

Contents

PREFACE

The purpose of this bachelor's thesis is to better understand the parameters that affect the average strain in reinforced concrete structures. Static testing of reinforced concrete prisms was conducted, and the focus of this project was the experimentation itself rather than the mathematical background.

Experimental work was conducted in the concrete laboratory at Chalmers University of Technology in Gothenburg, Sweden. Post-testing analysis and the writing process took place at Chalmers with the help of Norconsult AB. This study is supplementation to on-going research with the Swedish Fortification Agency at Chalmers.

Foremost, I would like to express my immense gratitude to my advisor Morgan Johansson for not only giving me the opportunity to be a thesis student at Norconsult, but also for his guidance, expertise, and motivation throughout the project. His guidance and knowledge have made this thesis one of the most valuable experiences at Chalmers. I am also grateful for the continuous support and advice provided by my examiner, Joosef Leppänen. His positivity and involvement in the project have been appreciated throughout the semester. I would also like to give thanks to Sebastian Almfeldt for his role in the experimental aspects of this thesis. His patience and vast laboratory knowledge resulted in an educational and successfully conducted experiment. In addition, I am thankful for the help Mathias Flansbjer offered in the DIC preparation process. His knowledge of DIC and the meticulous methods involved also led to the success of the experiment. Finally, I would like to thank my parents Pia and Sefa Köseoğlu for giving me the opportunity to live and study in Sweden. My bachelor's thesis and degree would not have been possible without their endless support and encouragement.

NOTATIONS

Abbreviations

2D	Two-dimensional
3D	Three-dimensional
DIC	Digital Image Correlation
FE	Finite Element
PVC	Polyvinyl Chloride
SLS	Serviceability Limit State
ULS	Ultimate Limit State

Roman uppercase letters

A	Area, parameter for rotational capacity
A_c	Cross-sectional concrete area
A_s	Cross-sectional steel area
E	Modulus of elasticity
F	Force
F_{tot}	Total force
L	Length
M	Moment
M_{cr}	Cracking moment
M_u	Ultimate moment
M_y	Yield moment
R	Capacity
$S_{r,max}$	Maximum crack spacing
$S_{r,min}$	Minimum crack spacing

Roman lowercase letters

a	Half of plastic hinge length
c	Concrete cover
d	Effective height
f_{ck}	Characteristic compressive strength
f_{cm}	Mean compressive cylinder strength of concrete
$f_{cm,cube}$	Mean compressive cube strength of concrete
f_{ct}	Tensile strength of concrete
$f_{ct,sp}$	Splitting tensile strength of concrete
f_{su}	Ultimate stress of steel
f_{sy}	Yield stress of steel
h	Height of beam cross-section
k	Stiffness
k_1	Reinforcement coefficient
l	Length
q	Uniformly distributed load
r	Rotational radius
u	Deformation
u_{el}	Elastic deformation
u_{pl}	Plastic deformation

w_k	Characteristic crack width
x	Compression head height

Greek letters

ΔL	Difference in length
Δr	Local bond failure distance
ε	Strain
ε_{cm}	Mean strain in concrete
ε_{cu}	Ultimate strain in concrete
ε_s	Reinforcement strain
$\varepsilon_{s,fsu}$	Ultimate strain capacity in steel
ε_{sm}	Mean reinforcement strain
ε_{su}	Ultimate strain in steel
ε_y	Yielding strain in steel
ϕ	Diameter, reinforcement diameter
ρ	Volume
σ	Stress
σ_{ct}	Tensile stress in concrete
θ_f	Rotation, rotational capacity
τ_b	Bond stress
τ_{bm}	Mean bond stress
ω_s	Mechanical tensile reinforcement ratio
$\omega_{s,crit}$	Critical mechanical reinforcement ratio

1 Introduction

1.1 Background

Due to its versatility and capabilities, reinforced concrete is one of the most prevalent materials used in modern construction. This innovative combination of materials has been heavily researched, but not in every aspect. Reinforced concrete structures are most commonly subjected to static loading, and therefore most knowledge of the material is within this realm. However, impulse loading and its effects are of ever-growing interest amongst civil engineers. By subjecting structures to an impulse load rather than a static load, the structure may behave unusually. For example, in the case of an impulse load, greater plastic deformations are often of higher interest than total load capacity (Johansson & Laine, 2012). Moreover, the average strain of the reinforcement bar plays an important role in the plastic deformation capacity. In other words, the structure's capability to absorb the energy from the impulse load is of greater importance than its load capacity. In addition, the response to this load may differ than that of a static load, e.g. resulting in a failure mode that would otherwise not occur.

In cooperation with Norconsult AB and Chalmers University of Technology and their ongoing project with the Swedish Fortification Agency, this bachelor's thesis will explore the parameters that affect average strain and deformation capacity in reinforced concrete structures subjected to static tensile testing. Data from static testing can be used in further research as a basis for dynamic problem calculations. The input data provided by static tests aid in dynamic calculations which can be applied to impulse-loading research. As more research is needed, the research in this thesis will supplement current research, and will be conducted and analyzed using laboratory equipment provided by Chalmers University of Technology.

1.2 Aim

The aim of the bachelor's thesis is to enhance the understanding of the structural response in reinforced concrete prisms subjected to tensile forces until failure. Static tests on reinforced concrete prisms will provide information and data regarding the average strain and its effects in reinforced concrete structures. The study will seek to answer the questions of how average strain is affected by different reinforcement diameters and how average strain is affected by reducing the bond between the reinforcement and concrete. By having a wide variety of prisms with different layouts of PVC tubing around the reinforcement and different reinforcement bar diameters, the data will present differences in average strain due to the altered parameters. With this information, the prisms' plastic deformation capacity can be studied, which is of great importance for impulse loaded structures. The experimental test results can be used as empirical data and as a comparison for future non-linear FE analyses.

During testing DIC (Digital Image Correlation) technology will be used to analyze the prisms' behavior during loading. This method of analysis will be used to calculate total displacement, crack development, crack spacing, and crack widths. DIC helps visualize the test results in a more intuitive method, which will simplify the analysis.

Ultimately, the thesis project will give insight into how the average strain, and therefore plastic deformation capacity, is affected by different parameters e.g. reinforcement amount and different PVC configurations in reinforced concrete prisms. The aim is to broaden the knowledge within this realm of Structural Engineering and to spread this information within the general civil engineering population.

1.3 Limitations

The experiment conducted in this thesis is limited to reinforced concrete prisms containing one reinforcement bar with varying diameters. In addition, rather than using full-scale reinforced concrete beams, prisms will be used leading to simplified production and testing. As this is a bachelor's thesis, the focus of the project is geared towards the experimentation itself and the analysis of the results, rather than calculations and theoretical studies.

1.4 Methodology

For better comprehension and a more thorough thesis a literature study was done in the early stages of the project. This provided a general understanding of the theory and mathematical concepts behind the project, previous research and/or projects, and important information regarding DIC technology.

Static tensile testing was conducted on reinforced concrete prisms with varying reinforcement bar diameters and PVC configurations until failure. The reinforced concrete prisms used in testing had a two-week construction period in which forms were assembled, reinforcement bars cut, and concrete casted directly after. After casting, the prisms underwent DIC preparation to ensure proper results and analysis post-testing. An analysis took place in which the number of cracks, crack widths, average strain, and total displacement were determined. Test results were studied using Microsoft Excel and GOM Correlate 2018 (GOM, 2018). Figures and diagrams are presented along with 3D strain fields and visual representations of crack development from the DIC technology. Ultimately, the DIC technology and software was able to interpret and calculate data and assist in visualizing the results to improve the analysis.

The prisms require a standard 28-day curing period, and after this period material testing will take place. Material testing of the concrete batch will take place on the final day of curing (day 28), and on the day of testing. In addition, static testing of the reinforcement bars will be conducted on six ϕ 10, 12, and 16 bars. Determining the material properties will be of use in the analytical stages of the thesis. Tensile testing

Post-testing results will provide data to show crack pattern, total number of cracks, and individual crack width during loading. These results will be used to comprehend the modes of failure and pinpoint the development of the cracks themselves.

2 Theoretical Background

Various theoretical concepts are explained in this chapter and provide a background and foundation for the experiment and analysis. In addition, previous research is presented and discussed to make predictions.

2.1 Concrete

Concrete's versatility has made it one of the fundamental materials in civil engineering. Concrete is a composite material containing a mixture of cement, sand, aggregate, and water. Due to its composition, concrete is known for its strength in compression and lack of strength in tension.

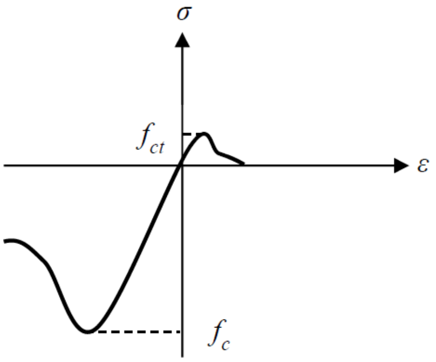

Figure 2.1 Stress-strain curve for the compressive and tensile strength of concrete (Jönsson & Stenseke, 2018).

As seen in Figure 2.1, the compressive strength significantly greater than the tensile strength. The load capacity of the concrete alone is low, and the material is not used to its full potential. Due to these material properties, concrete without added steel reinforcement leads to brittle failure modes when loaded in tension. These failures modes are undesirable, and a more ductile failure is desired.

2.1.1 Compressive strength

Determining the compressive strength is carried out by applying a uniaxial load to the concrete cubes until failure. The results represent the compressive strength for a concrete cube. However, according to Eurocode 2 CEN (2005), the results from the concrete cube tests should be converted to values for concrete cylinders and is calculated using the conversion equation given by Eurocode 2 CEN (2009b):

$$f_{cm} = 0.8 f_{cm,cube} \tag{2.1}$$

where f_{cm} is the mean compressive strength of a concrete cylinder (ϕ150x300 mm) and $f_{cm,cube}$ is the mean compressive strength of a concrete cube (150x150x150 mm), CEN (2012).

2.1.2 Tensile strength

True tensile strength tests of concrete cubes are difficult to carry out and therefore splitting tests are often used to determine the tensile strength. A uniform load applied to a centrally placed notch in the concrete cubes allows for an even distribution of the tensile load on the cubes. By loading the cubes in this manner, failure in tension is achieved in a vertical plane in the cube resulting in the tensile capacity for that batch of concrete. Split tests are used to determine the tensile strength of the concrete, but the results from these tests need to be converted in accordance to Eurocode 2 to axial tensile strength using the following formula

$$f_{ct} = 0.9 f_{ct,sp} \tag{2.2}$$

where f_{ct} is the concrete tensile strength, and $f_{ct,sp}$ is the tensile strength from the splitting tests.

Additionally, according to e.g. Eurocode 2 CEN (2009c), calculation of tensile strength can be done based upon the characteristic compressive strength rather than the splitting test results and is calculated by

$$f_{ct} = 0.3 {f_{ck}}^{2/3} \tag{2.3}$$

where

$$f_{ck} = f_{cm} - 8 \tag{2.4}$$

Both compressive and tensile strength are given in the unit [MPa].

2.2 Steel Reinforcement

As steel reinforcement is a key component of reinforced concrete, this chapter will discuss the material and its properties. The important characteristics of steel reinforcement and steel reinforcement material testing will also be mentioned in the subsequent subchapters.

2.2.1 Yielding

As discussed in previous chapters, materials may have an elastic, plastic, or combination of responses. For steel reinforcement, elasticity is dominant in the early stages of loading during low strains and is surpassed early on. As the load increases, the strain increases, and the material reaches a level of deformation in which elasticity is no longer dominant. This level of stress in the stress-strain curve is called the yielding point and is defined as f_y for a single reinforcement bar. The yielding point has a respective yielding strain, ε_y.

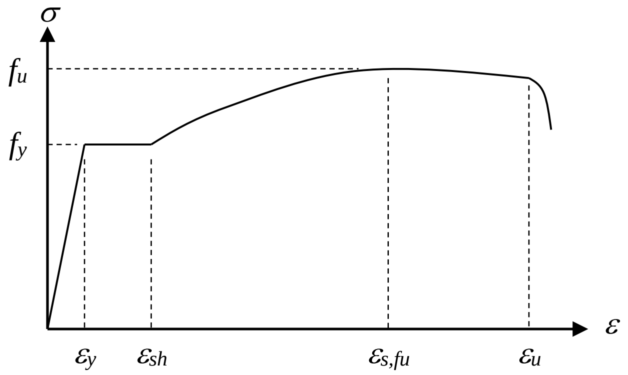

Figure 2.2 Stress-strain curve for a steel reinforcement bar (Johansson & Laine, 2012).

The yielding point is seen as a plateau in stress as the strain increases. Prior to the yielding plateau, deformations are elastic, and the material will return to its original state. Past the yielding plateau, deformations are plastic and permanent deformations reach the ultimate strength of the steel, f_u, and the failure strain $\varepsilon_{s,fu}$, see Figure 2.2. As the load is increased past this point, dislocations occur, and the material begins to reach failure and will eventually lead to rupture of the bar at the maximum strain, ε_u (Johansson & Laine 2012).

2.2.2 Strain hardening

Beyond the yielding point of steel, the behavior and integrity of steel is altered. As steel reinforcement is subjected to tensile loading, and thus higher strain, the yielding point is surpassed, and the material begins to harden and strengthen as the load is increased. In other words, a greater amount of force is required for further deformations.

An increase in deformation and load results in additional points of dislocation in the steel. These added points of dislocation are continuously added to each other creating a dislocation entanglement. This dislocation entanglement restricts the deformation of the steel and leads to an increase in required load for further deformations. This phenomenon is seen directly after the yielding plateau in the stress-strain curve for a steel reinforcement bar. Ultimately, the steel hardens (i.e. gains strength) as the strain increases, hence the term strain hardening.

2.2.3 Necking

Dislocations and points of failure in the atomic structure of steel occur as a load is applied and the strain is increased. During a sufficiently high load, dislocations in a certain point along the steel specimen will result in necking. Necking can be described as a decrease in the specimen's cross-sectional area due to the accumulation of dislocations in that certain region, see Figure 2.1 in Appendix A.

Within this necking region, deformations increase locally due to the increase in stresses and a decrease in cross-sectional area. The relationship between the internal stress and the applied force is seen in the following formula:

$$\sigma = \frac{F}{A} \tag{2.5}$$

where σ is the internal stress of the steel reinforcement, F is the applied tensile force, and, A is the cross-sectional area. As A is reduced, σ increases leading to greater deformations and a necking region. When the point of necking is reached, the maximum load the steel can resist, the failure load, is reached. The reduction of cross-sectional area then escalates resulting in less load required to deform the steel specimen further (Engström 2013). Necking is an indication of near-failure and is distinguished by the plateau in in load at maximum stress in the stress-strain curve.

2.3 Reinforced Concrete

Concrete's poor performance in tensile loading leads to the need of steel reinforcement. By combining the two materials, equilibrium is achieved by the steel carrying the tensile stresses and the concrete carrying the compressive stresses. In addition, the steel reinforcement provides ductility, leading to a safer and desirable failure mode. This chapter discusses the properties of reinforced concrete and the behavior of the material during loading.

2.3.1 Stages during loading

Studying the behavior of a reinforced concrete structure's cross-section allows for a better understanding of the internal mechanisms at play within the structure. A graphical representation of these internal forces and cross-section curvature provides insight into the three main stages of reinforced concrete's behavior, see Figure 2.3.

During the early stages of loading and service, or SLS (Stage I), reinforced concrete possesses a linear elastic response and can return to its uncracked original state. During this uncracked stage, the strains within the concrete and steel reinforcement are equal. However, during a reinforced concrete structure's lifetime, cracking will, and should, occur due to failure in tensile capacity in the concrete (Stage II). To maintain force equilibrium, steel reinforcement plays its important role in transferring the tensile loads in the structure after cracking has initiated. The steel reinforcement within the structure is crucial after crack development process, and the result of this is uneven strains between the two materials. This difference in strain allows for the cracks to widen and leads to a linear elastic response, but with reduced stiffness compared to the uncracked stage. Within the cracks themselves, the reinforcement bar is no longer restricted by the surrounding concrete and therefore can fully utilize its tensile capacity. Moreover, the cross-section reaches a point in which the material(s) exhibits a non-linear response (Stage III), see Figure 2.3. At this point, the cross-section has reached the ultimate limit state (ULS) and failure occurs within the structure in the form of concrete crushing or rupture of the reinforcement.

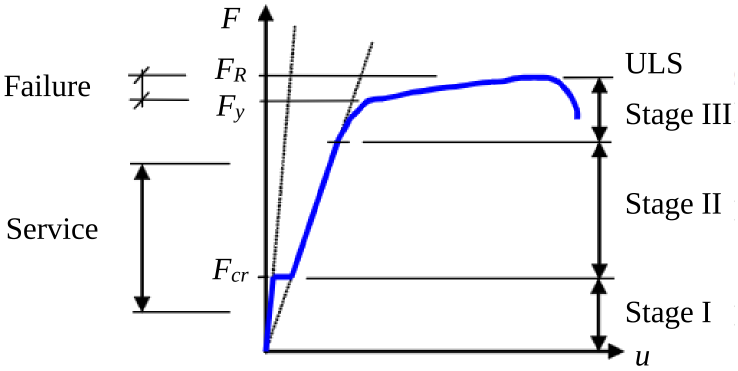

Figure 2.3 Stages I-III of reinforced concrete subjected to loading. Figure based on Engström, 2011.

2.3.2 Crack development

For the steel reinforcement to function as intended, the surrounding concrete must crack, which allows the steel reinforcement to contribute in the carrying of tensile forces. When the applied load reaches the so-called cracking load, cracks occur with a certain crack spacing interval. This crack spacing depends on the steel reinforcement configuration, the tensile strength of the concrete, and the bond between materials. The location of these initial cracks is dependent on the properties of the applied load. The examples given in this chapter represent prisms loaded with constant tensile loads over the specimen. Crack development is a rather calculable process in which the number of cracks and crack spacing can be predicted.

In the example of an uncracked reinforced concrete prism in tension, the concrete stress increases from the ends and reaches a plateau near the midspan of the prism whilst the steel stresses decrease from the ends also reaching a plateau, see Figure 2.4. The stresses within the steel reinforcement and the surrounding concrete are equal and the structure is in equilibrium with concrete and steel strains being equal.

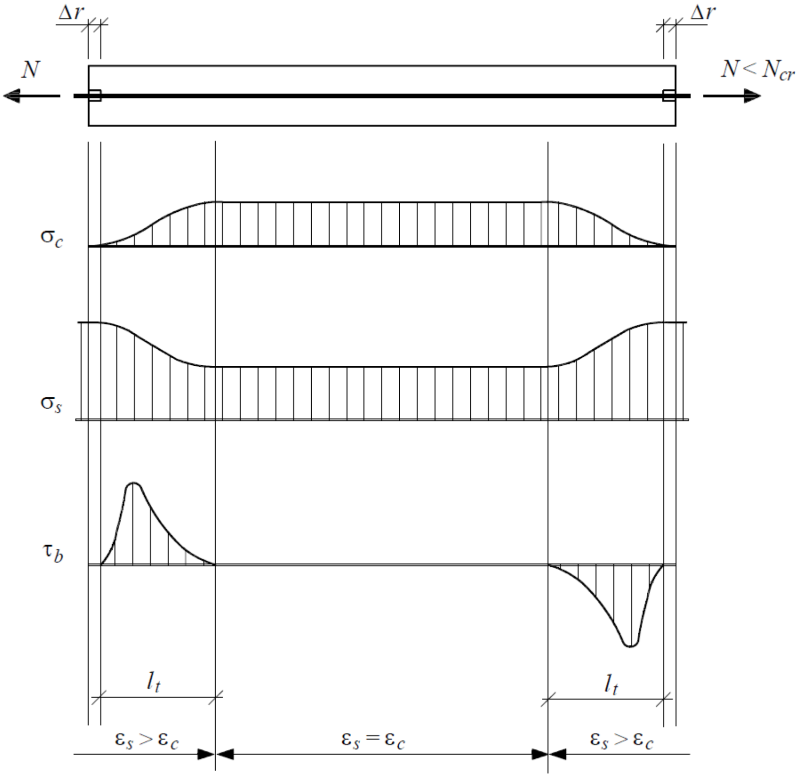

Figure 2.4 Distribution of concrete, steel, and bond stresses in a reinforced concrete prism subjected to a tensile load below the cracking load (Engström, 2011).

The plateau in this case indicates that a new crack is possible as

$$\sigma_{ct} = f_{ct} \tag{2.6}$$

where σ_{ct} is the tensile stresses within the concrete, and f_{ct} is the tensile capacity of the concrete, see Figure 2.5. As a crack develops, tensile stresses in the concrete are relieved and eventually, with enough cracks, most tensile stresses are carried by the reinforcement bar. This stage in crack development is therefore the stabilized cracking stage, meaning no more cracks are possible and the structure has stabilized. After the maximum number of cracks has developed, and as the applied force increases, the crack widths of the existing cracks increase.

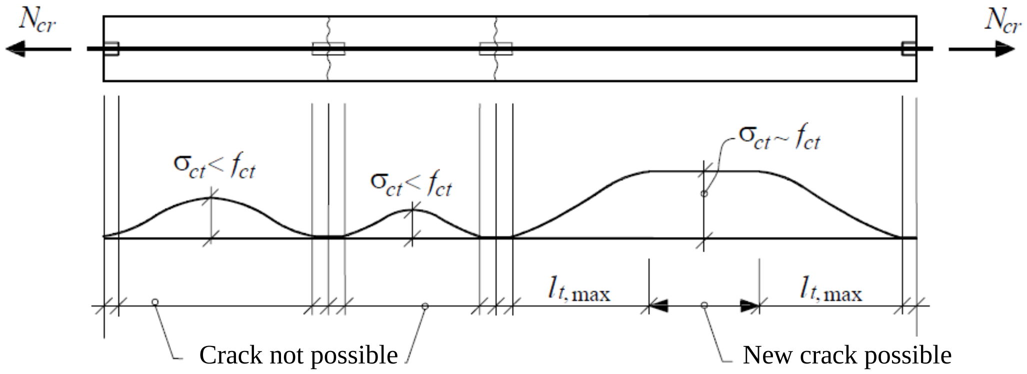

Figure 2.5 Example of the crack development process in a reinforced concrete prism as well as the distribution of concrete stress as new cracks arise. Figure based on Engström, 2011.

Between cracks in the stabilized cracking stage, concrete stresses are less than the tensile capacity of the concrete resulting in a maximum crack spacing, $s_{r,max}$. This distance between cracks is determined by the load transfer capabilities between the steel reinforcement and the surrounding concrete and has an upper and lower limit, $s_{r,max}$ and $s_{r,min}$, see Figure 2.6.

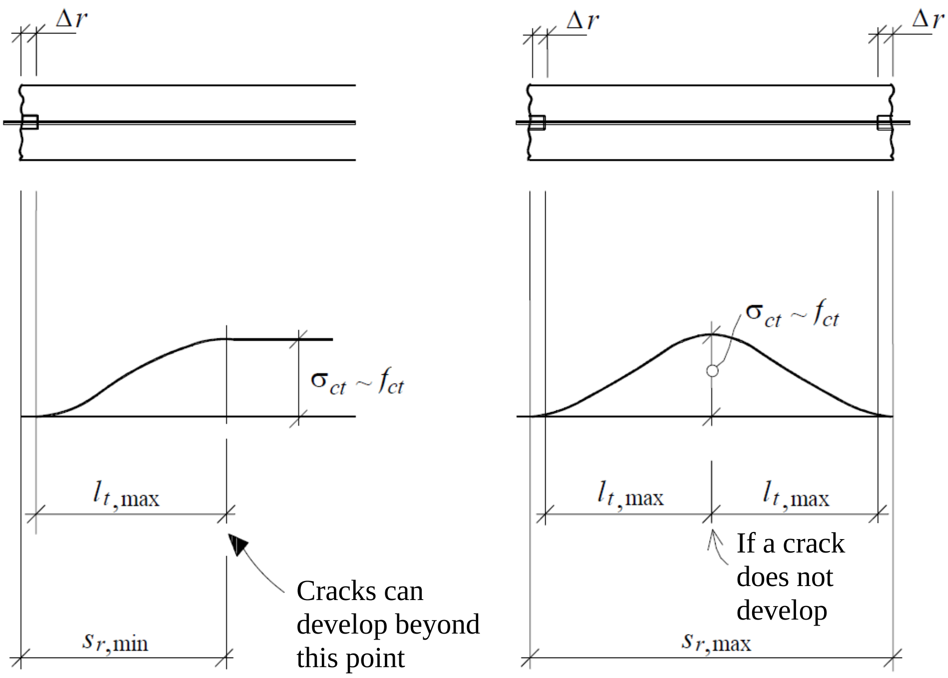

Figure 2.6 Upper and lower limits of crack spacing. Figure based on Engström, (2011).

2.3.3 Bond stress

Reinforcement bars used in reinforced concrete structures are ribbed to ensure an adequate bond between the two materials allowing proper load transfer. These ribs prevent slipping between the materials and allow tensile forces in the reinforcement bars to be transferred to the surrounding concrete. By doing so, the surrounding concrete then aids in carrying the tensile loads and the materials function as a system. The region in which these forces are transferred is called the transmission length, and within this region, the forces are transferred by means of bond stress, τ_b.

In the case of a reinforced concrete prism, bond stress is only activated over the transmission length. In other words, the bond stresses near the ends of the prism are zero and are then initiated in the transmission zone. The lack of bond stresses near the ends of the prism are due to local bond failure between the materials and is represented by Δr, see Figure 2.6. The surrounding concrete near the ends is insufficient in allowing load transfer, resulting in cracking and bond failure. The length of this zone in which bond failure exists can, according to Engström (2011), be calculated with the reinforcement diameter ϕ:

$$\Delta r \approx 2\phi \qquad (2.7)$$

Bond stress plays an important role in crack development, specifically crack spacing and a mean bond stress throughout a reinforced concrete prism can be calculated by

$$\tau_{bm} = \frac{3}{2 \cdot k_1} \cdot f_{ct} \tag{2.8}$$

where k_1 is a factor depending on the surface of the reinforcement bar (ribs). With a known reinforcement bar diameter and tensile capacity of the concrete, the minimum crack spacing can be calculated using this average bond stress, τ_{bm}:

$$s_{r,min} = \Delta r + \frac{1}{4} \cdot \frac{f_{ct}}{\tau_{bm}} \cdot \frac{\phi}{\rho} \tag{2.9}$$

where Δr is the span in which τ_{bm} is zero, ϕ is the reinforcement diameter, and ρ is the volume of reinforcement. The volume of reinforcement, ρ , describes the ratio between cross-sectional areas and can be calculated by

$$\rho = \frac{A_s}{A_c} \tag{2.10}$$

where A_s is the area of steel reinforcement and A_c is the area of concrete. A known prism length allows for the calculation of minimum and maximum crack spacing distances and a prediction can be made on the total number of cracks in the stabilized cracking stage (Engström, 2011).

Similarly, crack widths can be calculated using the calculated maximum crack spacing and material strain values. Crack width can be calculated by

$$w_k = s_{r,max}(\varepsilon_{sm} - \varepsilon_{cm}) \tag{2.11}$$

where w_k is the characteristic crack width, ε_{sm} is the mean strain of the steel, and ε_{cm} is the mean strain of the concrete.

To summarize, bond stress is a key component in the functionality of reinforced concrete and following crack development and spacing. Bond stress allows for proper load transfer and can be applied to determine crack development. A reduction in bond stress hypothetically results in fewer cracks and, in turn, greater total displacement and reinforcement strain.

2.3.4 Tension stiffening

Within the cracks of a reinforced concrete prism, the steel reinforcement carries the tensile loads, and it is assumed that the concrete no longer carries tensile forces. This phenomenon creates a symbiotic relationship between the two materials as the compressive forces are carried by the concrete and the tensile forces are carried by the reinforcement bars crossing the cracks. However, between cracks, both materials transfer tensile forces leading to a stiffer structure and less deformation. As seen in

Figure 2.7, the contribution of the concrete between cracks to the overall stiffness of the structure is called tension stiffening

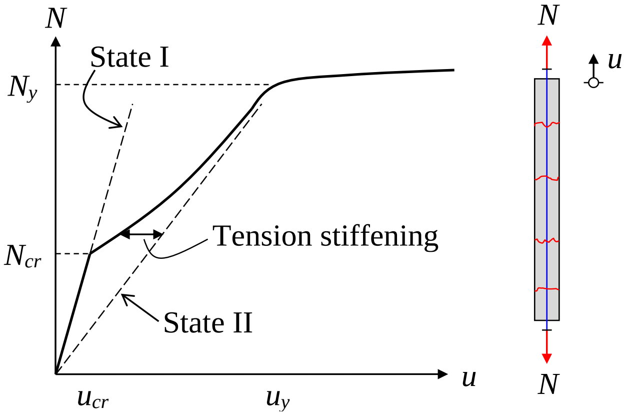

Figure 2.7 Effects of tension stiffening presented in a stress-strain curve (Plos et al., 2020).

This increase in stiffness of the structure is largely due to the internal connection between the two materials, or bond stress. Studying tension stiffening is of importance as this effect controls the crack development, crack spacing, and crack widths. As time passes and the load increases, tension stiffening diminishes and its advantages are lost, resulting in greater displacement.

2.4 Structural Responses

Understanding the structural response(s) of a structure during loading is of importance when conducting experimental research. To properly conduct an analysis post-testing, the responses should be understood, and predictions should be made. The following chapter discusses the typical structural response of structures and their importance.

2.4.1 Introduction

As a load is applied, a structure will deform from its/their original state. The importance of a structure's response is seen when studying the failure modes of said structure. The most effective way to withstand significant loads, for example an impulse load, is to absorb the energy of the load in the form of deformations. However, force equilibrium must be reached in statically loaded structures. In the case of reinforced concrete, ductility is desired, and therefore a larger plastic response is advantageous prior to failure. In addition, ductility and a plastic response ensure a safe and predictable failure mode.

2.4.2 Linear elastic response

If a structure subjected to a load returns to its original state without remaining deformations, the structural response is deemed to be linear elastic. After unloading, the deformations created are reversed and the structure returns to its undamaged state.

The linear elastic response of a structure can be expressed by a structural capacity R, and is calculated by

$$R = ku \tag{2.12}$$

where k is a constant stiffness, and u is the deformation of the structure. The representation of this response in a capacity-deformation diagram is linear, hence the name linear-elastic, see Figure 2.8.

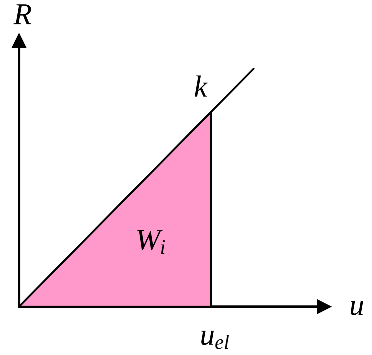

Figure 2.8 Structural response assuming pure elasticity (Johansson & Laine, 2012).

2.4.3 Plastic response

As loads often exceed the linear-elastic region, a plastic response is common amongst ductile materials, such as steel. If permanent deformations remain in the structure after unloading, the structure displays a plastic structural response in which returning to its original state is no longer possible.

Plastic deformations that are a result of a plastic response increase as the load increases. A high plastic deformation capacity ensures an increased energy absorption capacity and is a function of which load is required to generate this capacity. Moreover, the larger the plastic response, the more ductile that material is. For example, steel reinforcement has a large plastic response and therefore ductile failure mode. A plastic response is also clearly seen in the capacity-deformation diagram for a structure, see Figure 2.9.

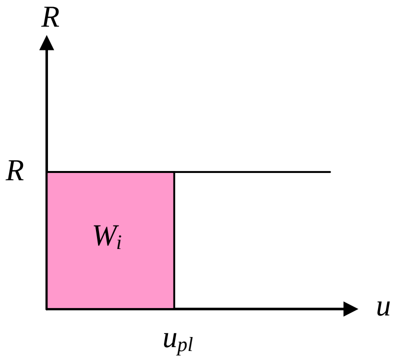

Figure 2.9 Structural response assuming pure plasticity (Johansson & Laine, 2012).

2.4.4 Elastic plastic response

A combination of an elastic and plastic response results in partial permanent deformations with some degree of elasticity. This form of structural response is seen in reinforced concrete where the interaction between the two materials leads to an elastic and plastic response. The steel reinforcement and its plastic nature adds to the ductility of the material, while the concrete adds stiffness and rigidity in the structure.

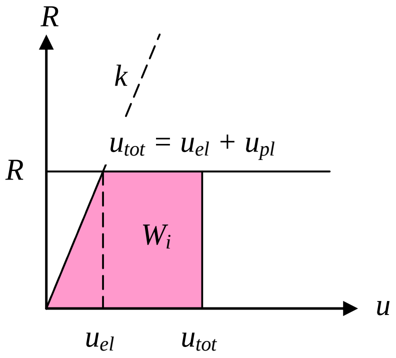

Figure 2.10 Structural response assuming a combination of elasticity and plasticity (Johansson & Laine, 2012).

The combination of elasticity and plasticity leads to two components of the total deformation, u_{tot}. The initial linear response results in an elastic deformation, u_{el}, and the plastic response results in a plastic deformation, u_{pl}. At this point, a certain elastic deformation is reached along with an irreversible plastic deformation. In the case of reinforced concrete prisms, the initial linear response represents the elastic deformation capacity. The response after elasticity represents the plastic deformation capacity and corresponds to the properties of the steel reinforcement within the prisms. For a reinforced concrete prism, the structural response is of importance when studying the energy absorption. The structure's energy absorption capacity presents the area under the force-displacement curve. Therefore, the plastic response after elasticity is of great importance as this determines the area beneath the curve.

2.5 Plastic Deformation Capacity of RC

Plastic deformations are inevitable due to the nature of reinforced concrete subjected to loading. The plastic deformations due to loading are crucial to ensure ductility in the structure and a safe failure mode. Crack development and plastic hinges in the structure lead to deformations whilst maintaining adequate load capacity. This plastic deformation capacity in the structure leads to an overall increase in energy absorption (Johansson & Laine, 2012).

2.5.1 Strain

Tensile stresses arise as a reinforced concrete specimen is subjected to loading and deformations. The strain in the reinforcement bar is of importance when studying the plastic deformation capacity of a structure as it is directly correlated to the plastic deformation capacity of said structure. Increasing the strain leads to greater deformations and therefore energy absorption. Strain in a reinforcement bar is calculated as

$$\varepsilon = \frac{u}{L} \tag{2.13}$$

where u is the change in length due to loading, and L is the initial length of the specimen. The significance of reinforcement strain and plastic deformation capacity in this instance is seen in rotational capacity of a certain cross-section.

2.5.2 Rotational capacity

A theoretical model coupled with a derivation of equations for rotational capacity is presented in the handbook published by the Swedish Fortification Agency (FKR, 2011). The model and derivation of equations to express rotational capacity is in accordance to the Bk 25:2 and is compiled by Johansson and Laine (Fortifikationsförvaltningen, 1973b). This derivation is based on a model of a simply supported beam and mathematically explains rotational capacity for a reinforced concrete structure with a given cross-section.

The correlation between reinforcement strain, plastic deformation capacity, and energy absorption is explained further when studying rotational capacity. The rotational capacity of a structure, $\theta_{f,}$, describes a cross-section's ability to rotate and deform as a result of loading, see Figure 2.11. A large rotational capacity warrants a larger plastic deformation capacity, and therefore greater ductility and energy absorption when subjected to loading (Johansson & Laine, 2012).

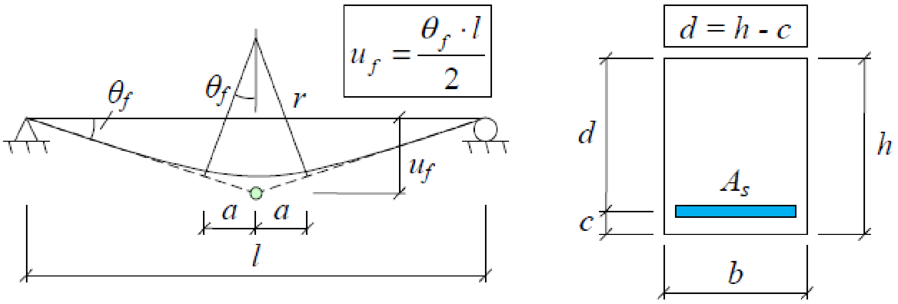

Figure 2.11 Rotational capacity model and cross-section for a simply supported beam (Johansson & Laine, 2012).

According to Johansson and Laine, the maximum rotational radius, r, is based on the strain of the steel reinforcement and the concrete. This relationship between rotational radius and strain is calculated by

$$\frac{1}{r} = \frac{\varepsilon_{cu}}{x} = \frac{\varepsilon_s}{d - x} \tag{2.14}$$

where ε_{cu} is the concrete's failure strain, ε_s is the steel reinforcement's average strain, x is the height of the cross-section's compressive zone, and d is the cross-section's effective height.

Furthermore, a failure criterion for a structure can be derived and written as

$$\omega_{s,crit} = \frac{0.8\varepsilon_{cu}}{\varepsilon_s} \tag{2.15}$$

where $\omega_{s,crit}$ is the mechanical reinforcement ratio used to determine if failure occurs in the form of bar rupture or concrete crushing. If the calculated value of ω_s is less than $\omega_{s,crit}$, bar rupture is assumed, and if the value is greater than $\omega_{s,crit}$, concrete crushing is assumed, see Figure 2.12.

$$\frac{x}{d} = \frac{\omega_s}{0.8} \tag{2.16}$$

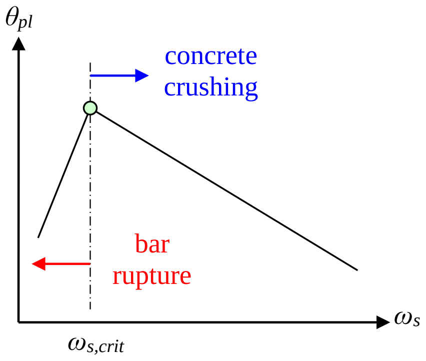

Figure 2.12 Illustration of the failure criterion for bar rupture and crushing of concrete (Johansson & Laine, 2012).

With the assumption that rupture of the steel reinforcement occurs, i.e. $\omega_s < \omega_{s,crit}$, the rotational capacity can be calculated as

$$\theta_f = \frac{a}{r} = \frac{0.5d + 0.15l}{r} = \frac{0.8\varepsilon_s}{d(0.8 - \omega_s)} \cdot (0.5d + 0.15l) = \frac{0.4\varepsilon_s}{0.8 - \omega_s} \cdot \left(1 + 0.3\frac{l}{d}\right) \qquad (2.17)$$

Ultimately, as seen in the derivation in equation (2.17), reinforcement strain directly affects the rotational capacity of a cross section. With this concept applied to reinforced concrete prisms, the greater the reinforcement strain, the greater the rotational capacity. As rotational capacity affects the plastic deformation capacity, a conclusion can be made that if the design strain is the reinforcement then this strain is directly related to the energy absorption capacity of a structure.

2.5.3 Catenary action

When a reinforced concrete structure is exposed to a load great enough to inflict permanent deformations a new equilibrium is sought out by the structure. The reinforced concrete structure seeks an alternative form of load transfer, and, therefore, catenary tensile forces are developed. The direction of these forces and their function in carrying external loads is parallel to the principles of a chain or hammock (Johansson, 2015). The development of these forces directed towards the supports allows for the structure to function even as the load is applied further. Catenary action is favorable as the phenomenon increases the overall strength and rigidity of the structure and allows for greater deformations, even after the structure is damaged (El-Tawil, 2016).

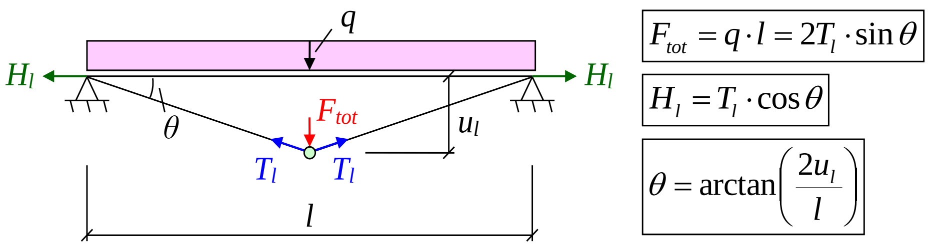

Figure 2.13 Illustration of catenary action in a beam with a uniformly distributed load, q, and a triangular deflection (Johansson, 2015).

Figure 2.13 presents the concept of catenary action in a beam and the development of forces towards the supports. An applied load increases the distance u_l, and, in turn, F_{tot}

continues to transfer the applied load to the supports. A requirement for catenary action to take place is steel reinforcement that remains in-tact. Additionally, the respective supports should be able to carry the horizontal forces, H_l, that arise. The lack of rupture in the bar allows for the catenary forces to continue their advantageous purposes. Catenary action essentially allows for greater deformations, which leads to overall greater plastic deformation capacity and energy absorption.

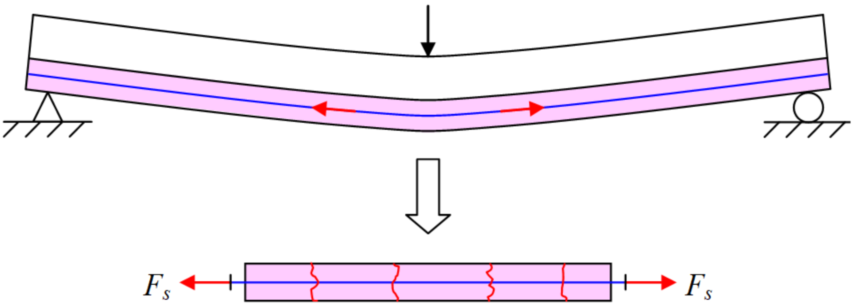

Figure 2.14 Schematic illustration of force action in the bottom of a reinforced concrete beam subjected to bending and a simplified description using a tensile loaded reinforced concrete prism.

A simplification of catenary action in a simply supported reinforced concrete beam can be done using reinforced concrete prisms, see Figure 2.14. The plastic hinge, the span in which plastic bending occurs, can be translated to reinforced concrete prisms. In this way, the prism is a small-scale representation of the catenary action in a beam and aids in the understanding of catenary action. Analyzing the tensile capacity and behavior of said prism allows for a better understanding of catenary action and its behavior in reinforced concrete structures.

2.6 KTH Experiments

Previous research is an important asset when conducting experimental research. Having a foundation of information and data can allow for predictions of test results and a better analysis. In this case, research done at KTH university in Stockholm, Sweden helps supplement this experiment and will be used as a comparison and reference.

Between years 2000-2005 the Swedish Armed Forces conducted a series of static and dynamic laboratory tests on concrete slab strips at KTH university in Stockholm, see Figure 2.15. These series of tests were conducted to compare and analyze the rotational capacity of reinforced concrete with new steel reinforcement (Ks 500) with previously used steel reinforcement. The simply supported concrete slab strips were configured with a two-point load in four-point bending with varying steel reinforcement quality, reinforcement diameters, and concrete qualities (Ansell & Svedbjörk, 2000, 2003, 2005). Reinforcement strain values for a chosen number of concrete slabs were recorded, calculated, and compiled by Johansson and Laine (2012) and can be used as a comparison in this project, see Table 2.1.

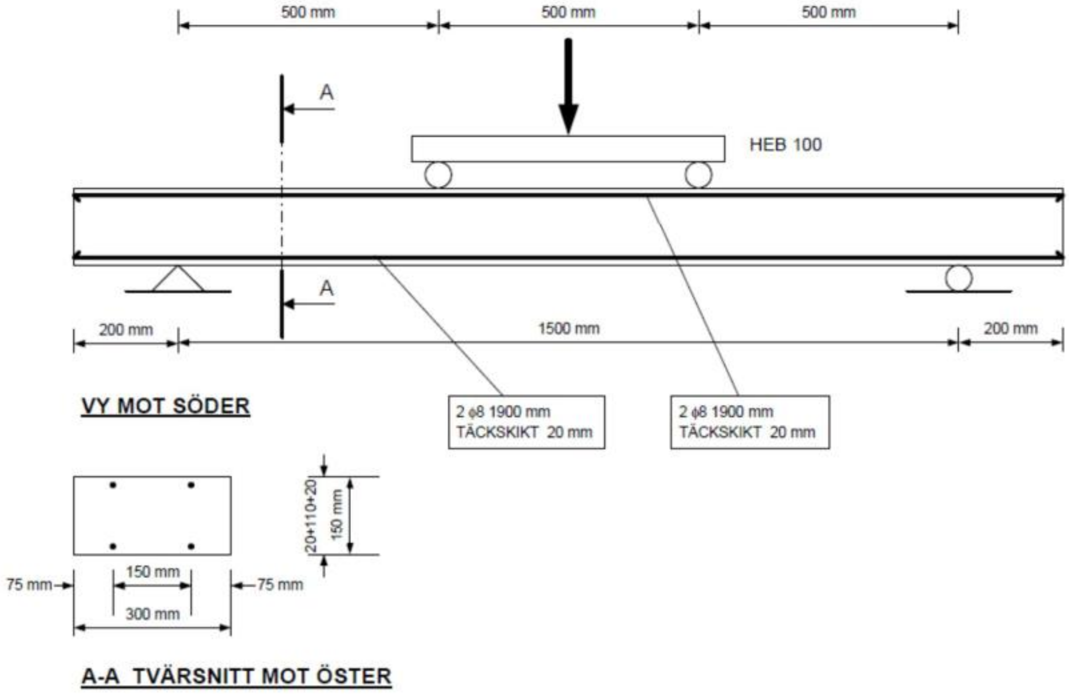

Figure 2.15 Illustration of the experiment configuration used in the KTH experiments (Ansell & Svedbjörk, 2000).

The series of experiments conducted at KTH are of similar nature to the reinforced concrete prisms tested in this project; however, lower reinforcement volume was used in the KTH experiments. Data presented from these experiments can be used to estimate prism test results. Beams were subjected to 4-point loading and the final plastic reinforcement strain was recorded over the beam’s entire length, see Figure 2.16 for an example of registered plastic reinforcement strains from one of the tests. Based on these measurements and the values presented in Table 2.1, an average strain of ~3-5 % is expected for the prisms subjected to tensile loading in this project. Surpassing an average strain of 3-5 % would hypothetically lead to failure of the steel reinforcement bars.

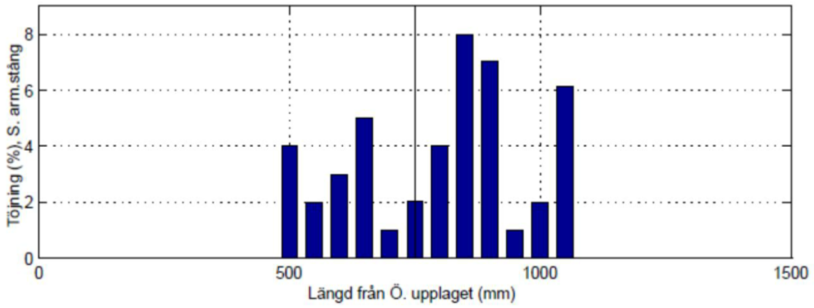

Figure 2.16 Measured strain distribution in the bottom reinforcement. B500 BT (Ansell & Svedbjörk, 2000).

Table 2.1 Presentation of results from previous experiments conducted at KTH (Johansson & Laine, 2012)

Reference 1)	Name	l [mm]	b [mm]	h [mm]	d [mm]	A_s [mm^2]	f_{cc} [MPa]	f_{sy} [MPa]	f_{su} [MPa]	γ [-]	ω_s [-]	ε_s [%]
(2000)	PLS 1	1500	300	150	126	101	28.1	500	575	1.15	0.047	3.2
	PLS 2	1500	300	150	126	101	28.1	500	575	1.15	0.047	3.2
	PLS 3	1500	300	150	126	101	28.1	500	575	1.15	0.047	3.0
	PLS 4	1500	300	150	126	101	28.1	570	660	1.16	0.054	3.1
	PLS 5	1500	300	150	126	101	28.1	570	660	1.16	0.054	3.4
	PLS 6	1500	300	150	126	101	28.1	570	660	1.16	0.054	3.6
(2003a)	PLS 2	1500	300	150	124	113	35.1	516	624	1.21	0.045	3.7
	PLS 3	1500	300	150	126	101	39.9	514	653	1.27	0.034	4.4
	PLS 4	1500	300	150	126	101	83.6	514	653	1.27	0.016	5.0
(2005)	PLS 1a	1500	530	150	122	201	45.0	534	643	1.20	0.037	1.0
	PLS 1b	1500	530	150	122	201	40.3	534	643	1.20	0.041	0.8
	PLS 1c	1500	530	150	122	201	37.9	534	643	1.20	0.044	1.6
	PLS 3a	1500	400	150	122	201	45.0	534	643	1.20	0.049	1.5
	PLS 3b	1500	400	150	122	201	40.3	534	643	1.20	0.055	1.9
	PLS 3c	1500	400	150	122	201	37.9	534	643	1.20	0.058	1.6
	PLS 4a	1500	320	150	122	201	45.0	534	643	1.20	0.061	3.2
	PLS 4b	1500	320	150	122	201	40.3	534	643	1.20	0.068	3.2
	PLS 4c	1500	320	150	122	201	37.9	534	643	1.20	0.073	1.6

1) Ansell & Svedbjörk

3 Experiment Description

Reinforced concrete prisms were constructed and tested to study the parameters that affect the average reinforcement strain. These RC prisms have lengths of 800 mm and a cross-sectional height and width of 100 mm. After casting and curing, the prisms were erected in an MTS 793 tensile testing machine in which the prisms were subjected to tensile forces until failure. This chapter explains the configuration and preparation of the reinforced concrete prisms. All experimental preparation took place in the Chalmers concrete lab.

3.1 Concrete prisms with centralized reinforcement bar

To simplify both the experiment preparation and testing, reinforced concrete prisms with centrally placed reinforcement bar were constructed, see Figure 3.1. By having less concrete and less reinforcement bar, the test specimens were easier to handle and lift onto the tensile testing machine. In addition, the analysis of average strain is also simplified by having a single centralized reinforcement bar. The results and analysis of the prisms can be later used in full-scale reinforced concrete beams.

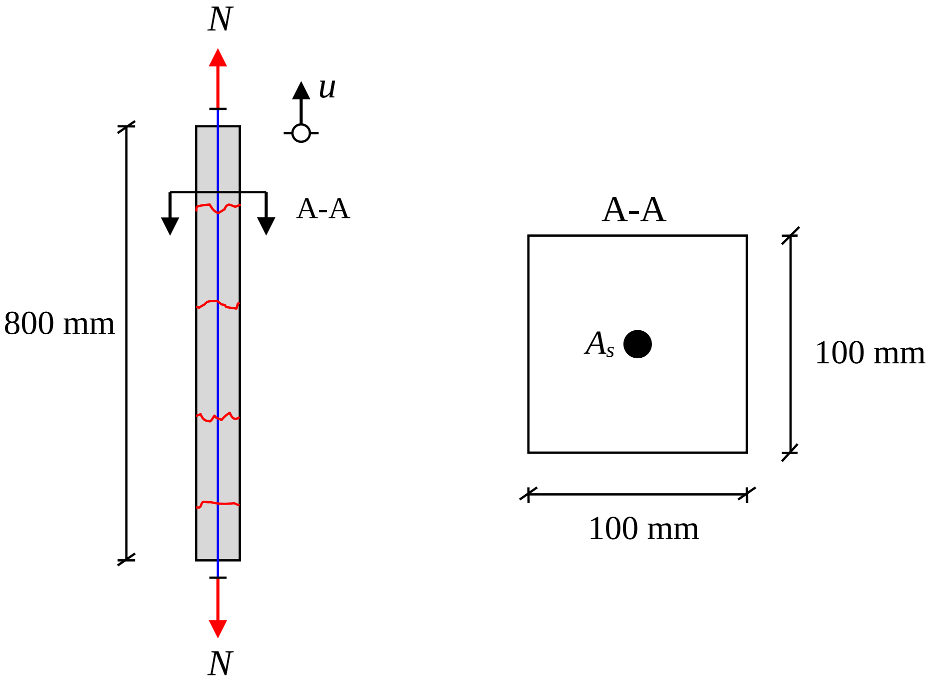

Figure 3.1 Reinforced concrete prism geometry and cross-section.

Eighteen reinforced concrete prisms were tested with varying reinforcement bar diameters (ϕ16, ϕ12, ϕ10) and layouts of low-friction PVC tubing, see Figure A.4. Varying reinforcement bar diameters provide three different reinforcement percentages: 2.0 % for ϕ16, 1.1 % for ϕ12, and 0.8 % for ϕ10. Prisms were grouped according to reinforcement diameter: three prisms with ϕ16, twelve prisms with ϕ12, and three prisms with ϕ10. Nine of the twelve prisms with ϕ12 reinforcement were configured with varying configurations of PVC tubing which had the following layouts:

4x50 mm, 8x50 mm, and 4x100 mm. Each layout corresponds to three prisms with ϕ12 reinforcement. The remaining prisms were configured without PVC tubing.

Each prism was labeled and numbered during preparation and then renamed during testing according to the order in which they were tested. Table 3.1 presents the prisms' names and the order in which they were tested. Prisms with a 4x50 mm PVC configuration are denoted with the letter A, prisms with an 8x50 mm PVC configuration with the letter B, and prisms with a 4x100 mm PVC configuration with the letter C.

Table 3.1 Naming of prisms based on order of testing and PVC configuration

Name	Bar Diameter [mm]	Configuration
ϕ16–1	16	No PVC
ϕ16–2	16	No PVC
ϕ16–3	16	No PVC
ϕ12–1A	12	4x50 mm
ϕ12–2A	12	4x50 mm
ϕ12–3A	12	4x50 mm
ϕ12–4B	12	8x50 mm
ϕ12–5	12	No PVC
ϕ12–6B	12	8x50 mm
ϕ12–7B	12	8x50 mm
ϕ12–8C	12	4x100 mm
ϕ12–9C	12	4x100 mm
ϕ12–10C	12	4x100 mm
ϕ12–11	12	No PVC
ϕ12–12	12	No PVC
ϕ10–1	10	No PVC
ϕ10–2	10	No PVC
ϕ10–3	10	No PVC

PVC tubing around the reinforcement will create regions in which the surrounding concrete is inactive. Inactivity in the concrete and reduced bond stress is predicted to lead to greater deformations. In addition, lower number of cracks is expected with greater volumes of PVC.

3.2 Test setup

Testing of the prisms was conducted in the Chalmers concrete lab using an MTS 793 tensile testing machine, station manager, and GOM Correlate. The configuration of DIC cameras and settings in GOM Correlate were adjusted beforehand, and then kept constant throughout testing. Two cameras coupled with GOM Correlate result in 3D models and strain fields for each prism. Configuring the settings of the DIC cameras is an important aspect regarding post-testing analysis and data handling. Initially, the cameras were set to a frequency of 0.5 Hz, meaning one frame or picture was captured every 0.5 seconds. This setting was used for prism ϕ16-1 (prism 01) but was modified to reduce file sizes. A frequency of 1 Hz, or one frame per second, was used for the remaining 17 prisms. Modifying the settings from 0.5 Hz to 1 Hz effectively halved raw file sizes making post-testing analysis simpler.

Station manager was programmed to control the speed and applied force throughout the test and was regulated using two phases. To begin the test, phase one was initialized at 0.5 mm/min and manually switched to phase two at 10 mm/min after the yielding plateau. Phase one allowed for slower crack development and a more detailed force-displacement curve, and phase two sped up the testing process for the 18 prisms. As each prism reached failure, station manager was programmed to detect a drop in applied force by 2 % and then commanded to immediately drop the load to zero and stop the test. Ceasing loading at this point took place for safety reasons, i.e. to prevent bar rupture which could lead dangerous concrete debris in the laboratory.

3.3 Digital Image Correlation (DIC)

3.3.1 Introduction

DIC (Digital Image Correlation) technology is an ever-growing and powerful analysis tool in the engineering world. Two cameras and DIC software generate 2D and 3D models of surfaces and structures which aid in visualization of total displacement and strain during testing. This technology was an important component in testing and analyzing the prisms, and therefore, this chapter will be a description of DIC technology, and the setup used in this thesis.

3.3.2 Static Testing Setup

At its core, DIC technology is a system consisting of cameras and software. In order to recognize and successfully analyze a test subject, the system of cameras and software require a high contrast pattern. To create this contrast, a white backdrop is applied to the surface of the specimen, and thereafter, a black speckle pattern. The pattern is then used as a reference image in the software and any changes in the surface pattern are interpreted as displacement, or strain.

Two cameras and an Aramis system were used to acquire the 3D models in this case. The cameras were set up with the focal point at the center of the test specimen and were kept constant throughout testing to ensure consistent results and measurements. Images were taken with a certain frequency and later imported into GOM Correlate 2018 (GOM, 2018) for post-processing and analysis. Additionally, DIC-specific stickers can be placed on test specimens. GOM Correlate software detects these stickers as points of reference and can therefore calculate distances between them.

3.3.3 Post-Processing

After testing, raw ARAMIS files containing images of the prisms were imported into GOM Correlate and used to calculate total displacement, number of cracks, and crack widths. This post-processing process was kept constant throughout all prisms to ensure a proper analysis.

Total displacement for each prism was calculated using a two-point-extensometer with an original length varying for each prism. These digital extensometer functions as a measurement tool to determine distances between two user-defined points. As some data was lost near the ends, the two points were placed as close to the edges as possible without losing data throughout the test. After creating the extensometer, displacement in the x-direction is measured with the first picture as the reference stage. Displacement data was then exported along with force data from the machinery. Stickers were placed in each corner of the prism to calculate displacement between them. However, as data was lost near the edges, and thus near the stickers, this was unsuccessful. To avoid this, stickers could have been placed a certain distance from the ends, i.e. 1-3 cm from the edge of the concrete. This way there is adequate space around the stickers ensuring that data loss does not occur.

Crack widths for each prism were calculated using three extensometers for each crack (Left, Center, Right). With these three crack calculations, an average crack width can be calculated for each crack and then plotted. These cracks were chosen in the stabilized cracking stage and then followed throughout the test. Data from each extensometer and each crack was then exported and then imported into excel.

3.3.4 DIC Study

Analyzing results in GOM Correlate is a meticulous process and should be done consistently throughout all results. For example, calculation of crack width should be done with the same settings and techniques for all cracks across all prisms to ensure consistent results.

The important settings in this case were the initial reference points for calculating crack widths i.e. which two points to measure between, and facet size. Extensometers in GOM Correlate are created using one reference point and an initial length. Determining the initial reference point can be done in several different ways, and the altered initial parameters may result in altered crack widths.

Crack width calculations were conducted in the stabilized cracking stage for each prism. Once the yielding plateau is reached, the number of cracks is logged, and crack widths are calculated from that stage. Extensometer placement was consistent throughout all crack calculations with case C used, i.e. reference points placed in the yellow region, see Figure 3.2. However, a study was conducted to compare different extensometer placements (case A-E) and the resulting crack measurements. The impact of altering the initial reference points is negligible and results are presented in Table 3.2.

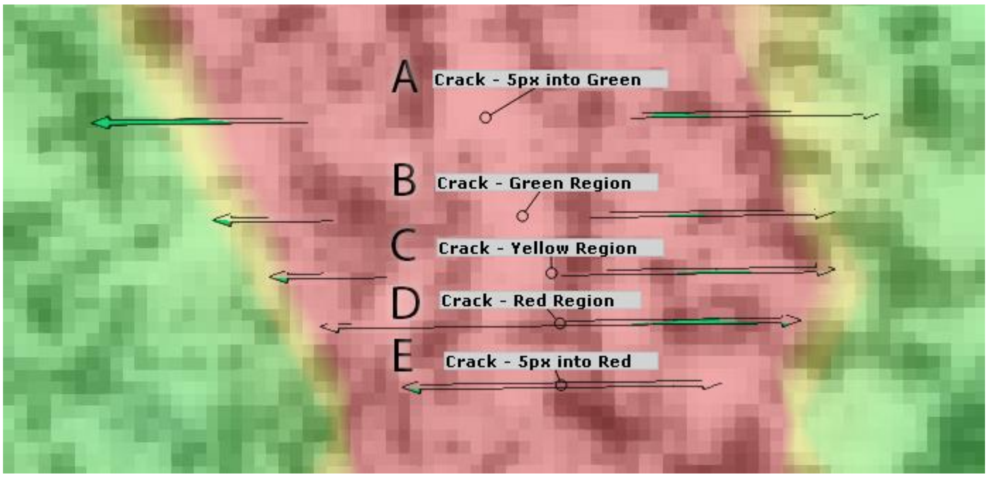

Figure 3.2 Different methods of extensometer placement for crack width calculation in GOM Correlate 2018.

Table 3.2 Maximum crack width results with varying extensometer placement and facet settings.

Facet [px]	**Max Width Case A [mm]**	**Max Width Case B [mm]**	**Max Width Case C [mm]**	**Max Width Case D [mm]**	**Max Width Case E [mm]**
17	13.420	13.423	13.427	13.427	13.425
19	13.419	13.420	13.425	13.427	13.427
21	13.417	13.420	13.424	13.425	13.429
23	13.413	13.419	13.422	13.425	13.429

Furthermore, facet size is an important factor when using DIC software. Facet size determines the accuracy of the measurements with larger facet sizes accumulating more data. The greater the amount of data, the more accurate the measurements. Altering the facet sizes (in case C) did not have substantial differences in the crack width measurements, see Table 3.3. A difference of 0.057 mm in maximum crack width between facet size 7 px and size 50 px may be insignificant in this project but could be of interest when studying initial crack development in early stages of loading.

Table 3.3 Maximum crack width results with varying facet sizes (Case C).

Facet [px]	**Max Width [mm]**
7	13.404
17	13.423
19	13.420
21	13.420
23	13.419
33	13.419
50	13.461

Ultimately, initial reference point placement and facet size do not have a substantial impact on the results in this case as the study is focused on total displacement. However, in studies with lower resolution images, the facet size may be of greater importance, and may affect the results. Additionally, studies of initial crack development in the early stages of loading may have to take extensometer placement and facet size into greater consideration.

4 Experimental Results

Results, discussion, and interpretation of the experimental results are presented in this chapter. In addition, material properties for both the concrete and steel reinforcement used are presented. Analysis of the experimental data was conducted using Microsoft Excel and GOM Correlate, and results are displayed as figures, graphs, and strain fields. Further details of the results presented can be found in Appendix C to Appendix E.

4.1 Material testing

Material parameters for the materials used in the reinforced concrete prisms are essential when conducting post-testing calculations. The parameters of interest for the concrete batch used are characteristic compressive strength, compressive strength, and tensile strength. Likewise, steel reinforcement parameters such as ultimate strain strength, yield strength, average strain, and yield to ultimate tensile strength ratio are determined.

4.1.1 Concrete

The batch of concrete used to cast the reinforced concrete prisms was tested to determine compressive and tensile strength. The results presented here represent an average compressive and tensile strength calculated from the six concrete cubes, see Table 4.1. Further results for each individual concrete cube are presented in Table B.1. Calculations and conversions are according to Eurocode 2, see Section 2.1, and values to calculate the averages are mean values. As the dimensions of the concrete cubes may have slightly exceeded 150 mm in length, width, and height, the resulting density of the cubes is higher than expected. For this reason, basing the tensile strength on the characteristic compressive strength is more representative of the actual tensile strength in this case.

Table 4.1 Average compressive and tensile strength of the batch used for the prisms.

Test Type **[-]**	**Strength f_{cm}, f_{ct}** **[MPa]**
Compression	47.2
Split	3.46

4.1.2 Steel reinforcement

Six stress-strain curves are plotted for each respective reinforcement diameter, see Figure 4.1. With a total of 18 reinforcement segments tested, an average curve for all six bars for each diameter was then calculated and plotted, see Figure 4.2. The results are plotted in stress-strain curves for each of the reinforcement bar diameters and provide data for material parameters. Complete material testing results for all 18 segments and their respective averages are presented in Appendix B.2. These average curves are then used as a comparison in the prism results, see Section 4.2.2.

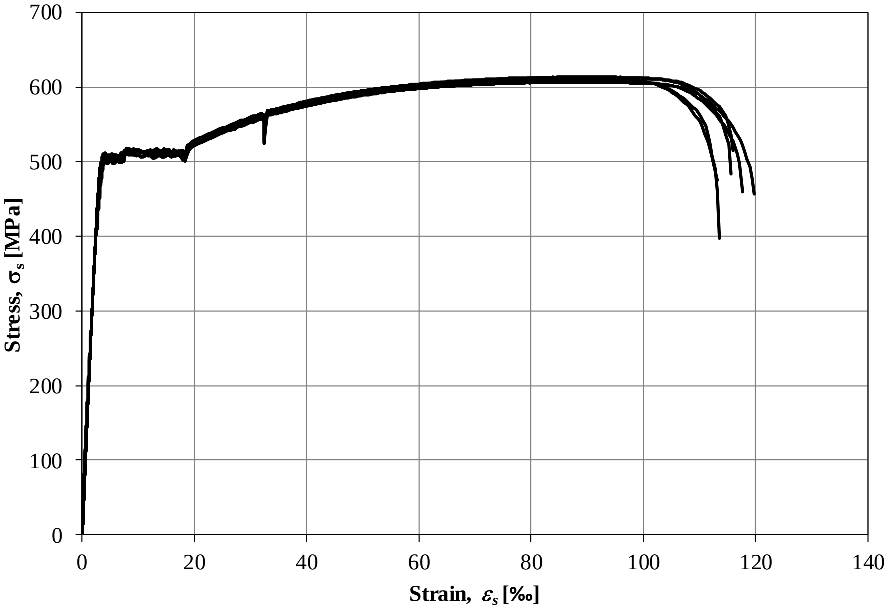

Figure 4.1 Stress-strain curves for six ϕ16 reinforcement segments.

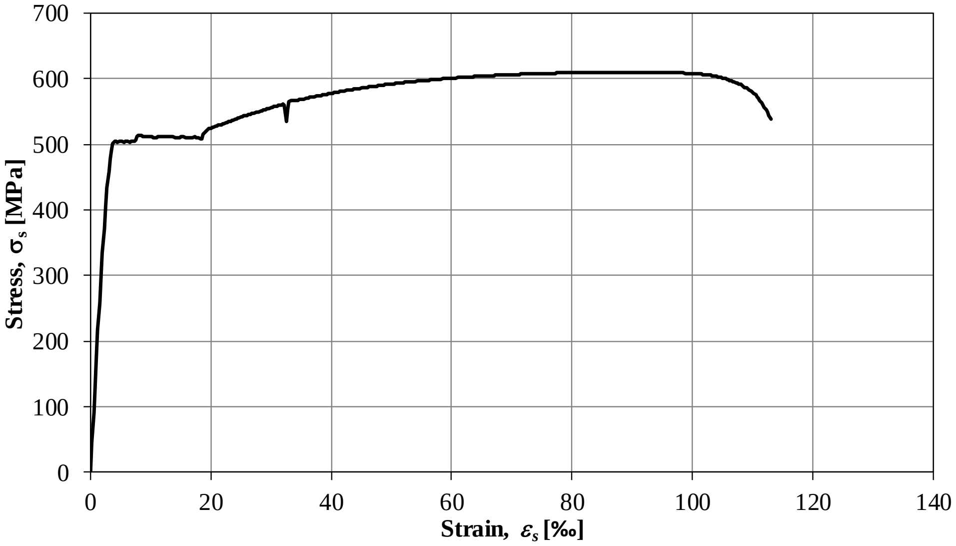

Figure 4.2 Average stress-strain curve for six ϕ16 reinforcement segments.

In addition, the material testing data allows for determination of average strain values and other steel reinforcement properties, see Table 4.2.

Table 4.2 Average strain, yield point, ultimate tensile strength, and f_u/f_y ratio for each reinforcement diameter.

ϕ [mm]	ε_{su} [‰]	f_y [MPa]	f_u [MPa]	f_u / f_y [-]
16	89	507	610	1.20
12	83	524	622	1.19
10	79	541	654	1.21

4.2 RC Prism Results

Processed data for each prism was exported from GOM Correlate and imported into Microsoft Excel, and then plotted according to force, displacement, strain, and crack widths, see Appendix C. Prisms were then grouped by reinforcement bar diameter and plotted together to spot similarities and differences, see Appendix C.8.

4.2.1 Method

Experimental results and processed data in GOM Correlate provide a variety of different results. Each prism's respective crack widths, total displacement, and force are plotted. For consistent results and analysis, prisms containing the same reinforcement bar diameter share the same diagram formatting, more information is found in Appendix C. An important aspect of the experiment results is the occurrence of premature unloading during testing. This was clearly seen in two prisms and, due to this, all eighteen prisms were studied to determine if premature unloading occurred in other prisms. The results of this are presented in Table 4.3 with more information about premature unloading in Appendix C.1.

Table 4.3 Determination of premature unloading in RC prisms.

Prism	**Premature Unloading?**
ϕ16-1	No 1)
ϕ16-2	No
ϕ16-3	No
ϕ12-1A	Yes 2)
ϕ12-2A	No
ϕ12-3A	No
ϕ12-4B	Yes 3)
ϕ12-5	No
ϕ12-6B	No
ϕ12-7B	No
ϕ12-8C	No
ϕ12-9C	No
ϕ12-10C	No
ϕ12-11	No
ϕ12-12	No
ϕ10-1	No
ϕ10-2	No
ϕ10-3	No

1) Successful test with a clear plateau in load and no new crack in GOM Correlate.

2) New crack commenced premature unloading.

3) Concrete piece dislodged and commenced premature unloading.

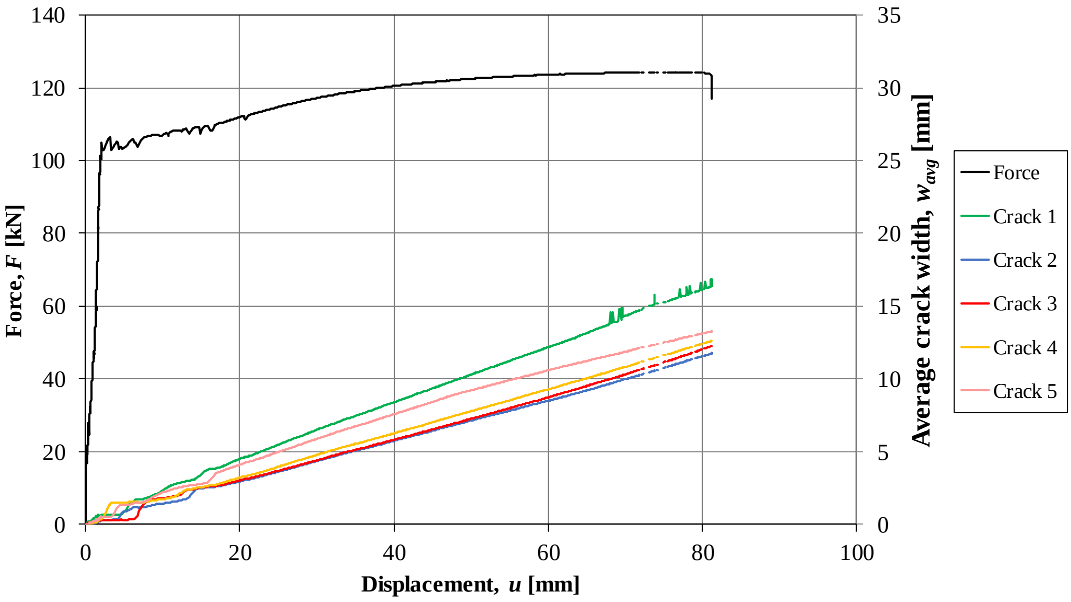

Figure 4.3 Example of experiment results in the form of total prism displacement, average crack widths, and force in prism ϕ16-1.

Figure 4.3 is an example of how results and processed data are presented for prisms containing ϕ16 reinforcement. Each respective crack is a combination of three different crack calculations in GOM Correlate. For example, crack 1 in Figure 4.3 is an average of the crack width on the right, center, and left of the prism. The number of cracks presented in these figures represents the number of cracks developed before the stabilized cracking stage, and therefore, new cracks initiated beyond this point are not accounted for here. These figures show the spread of crack widths for each prism and at which point during loading individual cracks developed. Comparisons can be made between different reinforcement configurations and will be presented in the following sections.

Additionally, cracks for each prism are combined to present the total crack width along with the total prism displacement. An example of these results is found in Figure 4.4 with additional results in Appendix C. Presenting the results in this manner explicitly displays the difference between a prism's total displacement and its total crack width.

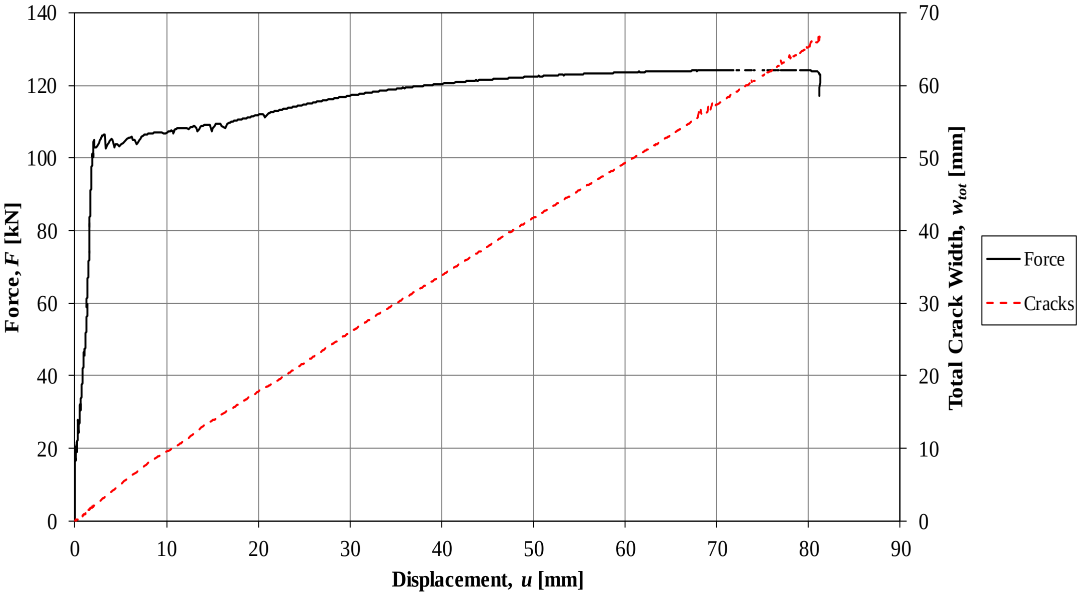

Figure 4.4 Example of experimental results in the form of total crack width, prism displacement, and force in prism ϕ16-1.

Furthermore, images of each prism in the stabilized cracking stage and at maximum load are presented and are used to visualize their behavior during loading. Figure 4.5 is an example of a GOM Correlate report for a prism at maximum load. An example of how crack and total displacement calculations are executed in GOM Correlate are also presented, see Appendix E for more detail.

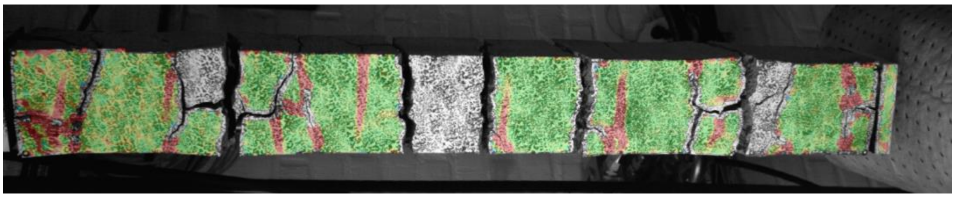

Figure 4.5 Example of a GOM Correlate report for prism ϕ16-1 at maximum load.

4.2.2 Prisms without PVC

Some form of reference data is a key component of any experimental work. In this study, the prisms without PVC tubing were used as comparisons and provided standard strain values for each of the reinforcement bar diameters. These test results provide insight into how varying reinforcement bar diameters affect the average strain. By having a foundation, the effects of the altered parameters can be studied. With the material properties and stress-strain curves predetermined, a comparison can also be made between plain reinforcement bars and the reinforced concrete prisms.

4.2.2.1 ϕ16 prisms

The group of ϕ16 prisms without PVC are presented in Figure 4.6 and resulted in the most cracking and overall damage during testing. The strain for each prism is calculated according to equation (2.13) where the initial length is specific to each respective prism. These initial lengths were determined in GOM Correlate by setting two reference points where data loss would not occur. Consequently, initial lengths vary between prisms, but this is taken into consideration during strain calculations. The interaction between the steel reinforcement and surrounding cracking was limited, which lead to large total displacement, high average strains, and spalling of the concrete. The large number of both vertical and horizontal cracks indicates that load transfer between reinforcement and the surrounding concrete to a large extent was lost, and consequently, the concrete between the cracks had little influence on the response of the prism. The longitudinal cracks displayed in Figure 4.7 were due to spalling and led to a lack of interaction between reinforcement and surrounding concrete and was due to the overall large volume of reinforcement, *ρ*.

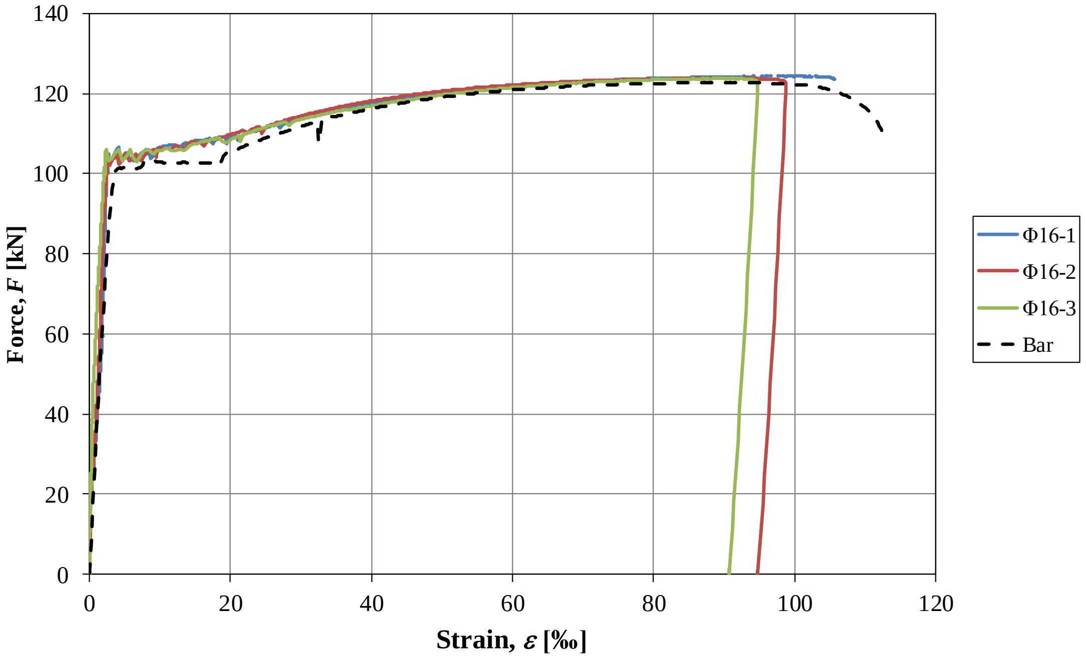

Figure 4.6 Results from ϕ16 prisms without PVC and the average ϕ16 material testing results (Bar).

The force-strain curve for a single reinforcement bar in Figure 4.6 is a representation of the average of six bars tested during material testing. In this case, the ϕ16 material testing results have a low spread, see Figure B.1. This implies that the average curve is an adequate representation of the six bars and can be used as a comparison. Additionally, the prism curves lie above the reinforcement curve (Bar), especially in the early stages of loading or during lower strains, which displays the effects of tension stiffening. In other words, the concrete in the prisms contributed to the stiffness of the structure.

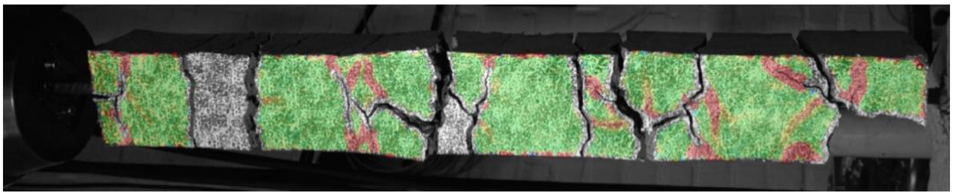

Figure 4.7 Spalling in the concrete and local bond failure at the ends of prism ϕ16-3 at maximum load.

The measured strains at maximum load in the ϕ16 prisms lie between 8-10 %, whilst the average plain reinforcement bar strain reaches 9 %. This difference of less than 1 % is an indication of little/negligible influence of uncracked concrete between cracks. A stronger interaction between the steel reinforcement and surrounding concrete would lead to a more distinct difference in final strain due to an increase in stiffness. A difference of less than 1 % is not entirely of surprise as spalling cracks are prevalent and local bond failure is clearly seen at the prisms' ends, see Figure 4.7.

Furthermore, average crack widths amongst ϕ16 prisms were relatively consistent. Average crack widths for individual cracks were consolidated and the same trend was consistent for all three prisms, see Appendix C for all crack development figures. In addition, crack development occurred simultaneously in these prisms, i.e. in the early stages of loading, see Figure 4.8.

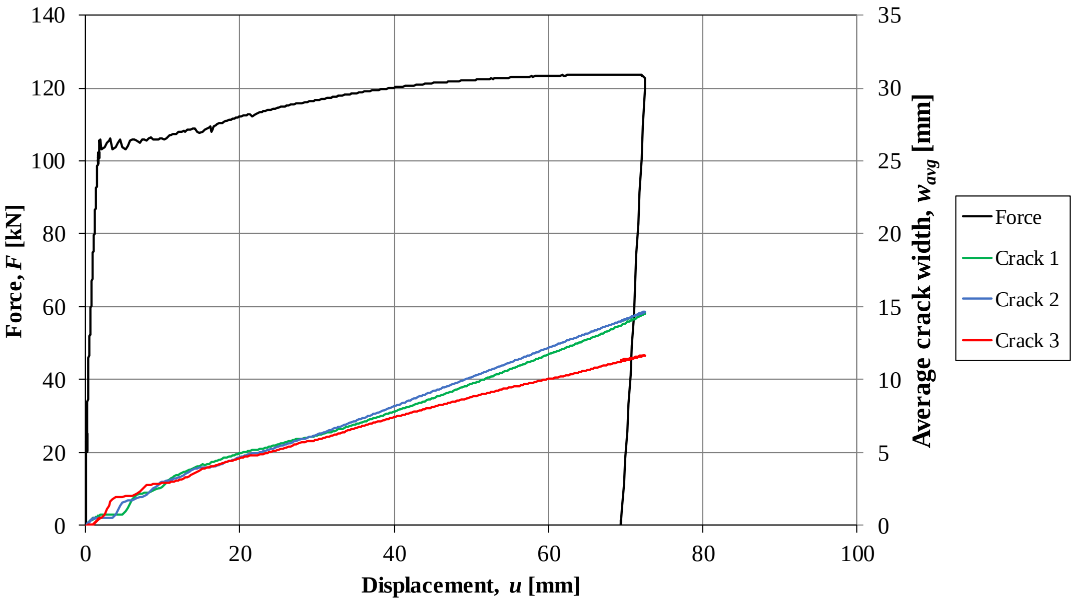

Figure 4.8 *Example of consolidation of average crack widths and crack development in prism ϕ16-3.*

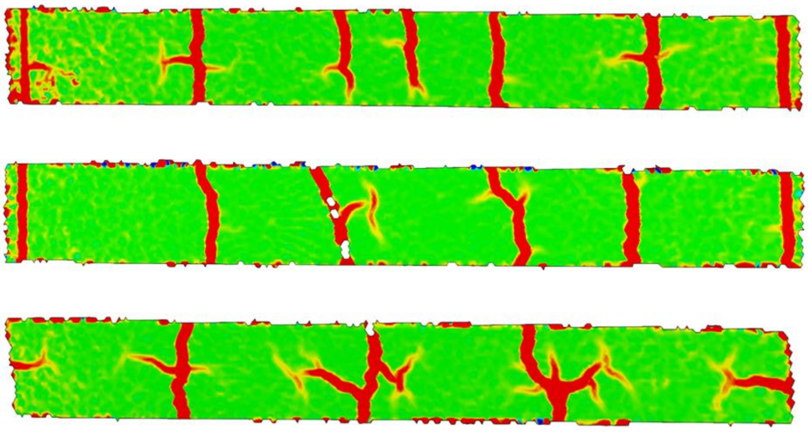

Figure 4.9 *Strain fields for ϕ16 prisms.*

4.2.2.2 ϕ12 prisms

As the reinforcement percentage is decreased in the prisms with ϕ12 reinforcement, a somewhat improved interaction between the materials was attained in these prisms. A comparison between ϕ12 prisms without PVC and the average curve for ϕ12 reinforcement is presented in Figure 4.10. However, local bond failure and bursting cracks were prevalent amongst these prisms, see Figure 4.11.

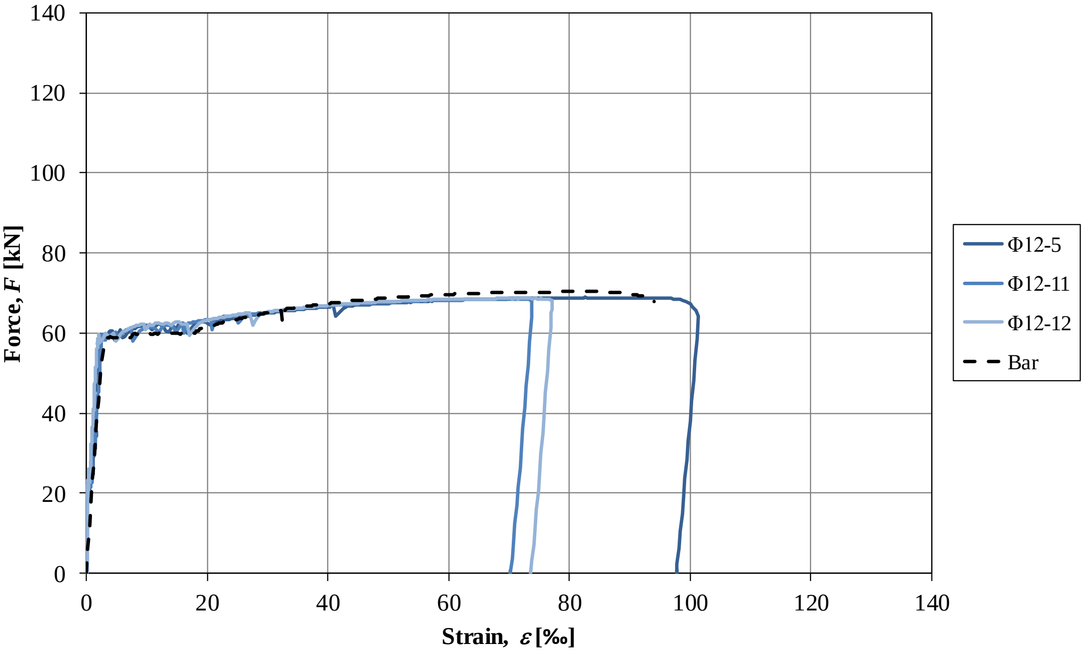

Figure 4.10 Results from ϕ12 prisms without PVC and the average ϕ12 material testing results (Bar).

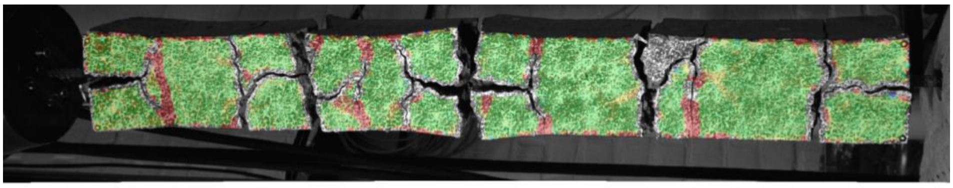

Figure 4.11 Local bond failure and bursting cracks in prism ϕ12-5 at maximum load.

Average strains of around 7 % were achieved in ϕ12 prisms without PVC with an outlier reaching over 8 %. This range in results may be correlated to differences in material properties. For example, the ϕ12 material testing results were widely spread which led to the average curve being somewhat misrepresentative, see Figure B.3. The range in steel reinforcement performance can also be translated to the prisms. For example, certain prisms may have resulted in higher strains than others due to different properties in the steel reinforcement. The discrepancies in steel reinforcement also resulted in differences in tension stiffening effects. Prism ϕ12-5 in Figure 4.10 shows an increase in load capacity in the early stages of plastic deformation.

Further, average crack widths in relation to prism displacement and applied force for ϕ12 prisms without PVC are presented in Figure 4.12. Crack development took place at several different stages of loading, and the range in average crack widths is high in comparison to those shown in Figure 4.8. The broad range of average crack widths and points of crack development is apparent in ϕ12 prisms without PVC, and comprehensive results are found in Appendix C.3.

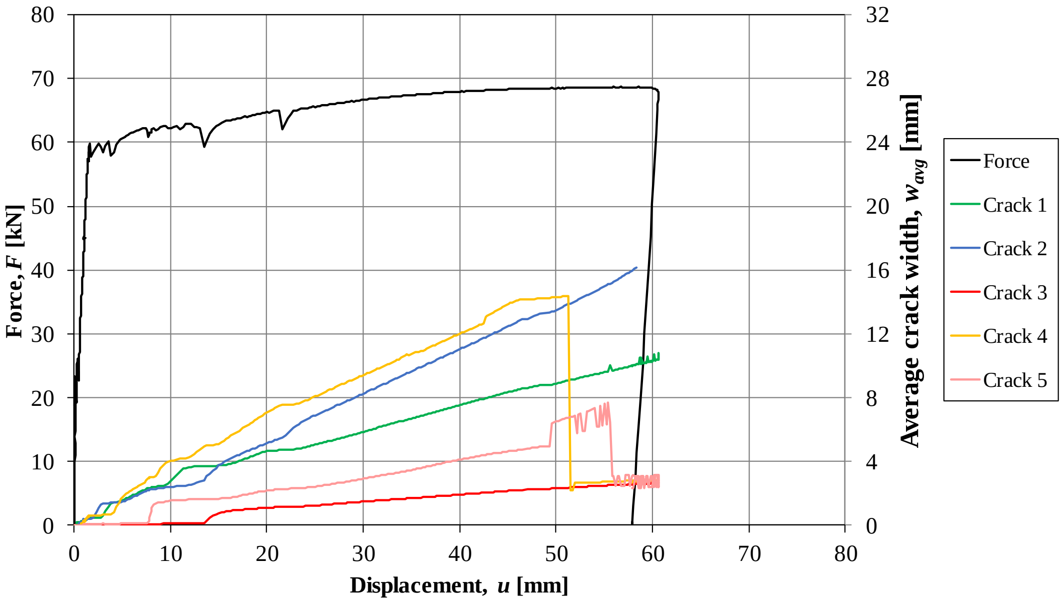

Figure 4.12 Average crack widths and crack development as a function of total displacement and force in prism ϕ12-12.

As seen in Figure 4.12, cracks 4 and 5 dropped after a prism displacement of about 50-55 mm. However, this abrupt drop in average crack width is due to data loss in GOM Correlate. As concrete spalled and pieces began to fall off, the strain field data was lost in some areas. The area around cracks was especially prone to data loss as the black speckle pattern is deformed and lost. This sudden change is average crack width was a common trend due to many prisms experiencing concrete spalling, and therefore, data loss.

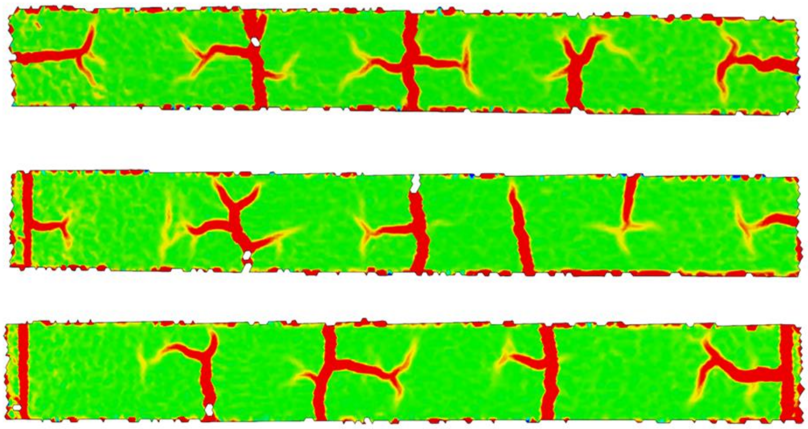

Figure 4.13 Strain fields for ϕ12 prisms.

4.2.2.3 ϕ10 prisms

Results from ϕ10 prisms without PVC are presented in Figure 4.14 and Figure 4.15. These results display the effect of the concrete on the overall stiffness of the specimen. A stiffer prism with fewer spalling cracks led to decreased displacement and overall reinforcement strain.

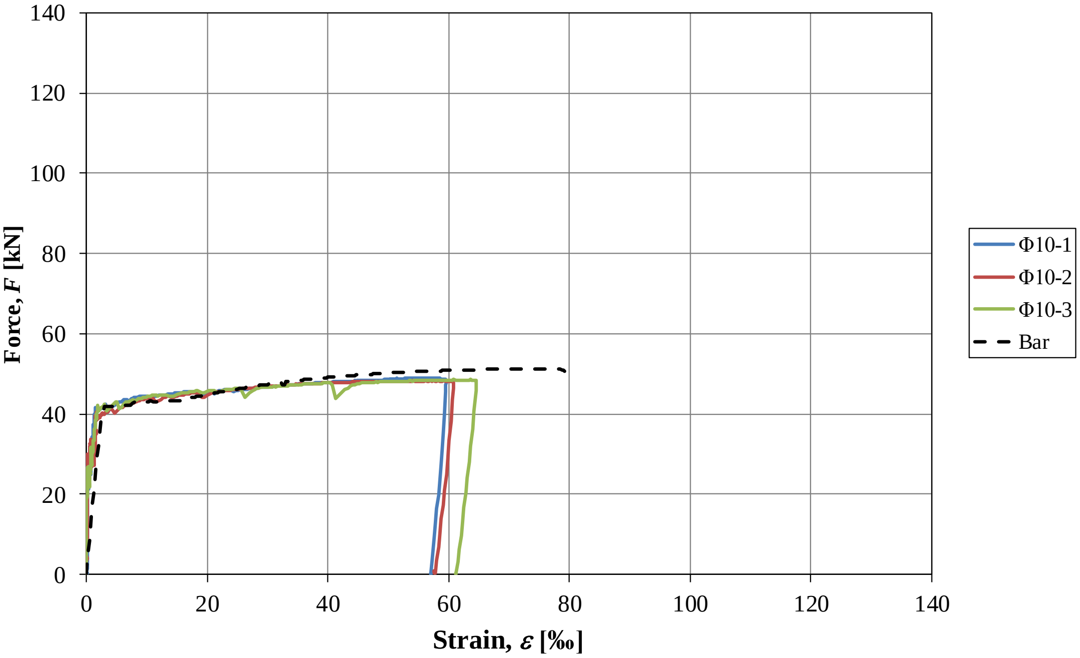

Figure 4.14 Results from ϕ10 prisms without PVC and the average ϕ10 material testing results (Bar).

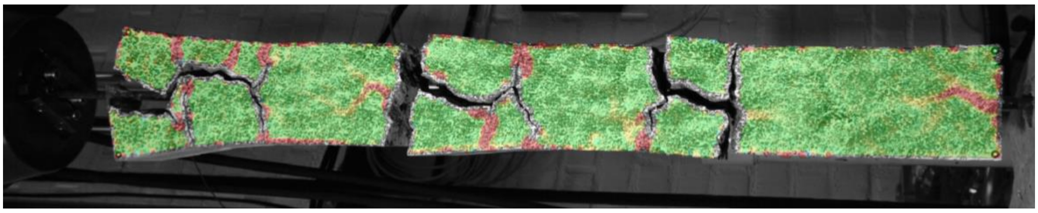

Figure 4.15 Fewer cracks and less local bond failure near the ends of prism ϕ10-1 at maximum load.

The lower amount of reinforcement led to fewer cracks and points of local bond failure even at maximum load, see Figure 4.15. As seen in Figure 4.14, the average strain values for the prisms are within the 6 % range, whilst the plain ϕ10 reinforcement bar average reaches just under 8 %. This difference in strain demonstrates the effects of the surrounding concrete and its contribution to the overall stiffness of the prisms.

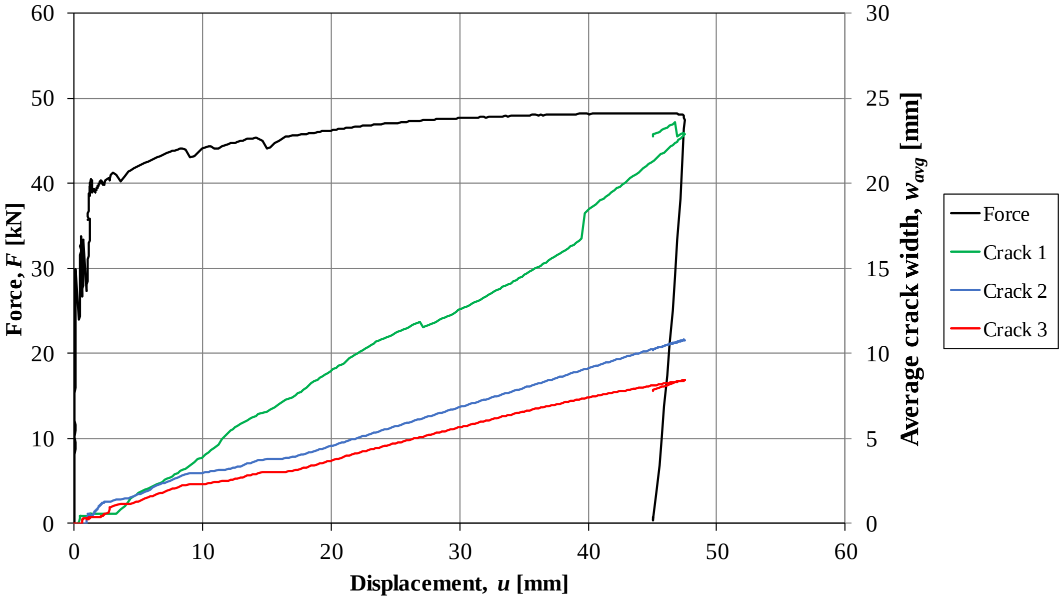

Figure 4.16 Average crack widths and crack development as a function of total displacement and applied force in prism ϕ10-3.

Prisms containing ϕ10 reinforcement without PVC developed only two or three cracks before reaching the stabilized cracking stage. The results are somewhat scattered as crack data loss occurred in several of these prisms. However, Figure 4.16 is used as an adequate representation of the ϕ10 prism crack behavior, see Appendix C.7 for crack widths in all ϕ10 prisms. Average crack widths are varying with crack development occurring simultaneously, i.e. in the early stages of loading.

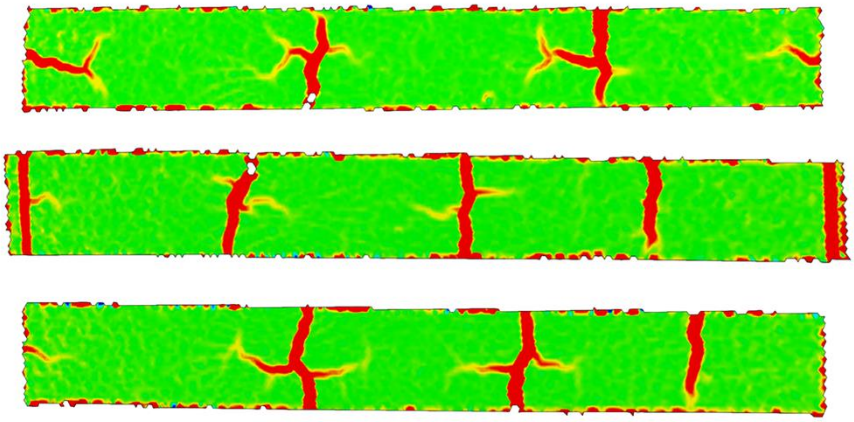

Figure 4.17 Strain fields for ϕ10 prisms.

4.2.3 ϕ12 Prisms with PVC

4.2.3.1 4x50 mm PVC

Results for prisms with PVC configurations are presented in the same manner as prisms without PVC. However, these prisms are compared to both the prisms without PVC and the average curve from material testing. Figure 4.18 is an example of how these results are presented in a comparative fashion. This diagram structure is continued in the following subchapters and allows for easier visualization of test results.

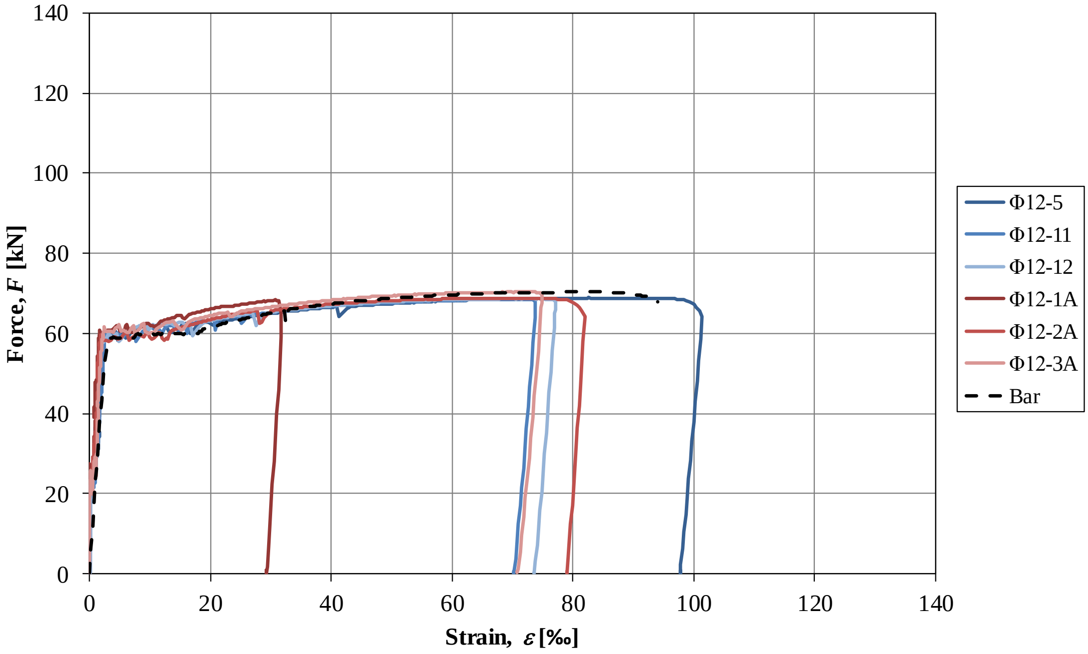

Figure 4.18 Results from ϕ12 prisms without PVC, prisms with 4x50 mm PVC, and the average ϕ12 material testing results (Bar). Specimen ϕ12-1A was subjected to premature unloading, see Figure C.2 in Appendix C.

Average crack widths for the prisms with 4x50 mm are somewhat skewed. The first of these prisms tested, prism ϕ12-1A, prematurely unloaded which resulted in incomplete test results. The second, prism ϕ12-2A lost a significant amount of data in GOM which is clearly seen by steep drops in average crack widths, see Appendix Appendix C.4. The final of these three prisms was successful and showed crack development in the early stages of loading and rather consolidated average crack widths, see Figure 4.19 and Figure 4.20.

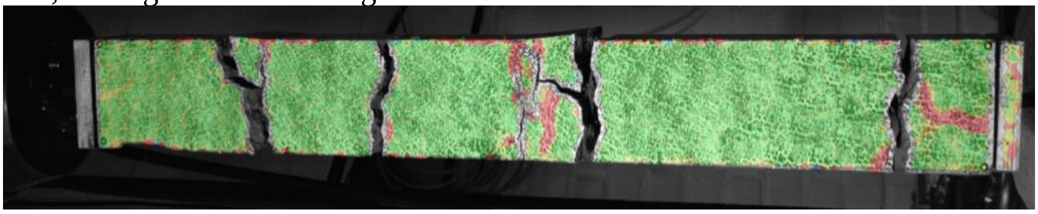

Figure 4.19 Similar crack widths seen in prism ϕ12-3A at maximum load.

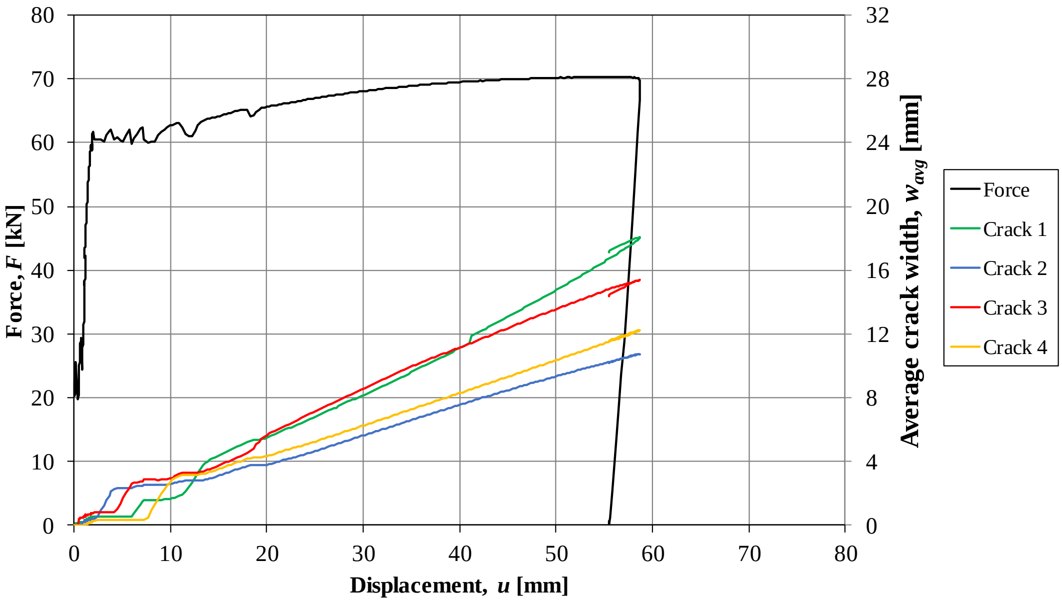

Figure 4.20 Average crack widths and crack development as a function of total displacement and force in prism ϕ12-3A.

The predicted effects of the PVC tubing on the prisms were primarily greater total displacements and therefore greater plastic deformation capacity. PVC tubing surrounding the reinforcement bars would theoretically inhibit the concrete from bonding to the steel in those regions. Reducing the bond stress at these points should inevitably lead to additional cracks and higher strains should be achieved.

However, the behavior of the 4x50 PVC prisms seem to have a different response than expected. The same or fewer cracks were generally obtained but lower displacement values were the result. Comparing ϕ12 prisms without PVC tubing to the ϕ12 prisms with the 4x50 configuration shows the difference in total displacement. For example, prism ϕ12-2A (4x50) resulted in a total displacement of ~63 mm whilst prism ϕ12-5 (no PVC) resulted in a total displacement of nearly 80 mm. Additionally, prism ϕ12-5 developed five cracks in the stabilized cracking stage, whilst prism ϕ12-2A only reached four cracks. Consequently, the PVC configuration had inverse effects in this case and was disadvantageous regarding total displacement, average strain, and crack development.

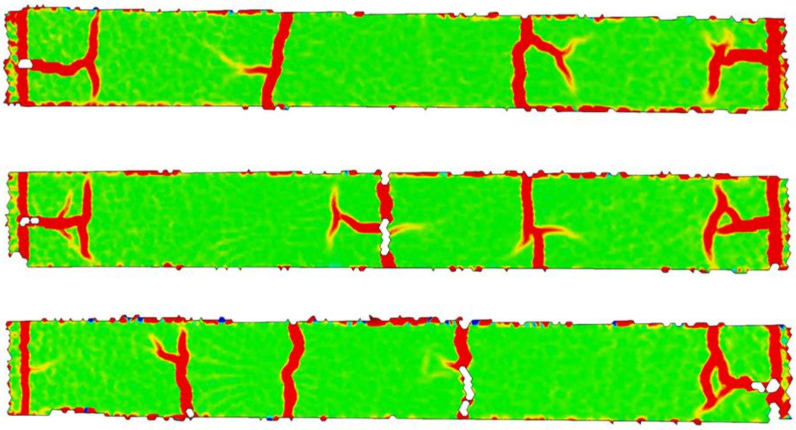

Figure 4.21 Strain fields for ϕ12 prisms with 4x50 mm PVC. Note the reduced number of cracks due to the PVC.

4.2.3.2 8x50 mm PVC

With an even higher volume and frequency of PVC tubing segments, the 8x50 configuration was predicted to result in higher strains. However, the inverse effect of the PVC tubing is displayed with this configuration as well, see Figure 4.22.

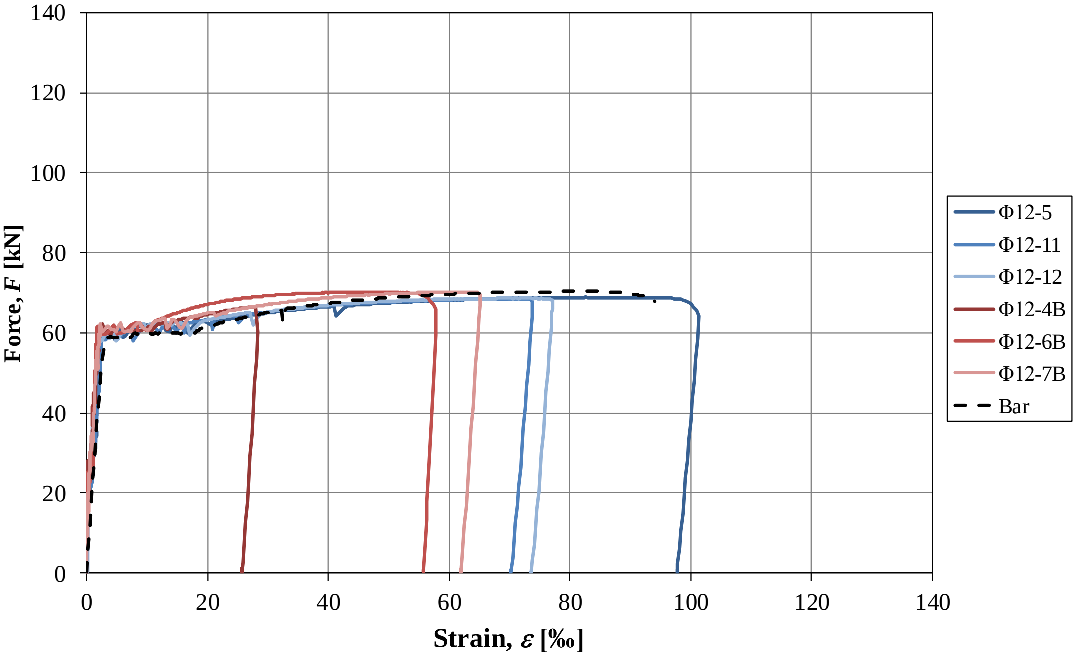

Figure 4.22 Results from ϕ12 prisms without PVC, prisms with 8x50 mm PVC, and the average ϕ12 material testing results (Bar).

Average strains of nearly 8 % are achieved in some ϕ12 prisms without PVC. Therefore, with an 8x50 PVC configuration, strains were predicted to be greater in these prisms. This was not the case as the prisms with eight segments of PVC resulted in strains reaching the 4-6 % region, or around 2 % lower in average strain than the prisms without PVC. An outlier (prism ϕ12-4B) only reached a final strain of ~2.5 % due to premature unloading. This trend displays that the greater the volume of PVC, the lower the strains and total displacement.

A distinct difference in crack development is seen in prisms containing 8x50 mm PVC, see Figure 4.25. Unfortunately, one of three prisms, prism ϕ12-4B, prematurely unloaded resulting in incomplete data. However, the remaining two, prism ϕ12-6B and prism ϕ12-7B, showed similar results with only three cracks in the stabilized cracking stage and a wide range of average crack widths, see Figure 4.23 and Figure 4.24.

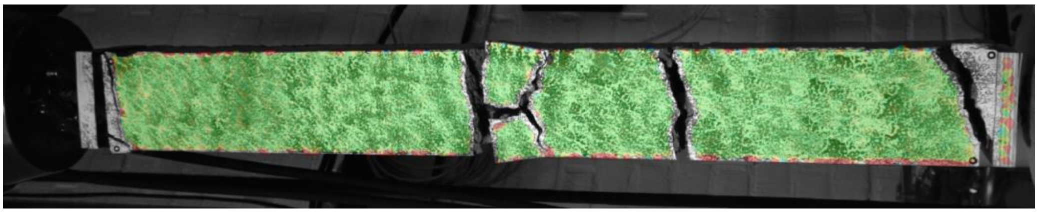

Figure 4.23 Prism ϕ12-7B at maximum load. Notice only three cracks developed with an uncracked span of ~0.35 m even at maximum load.

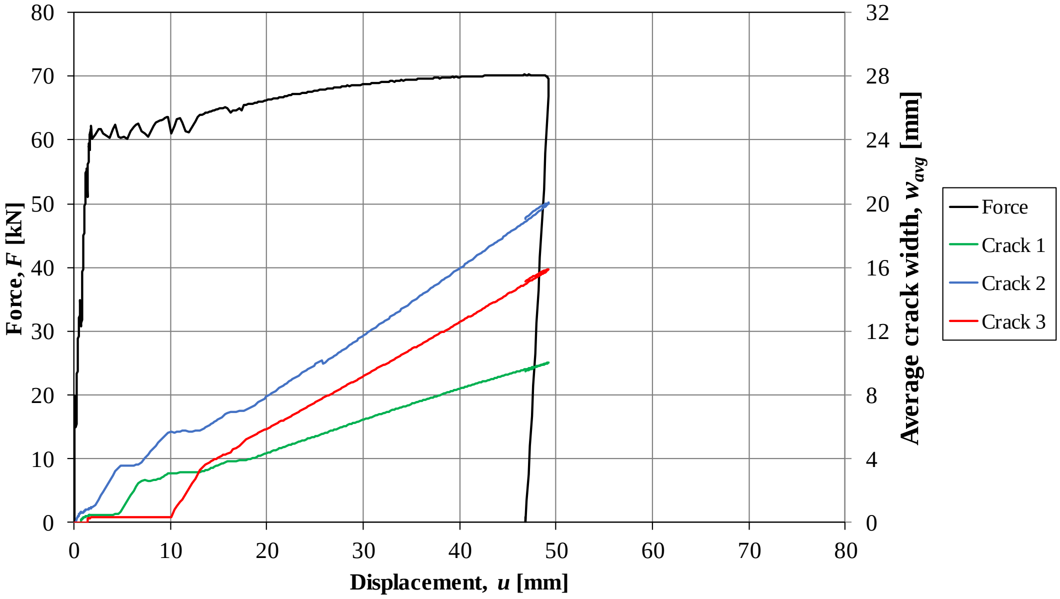

Figure 4.24 Average crack widths and crack development as a function of total displacement and applied force in prism ϕ12-7B.

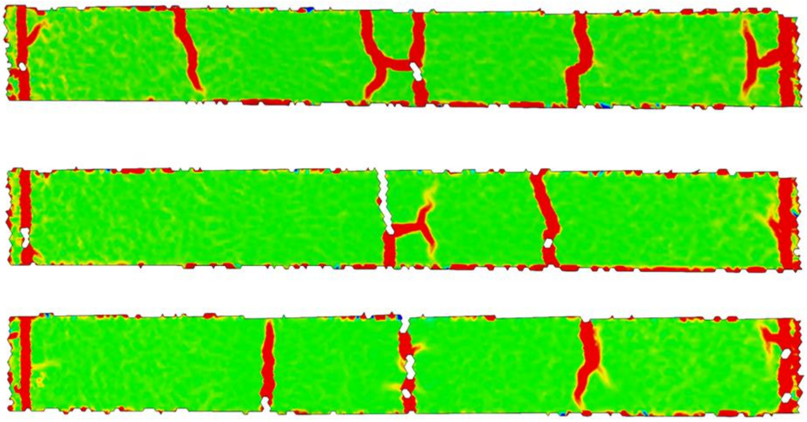

Figure 4.25 *Strain fields for ϕ12 prisms with 8x50 mm PVC. Note the reduced number of cracks due to the PVC.*

4.2.3.3 4x100 mm PVC

Lastly, prisms with a total of 400 mm of PVC tubing resulted in the fewest number of cracks in the stabilized cracking stage, and even near failure, see Figure 4.27. The lack of cracking was consistent throughout all 4x100 mm prisms and resulted in lower total displacement and strain, which is clearly seen in both the 3D strain fields and displacement graphs, see Figure 4.29.

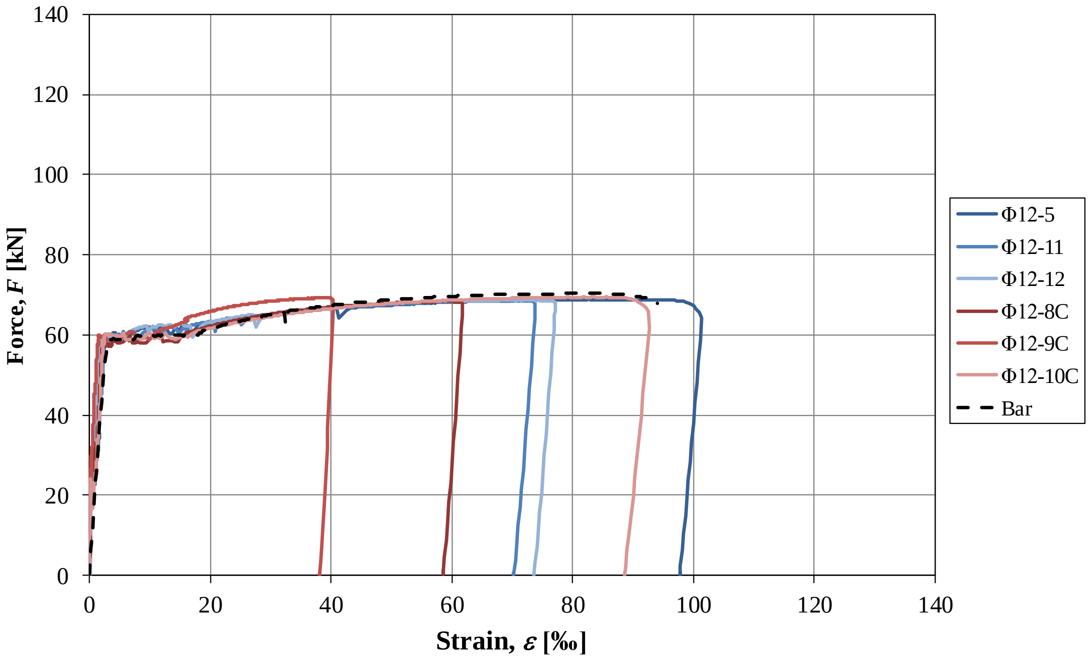

Figure 4.26 *Results from ϕ12 prisms without PVC, prisms with 4x100 mm PVC, and the average ϕ12 material testing results (Bar).*

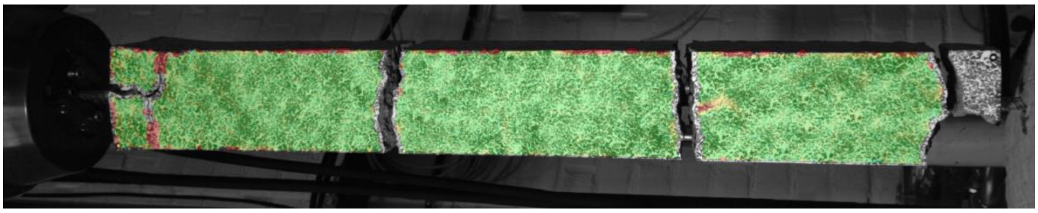

Figure 4.27 Fewer total cracks at maximum load due to the 4x100 mm PVC configuration in prism ϕ12-10C.

Strain in these prisms vary greatly compared to other prism configurations with a lower strain of just below 4 % in prism ϕ12-8C and an outlier with over 8 % in prism ϕ12-10C, see Figure 4.26. Ultimately, the lack of cracking in the 4x100 mm PVC prisms was expected, but lower average strains were obtained.

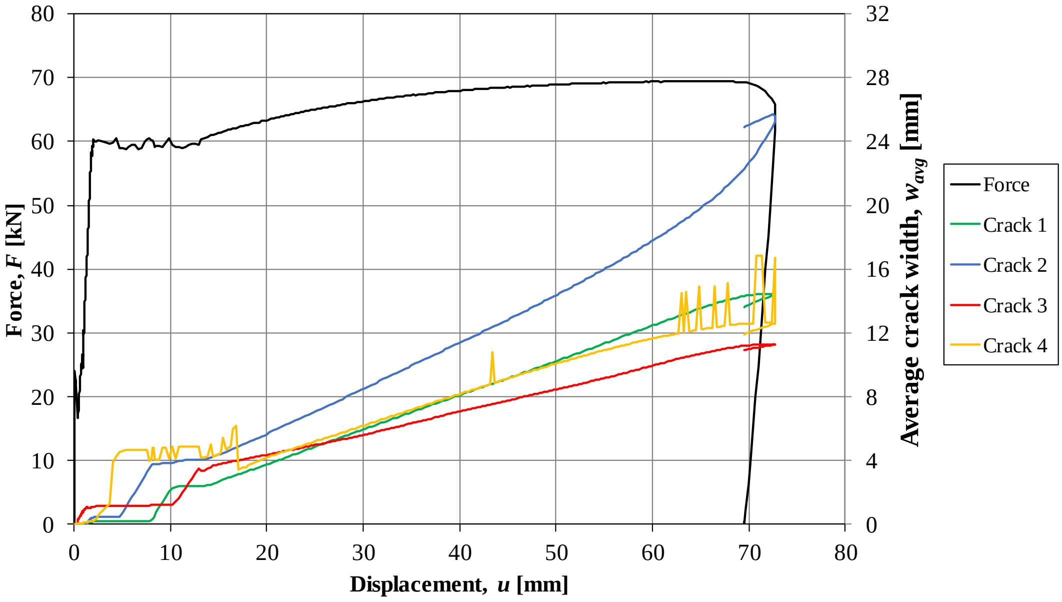

Figure 4.28 Average crack widths and crack development as a function of total displacement and applied force in prism ϕ12-10C.

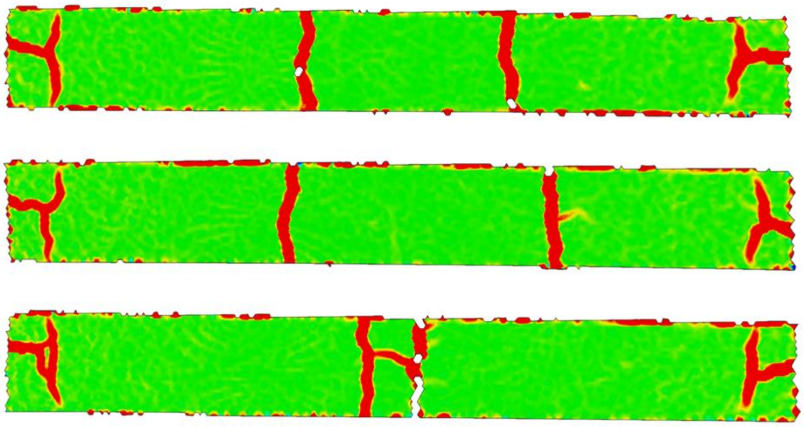

Figure 4.29 Strain fields for ϕ12 prisms with 4x100 mm PVC. Note the consistent number of total cracks and fewer spalling cracks.

Prisms with the 4x100 mm PVC configuration all resulted in four cracks in the stabilized cracking stage, but these cracks accounted for nearly all the total displacement in the prism. Small peaks in average crack width are indications of data loss with immediate recovery. The DIC pattern changes throughout testing and GOM detects these changes in pattern, but, at times, may lose some of this data. The results in Figure 4.28 clearly show the local data losses, but these effects didn’t result in an unsuccessful test in this case.

4.3 Comparison of the results

The effects of the PVC tubing on the reinforcement strain were clearly seen in the results but were not as predicted. Lower strains were achieved due to the PVC tubing and the greater the PVC volume the lower the resulting strains. However, results were somewhat scattered with some outliers reaching strains close to the average strain of a single reinforcement bar, see Figure 4.30.

In addition, premature unloading affected two prisms which were deemed unsuccessful and incomplete tests, further details on premature unloading are found in Appendix C.1. Crack development and average crack widths were affected by the decreased bond stress, but predictions were also proven to be somewhat wrong. The volume of PVC used is directly related to the number of cracks, with less cracks arising with greater volumes of PVC.

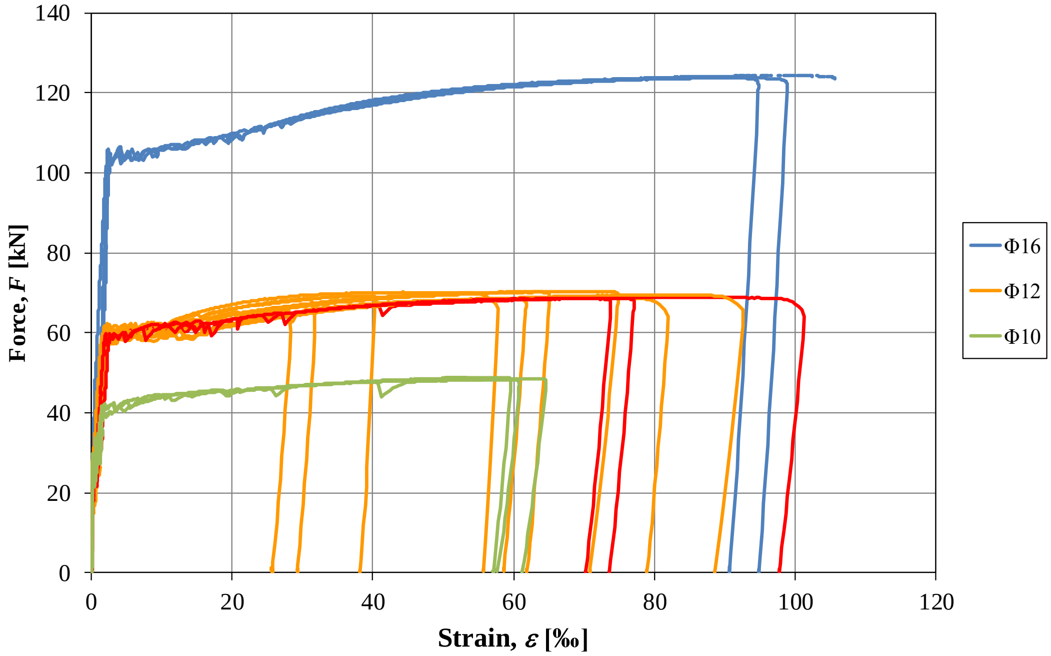

Figure 4.30 Results for all reinforced concrete prisms. Red curves represent ϕ12 prisms without PVC and orange curves represent ϕ12 prisms with PVC.

The lack of surrounding concrete in the prisms may have bottlenecked the potential influence of the PVC tubing. For example, spalling cracks and overall failure of interaction between the reinforcement and surrounding concrete took place in the prisms but may not occur in the same way in beams due to uneven concrete covers available above and below the reinforcement. Furthermore, a single centrally placed reinforcement bar is not used in practice. Large-scale beams may consist of reinforcement configurations with multiple reinforcement bars per layer, or even multiple layers of bars. A complex reinforcement configuration may lead to varying results due to a more complex response compared to prisms. Such factors may be a reason why larger strains than expected were achieved in the prisms than those previously observed in tests on beams.

Compiling the experiment data for all prisms allows for a comparison and analysis of the results. Each prism's total number of cracks in the stabilized cracking stage along with crack width and deformation results are presented in Table 4.4. The total crack width w_{tot} is used as a comparison to the total prism displacement, u_{tot}. The difference between these measurements indicates the effects of the PVC tubing and the influence of the cracks on the prism deformation. In addition, a ratio between w_{tot} and u_{tot} is presented to compare the prisms' behavior. Each prism had varying results and varying degrees of data loss in GOM Correlate which resulted in some skewed results.

Table 4.4 Compiled crack data for all prisms. Note that [-] indicates missing information due to data loss in GOM Correlate.

Prism [-]	**Cracks [#]**	**Max Width [mm]**	**Mean Width [mm]**	**Min Width [mm]**	w_{tot} **[mm]**	u_{tot} **[mm]**	w_{tot}/u_{tot} **[-]**
ϕ16-1	5	16.8	13.4	11.8	66.8	81.3	0.82
ϕ16-2	4	23.8	17.6	13.2	63.7	77.5	0.82
ϕ16-3	3	14.6	13.6	11.7	40.9	72.5	0.56
ϕ12-1A	4	8.1	5.6	2.8	22.5	25.0	0.9
ϕ12-2A	4	17.7	10.8	6.0	39.5	64.0	0.62
ϕ12-3A	4	18.1	14.1	10.7	56.4	58.7	0.96
ϕ12-4B	5	5.9	4.3	1.9	-	22.3	-
ϕ12-5	5	24.2	14.8	7.2	61.4	78.6	0.78
ϕ12-6B	3	22.8	15.3	6.9	-	44.3	-
ϕ12-7B	3	20.0	15.3	10.0	45.9	49.2	0.93
ϕ12-8C	4	15.3	10.5	1.1	41.1	44.8	0.92
ϕ12-9C	4	15.3	11.7	2.3	-	29.8	-
ϕ12-10C	4	16.8	17.1	11.3	67.6	72.8	0.93
ϕ12-11	4	14.8	10.5	7.8	41.2	58.0	0.71
ϕ12-12	5	16.1	10.3	2.7	46.4	60.6	0.77
ϕ10-1	2	23.7	16.5	9.4	31.3	47.0	0.67
ϕ10-2	3	23.6	14.3	8.4	42.5	47.5	0.89
ϕ10-3	3	20.0	13.6	7.5	37.5	50.4	0.74

With the results in Table 4.4, a conclusion can be made that total crack widths accounted for the majority of the total deformation in prisms with high volumes of PVC tubing. For example, prisms ϕ12-8C and ϕ12-10C resulted in total crack widths that accounted for over 90 % of the total deformation. Although these prisms resulted in the fewest number of cracks, these cracks accounted for most of the deformation.

In addition to crack and deformation data, the average strain can be calculated for each prism. This comparison and presentation of results focuses on the aim of this thesis and is seen in Figure 4.31. The average strain for each prism is plotted alongside the average strain in a single reinforcement bar of the same diameter (Bar). This allows for a clearer analysis between prisms, but also shows the distinct differences in average strain between reinforcement bar diameters. Comparing average strains in this way continues to show the inverse effect of the PVC tubing.

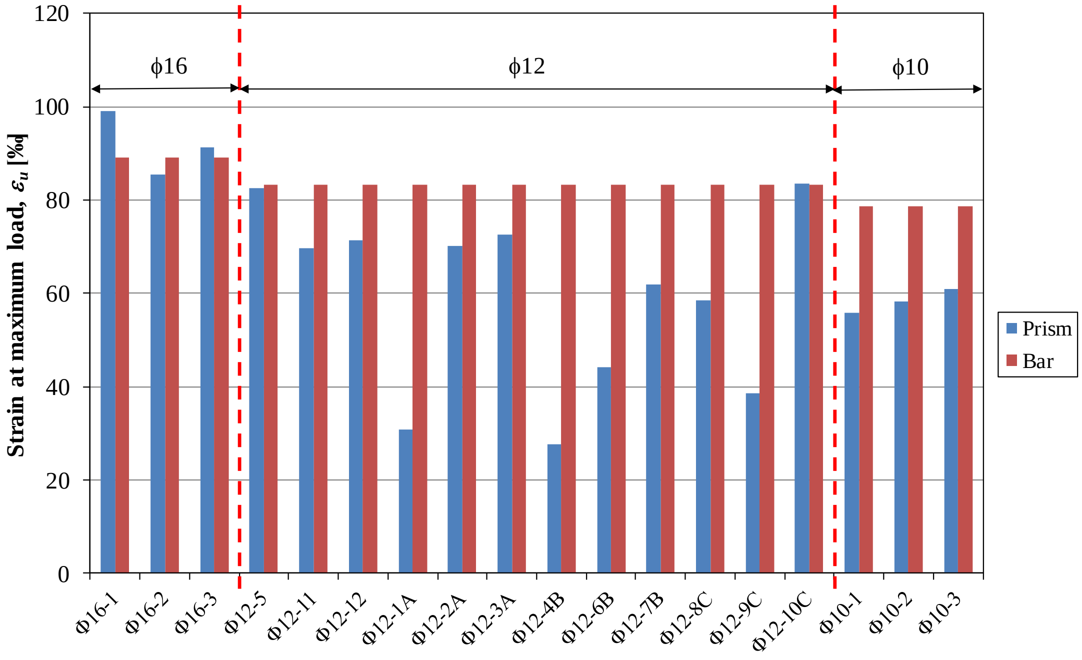

Figure 4.31 Average strain in prisms at maximum load.

Furthermore, with the average strain data for each prism and respective reinforcement, a ratio between the two can be calculated see Figure 4.32. Lower ratios indicate the inverse effects of the PVC tubing and can be compared to the relatively high ratio for the ϕ12 prisms without PVC. In addition, a ratio greater than one indicates that the average strain in prisms was greater than the average strain in the reinforcement bars. This was seen in ϕ16 prisms due to the lack of interaction between materials.

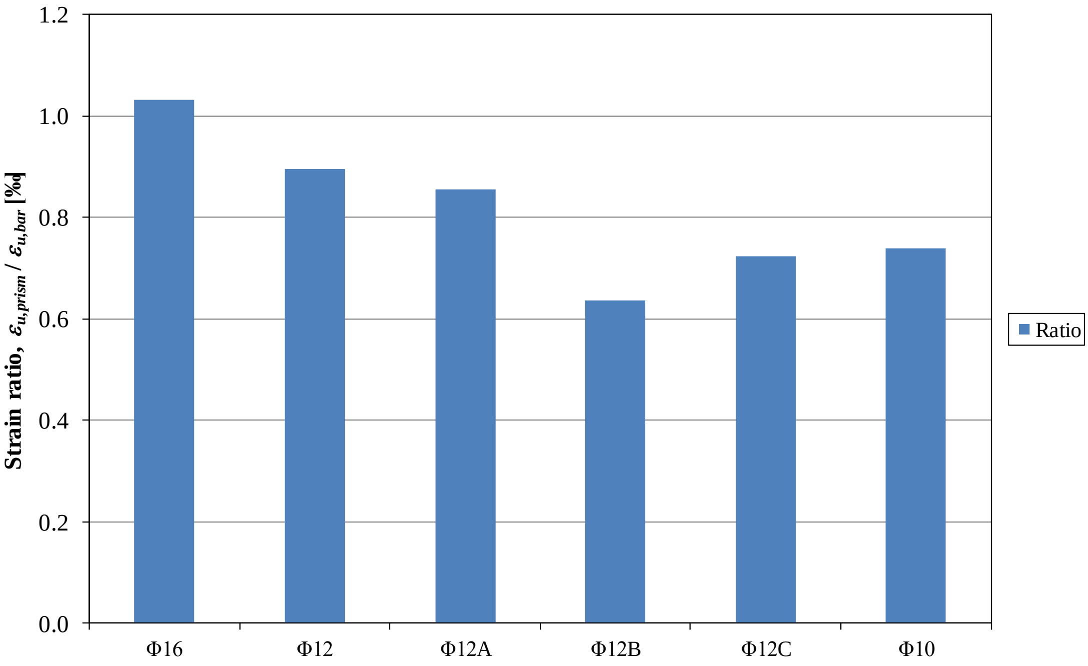

Figure 4.32 Ratio of average strain in prisms compared to reinforcement bars.

The length of the PVC and the spacing between segments may have contributed to these disadvantageous effects. For example, prisms with the 4x50 mm configuration resulted in more cracking than 8x50 mm or 4x100 mm and may be a better configuration regarding crack development. Additionally, the 8x50 mm configured prisms resulted in even fewer cracks than the prisms with 4x100 mm PVC indicating that the spacing and PVC volume plays a significant role in the number of cracks developed. A continuation of this study could be conducted with a few altered parameters. Conflicts with premature unloading took place due to the configuration and programming of the tensile testing machine, and the simplicity of studying reinforced concrete prisms, rather than beams, may be a poor representation of the effects PVC might have in a beam.

5 Conclusions

This study investigated the parameters that affect reinforcement strain in reinforced concrete structures loaded until failure. In total, eighteen reinforced concrete prisms with centrally placed reinforcement bars were constructed, tested, and analyzed. Measurements and calculations were conducted using DIC technology to determine individual crack widths and prism deformation. Results were compiled using GOM Correlate and Microsoft Excel and then analyzed to study the effects of altered parameters on reinforcement strain. Varying reinforcement bar diameters was an altered parameter that led to discrepancies in reinforcement strain. In addition, configurations of PVC tubing around the reinforcement in various prisms were an additional parameter that inevitably resulted in differences in reinforcement strain.

5.1 Summary of results

First, prisms without PVC, but with varying reinforcement diameters (ϕ16, ϕ12, ϕ10) resulted in differences in average strain. Increased reinforcement diameters displayed less interaction at failure between the reinforcement bar and the surrounding concrete, and hence, displayed increased average reinforcement strain. This trend was consistent and seen throughout the reinforcement bar diameters with the most interaction in prisms with ϕ10 and the least interaction in prisms with ϕ16. Additionally, the effects of tension stiffening were clearly seen in these results when prisms were compared to a plain reinforcement bar.

Second, the average strain in the reinforced concrete prisms was negatively affected by the addition of PVC tubing. Initial predictions concluded that PVC tubing would reduce the bond between the materials and therefore lead to sections of reduced bond stress. By reducing the bond stress along the reinforcement bar, fewer cracks should develop resulting in higher average reinforcement strain. The total displacement for prisms with PVC tubing were expected to be greater than those without PVC due to the increase in average strain. Consequently, this increase in average strain and overall displacement should be advantageous regarding the prisms' rotational and plastic deformation capacity.

However, testing of the reinforced concrete prisms presented that the PVC tubing has an inverse effect. The results indicated that the predictions were false, and that lower average strains and total displacements were achieved. Increasing the volume and segment length of PVC led to fewer cracks, but less deformation and this trend was consistent throughout each PVC configuration. Although the inverse results indicate that the tubing is not beneficial to the average reinforcement strain, a conclusion that this theory is false cannot be made. Reinforced concrete structures range vastly in configuration and design, and these results provide a better understanding of the internal mechanisms of structures, not overall behavior.

Moreover, crack widths and crack development were affected by the PVC tubing, meaning these regions of reduced bond stress did, in fact, affect the prisms. Prisms with highest volume of PVC tubing resulted in the fewest number of total cracks in the stabilized cracking stage and even at failure. These results were constant throughout all prisms with this configuration leading to the conclusion that the PVC tubing did affect crack development. Additionally, the spacing between and lengths of the PVC segments played a role in crack development.

Ultimately, these results create a foundation for further research within this realm as impulse loads and plastic deformation capacity are of ever-growing interest. Analyzing prisms provides insight into the internal mechanisms at play in larger reinforced concrete structures. For example, static testing results presented in this study can be used as input data in further studies. Dynamic loading calculations require some form of static testing results and the prisms in this case are a prime example of this input data. Lastly, improvements in further studies can be made such as reprogramming of the MTS tensile testing machine to ensure correct unloading, and the use of reinforced concrete beams rather than prisms.

5.2 Future research

Reconfiguration of the MTS 793 tensile testing machine would ensure that each prism reaches near-failure before unloading. As seen in the results, the development of a new crack or dislodgment of a concrete piece resulted in a drop in applied load signaling the machine to halt loading. An indication of 2 % load loss was disadvantageous in this case and would require a different unloading signal. Reprogramming station manager would allow for these processes to take place without unloading prematurely. For example, manually commanding the unloading of the prisms based on the expected maximum load would be a better solution to ensure the correct test results even with the development of a new crack. This test setup would require some human intervention and observation during testing, rather than an automatic test in which loading and unloading are automatic. Ultimately, taking premature unloading into consideration and avoiding this mishap would result in more accurate tests and a better understanding of the results.

The research and results of this thesis are representative for reinforced concrete prisms. The simplicity of reinforced concrete prisms may have inhibited these results from being applicable to larger and more practical structures, such as reinforced concrete beams. One centrally placed reinforcement bar fails to represent full-scale reinforced concrete structures used in modern civil engineering. Furthermore, the simplicity of using prisms led to easier construction of forms, casting, and testing. Testing of the prisms was manageable as each prism was light enough to handle and lift in and out of the testing machine. Full-scale beams with complex reinforcement cages would display the effects of PVC tubing on the beam performance but would lead to a more complex test configuration. The effects of the PVC on different forms of reinforcement, such as stirrups, was not studied in this project and may lead to the predicted results. Additionally, implementation of different reinforcement percentages could also be of interest in further studies.

In conclusion, ensuring proper unloading and using larger reinforced concrete structures would give better insight into the effects of altered reinforcement parameters. Premature unloading took place which led to incomplete data and results for two prisms. The limitations in this thesis allowed for simpler and more efficient testing but may have led to nonapplicable results. However, the results are still of importance and can be used in further studies.

6 References

Al-Emrani, M., Engström B., Johansson, M., Johansson, P. (2013). *Bärande konstruktioner: Del 1*. Gothenburg: Chalmers University of Technology

Al-Emrani, M., Engström B., Johansson, M., Johansson, P. (2011). *Bärande konstruktioner: Del 2*. Gothenburg: Chalmers University of Technology

Allam, S., Shoukry, M., Rashad, G., Hassan A. (2012) *Evaluation of tension stiffening effect on the crack width calculation of flexural RC members*. Structural Eng. Dept., Faculty of Engineering, Alexandria University, Alexandria, Egypt

Ansell A. och Svedbjörk G. (2000): *Statisk provning av fritt upplagda plattstrimlor av betong med armering av varierande seghet.* Avdelningen för Betongbyggnad, Kungliga Tekniska Högskolan, Teknisk rapport 2000:16, Stockholm, 50 sid.

Ansell A., Svedbjörk G. (2003a): *Kompletterande dynamisk provning av kontinuerliga plattstrimlor av betong med armering av varierande seghet.* Avdelningen för Betongbyggnad, Kungliga Tekniska Högskolan, Teknisk rapport 2003:3, Stockholm, 51 sid.

Ansell A., Svedbjörk G. (2005): *Statisk provning av fritt upplagda plattstrimlor med varierande tvärsnittsareor.* Avdelningen för Betongbyggnad, Kungliga Tekniska Högskolan, Teknisk rapport 2005:6, Stockholm, 58 sid.

CEN. (2005). SS-EN 1992-1-1:2005: *Design of concrete structures – Part 1-1: General rules and rules for buildings.* European committee of Standardization.

-(2009b). SS-EN 12390-3:2009: *Testing hardened concrete – Part 3: Compressive strength of test specimens.* European Committee of Standardization.

-(2009c). SS-EN 12390-6:2009: *Testing hardened concrete – Part 6: Tensile splitting strength of test specimens.* European Committee of Standardization.

-(2012). SS-EN 12390-1:2012: *Testing hardened concrete – Part 1: Shape, dimension and other requirements for specimens and moulds.* European Committee of Standardization.

El-Tawil, S. (2016) *Characterization of Catenary Action*. University of Michigan, College of Engineering, Civil & Environmental Engineering

Fortifikationsförvaltningen, (1973b). *Provisoriska anvisningar för dimensionering av armerade betongkonstruktioner som skydd mot verkan av konventionella vapen inom närmissområde – Kommenarer. (Preliminary instructions for the design of reinforced concrete structures as protection against the effect of conventional weapons – Comments. In Swedish.)* Fortifikationsförvaltningen, Befästningsavdelningen, Publ nr 25:2 Bk/1973, Stockholm.

Fortifikationsverket, (2011). *FortSkydd. Bilaga till Fortifikationsverkets Konstruktionsregler FKR 2011*. Dnr 4535/2011, Försvarsmakten

GOM. (2018). *GOM Correlate Professional* (Version 2018 hotfix 5) [Computer software]. Retrieved from https://www.gom.com/3d-software/gom-correlate-professional.html

Johansson, M., Laine, L. (2012). *Bebyggelsens motståndsförmåga mot extrem dynamisk belastning, Del 3 – Kapacitet hos byggnader. (The resistance of housing settlement subjected to extreme dynamic loading. Part 3: Building capacity. In Swedish.)* Myndigheten för samhällsskydd och beredskap (Swedish Civil Contingencies Agency), Publ. No MSB 142, Karlstad.

Jönsson, J., Stenseke, A. (2018). *Concrete Beams Subjected to Repeated Drop-Weight Impact and Static Load: Assessment of structural response in experimental testing and predicted response with numerical analyses* (Master's thesis, Chalmers University of Technology, Institution of Architecture and Civil Engineering)

Plos M., Johansson M., Zandi K., Shu J. (2020). *Recommendations for Assessment of Reinforced Concrete Slabs – Enhanced structural analysis with the finite element method.* Division of Structural Engineering, Chalmers University of Technology, Göteborg.

Rahimah, M., M.S. M., Deric J., Griffith M. (2016) *The Tension Stiffening Mechanism in Reinforced Concrete Prisms.* School of Civil, Environmental and Mining Engineering, University of Adelaide

Appendix A Experiment Preparation

Appendix A provides a description and documentation of the construction and preparation of the reinforced concrete prisms used in this experiment. Materials and material testing descriptions are also presented.

A.1 Preparation of prisms

A.1.1 Construction of forms

Existing forms from previous experiments were used to cast the 18 prisms. These forms were configured for prisms with a length of 1000 mm, which led to some necessary modifications. Holes for the reinforcement bars in the end blocks of the forms were drilled and shaped using a drill press, and then later screwed back into the forms with the new length of 800 mm between them, see Figure A.1.

Due to the previous experiments, the forms lacked the homogenous surface desired for DIC preparation, so excess dried concrete was removed. After removal of excess concrete, the forms were oiled and cleaned prior to casting to ensure proper demolding.

A.1.2 Reinforcement configuration

To acquire the centrally placed reinforcement bars, the ends of the forms supported the reinforcement bar during casting. Segments of steel reinforcement were cut using a rebar cutter, and later inserted through the holes in the forms, see Figure A.3. The ends of the reinforcement bars were marked using paint markers to detect any reinforcement movement during the casting process.

To reduce the bond between the reinforcement bars and the surrounding concrete, segments of low-friction PVC tubing were used along the bars. To fasten segments of PVC to the reinforcement bars, industrial hot glue was used to bond the tubing to the reinforcement. The importance of this step was to guarantee that no concrete would seep into the cavity between the tubing and reinforcement.

As the reinforcement bar diameters range from 10 – 16 mm and due to short prism lengths, no supportive wires were needed to prevent sagging of the reinforcement. Sagging is undesired as it could lead to an additional moment during tensile loading.

A.1.3 Reinforcement Material Testing

Steel reinforcement is a key component of this thesis and the average strain results in reinforced concrete prisms. This subchapter discusses the material testing process of steel reinforcement bars.

Segments of reinforcement bar were placed vertically in a tensile testing machine and subjected to tensile loading until rupture. The calculated strains are based on an initial length and the subsequent changes in length. In this case, steel reinforcement segments were cut with initial lengths of 420 mm, with 400 mm between the grasping points on the tensile machine. Six segments were cut for each reinforcement bar diameter, i.e. six ϕ16, six ϕ12, and six ϕ10. Loading of the bars was displacement controlled using two phases. Phase one had a determined speed of 0.5 mm/min and was applied up to the yielding point. Past yielding, phase two was initialized with a determined speed of 10 mm/min and was applied until bar rupture. With these two phases, station manager, and an external extensometer, force data and deformations were recorded.

A.1.4 Concrete casting

One batch of concrete was needed to cast the 18 prisms and six material testing cubes and was mixed in the concrete lab. Materials and ingredients were weighed and calculated and then mixed in a concrete mixer, see Appendix A for the concrete mixing process. A vibrator was used to eliminate the risk for air in the forms, and concrete cubes were submerged in water shortly after casting until test day. The recipe presented in Table A.1 was calculated in Microsoft Excel, and as some of the materials in the mix weren't dry, their moisture contents were taken into consideration.

Table A.1 Concrete recipe used for prisms and material testing cubes.

Material	Supplier	Amount [kg]
Byggcement CEM II/A-LL 42,5 R	Cementa	84.1
Sand 0/8 Sköllunga	Ucklums Grus	206.1
Aggregate 8/16 Vikan	Skanska	179.1
MasterGlenium	BASF	1
MasterSet R 401 Lent	BASF	0.3
Water	-	26.4

A.1.5 Concrete material testing

To properly study concrete structures and their behavior, material testing is necessary to determine the properties of a specific batch. Concrete material testing in this study was conducted via two tests- one to determine compressive strength and one to determine tensile strength.

These tests are commonly conducted using concrete cylinders, but in Sweden, concrete material testing is conducted using cubes. For this reason, concrete cubes were used, and therefore, results represent strengths in cube form. Standard dimensions in length, width, and height of the cubes are 150 mm. A conversion from strengths in cube form to strengths in cylindrical form is necessary according to Eurocode 2 CEN (2005).

A.1.6 Demolding and DIC Preparation

After a 28-day curing period, the prisms were ready to be demolded and prepared for testing. The DIC preparation was a crucial step in the preparation of the prisms. The DIC cameras and software require a high contrast and black speckle pattern to function as intended. For this reason, two of the smooth sides of each prism were painted white. A black speckle pattern was then applied to the surfaces of the prisms, after a tutorial on the meticulous technique by an expert from RISE (Research Institutes of Sweden). This application was done using a sea sponge and black paint, and the ideal pattern results in a surface with 50 % white and 50 % black paint, see Figure A.7. The DIC preparation resulted in some prisms having a better speckle pattern than other, but this variation did not affect the results.

Figure A.1 Construction of reinforced prism forms.

Figure A.2 Prism and material testing forms prepared for casting.

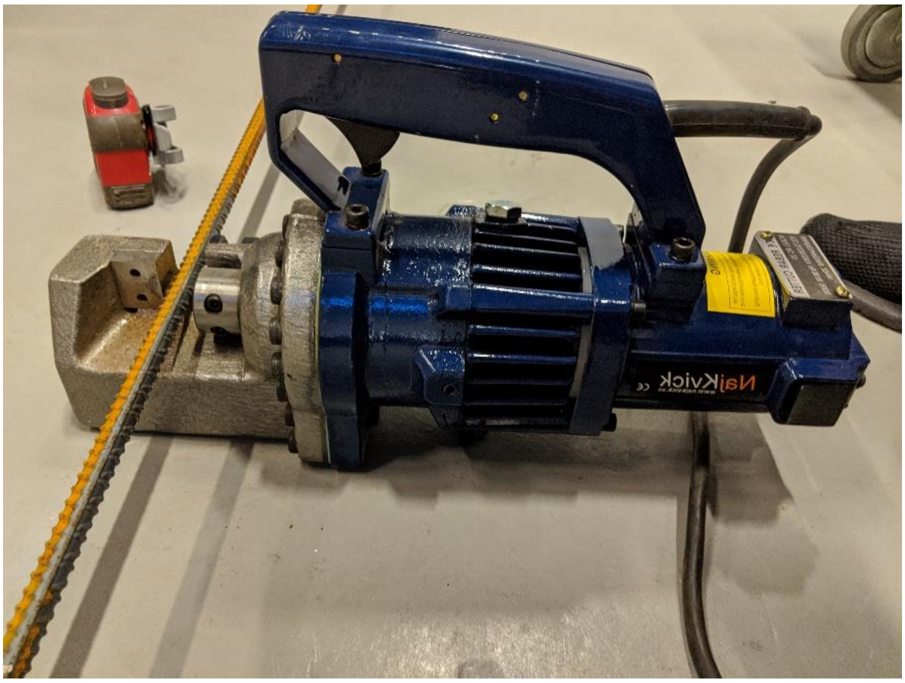

Figure A.3 Cutting of steel reinforcement for the prisms and material testing.

Figure A.4 Installation of three different PVC configurations- 4x50 mm (left), 8x50 mm (center), 4x100 mm (right). The bottom image displays a prism with 4x100 mm ready for casting from a top-down view. Note the spacing between PVC segments and from the wooden ends.

Figure A.5 Mixing of concrete batch on casting day.

Figure A.6 Casting of the reinforced concrete prisms.

Figure A.7 DIC preparation including application a white backdrop and a black speckle pattern.

Figure A.8 Example of the test set-up with cameras and the MTS 793 tensile machine.

Figure A.9 Segments of steel reinforcement for material testing.

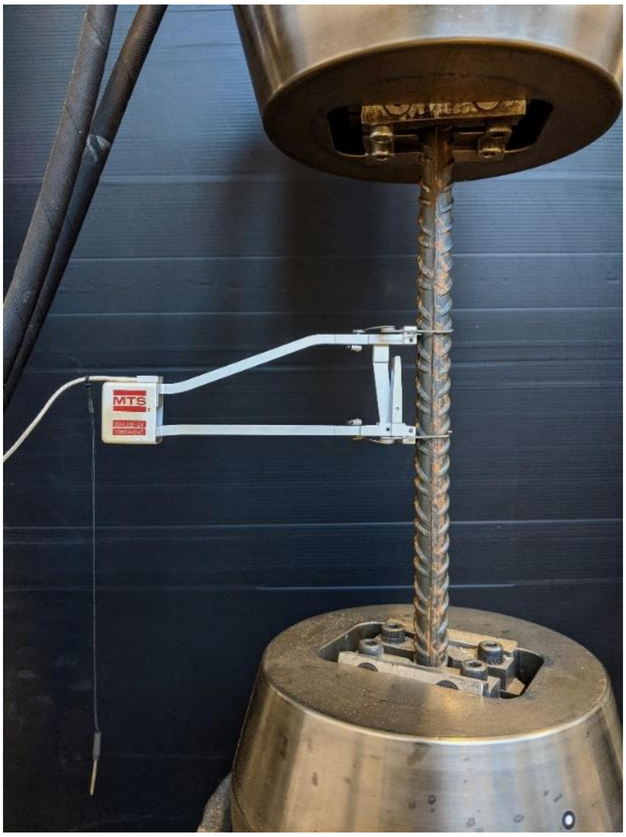

Figure A.10 Material testing steel reinforcement segments.

Figure A.11 Example of necking prior to failure in steel reinforcement.

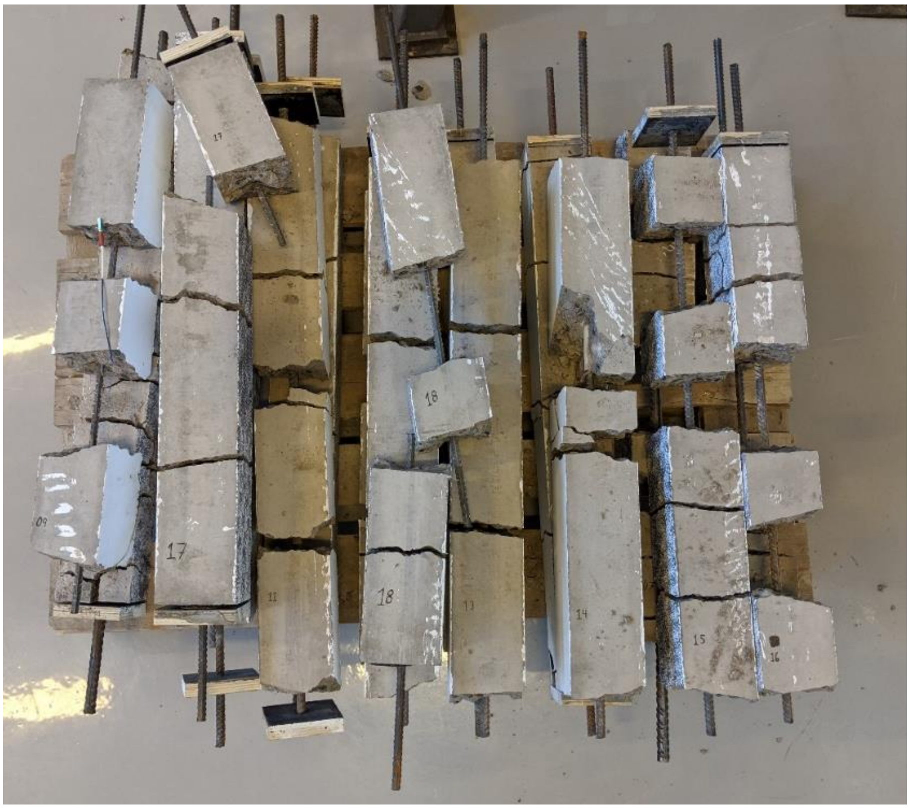

Figure A.12 Reinforced concrete prisms post-testing.

‘

Figure A.13 Split testing concrete cubes.

Appendix B Material Testing Results

B.1 Concrete properties

Concrete material properties were determined by means of concrete cube material testing. These tests for compressive and tensile strength were conducted on test day, i.e. after 28 days of curing.

Table B.1 Compressive and tensile strength results from concrete cube testing.

Cube [#]	**Test Type** [-]	**Strength $f_{c,cube}$, $f_{ct,sp}$** [MPa]	f_{ck} [MPa]	f_{cm} [MPa]	f_{ct} 1) [MPa]
1	Compression	58.6	38.9	46.9	3.44
2	Compression	58.5	38.8	46.8	3.44
3	Compression	59.7	39.8	47.8	3.50
4	Split	6.91			6.22
5	Split	6.93			6.24
6	Split	6.76			6.08

1) Calculation of *fct* based on characteristic compressive strength, see equation (2.3)

B.2 Steel reinforcement properties

Steel reinforcement properties were determined by static tests of six reinforcement bars per reinforcement diameter. Total, eighteen reinforcement bar segments were tested to determine the material properties of the steel.

Results from material testing of the steel reinforcement are presented in stress-strain curves. An average stress-strain curve for the six bars is also presented for each reinforcement diameter.

B.2.1 ϕ16 reinforcement

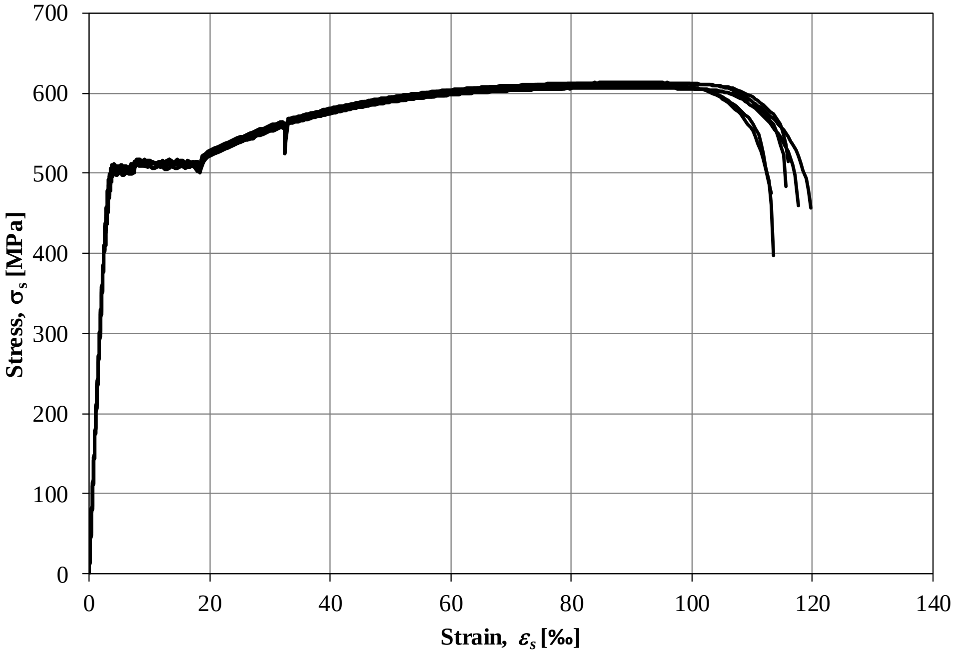

Figure B.1 *Stress-strain curve for six ϕ16 steel reinforcement bars.*

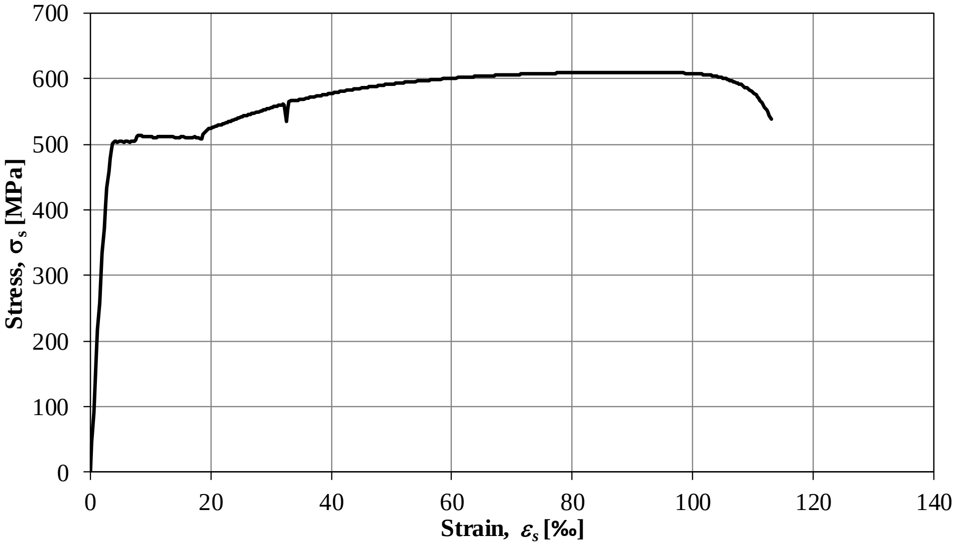

Figure B.2 *Average stress-strain curve for six ϕ16 bars.*

B.2.2 ϕ12 reinforcement

The wide range of results for the six ϕ12 reinforcement bars led to a somewhat skewed average. This average was then used as a comparison in the prisms results and is somewhat misrepresentative.

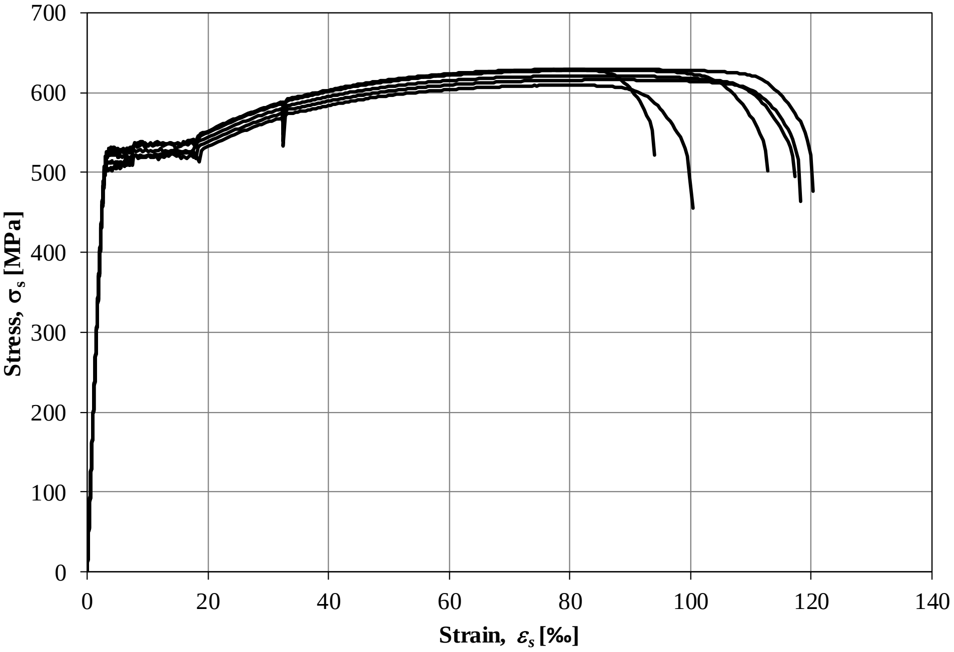

Figure B.3 Stress-strain curve for six ϕ12 steel reinforcement bars.

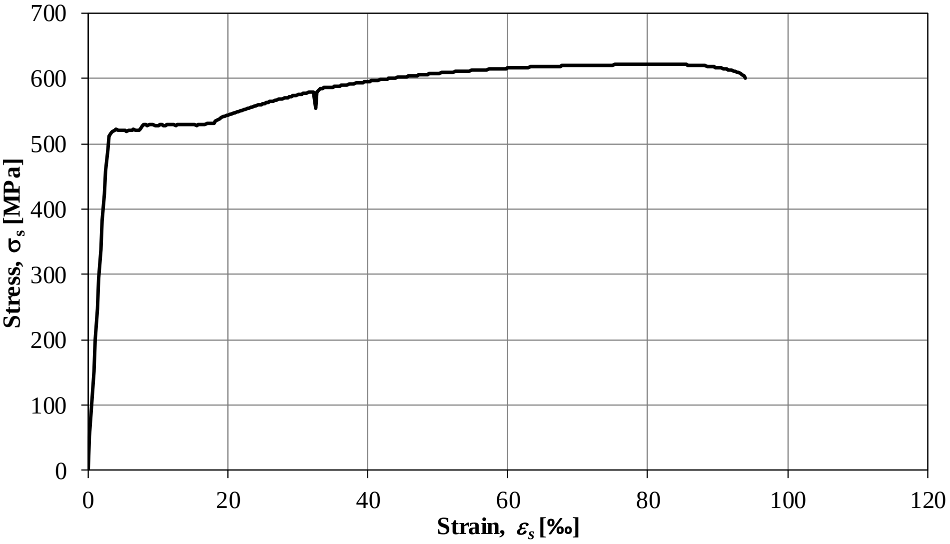

Figure B.4 Average stress-strain curve for six ϕ12 bars.

B.2.3 ϕ10 reinforcement

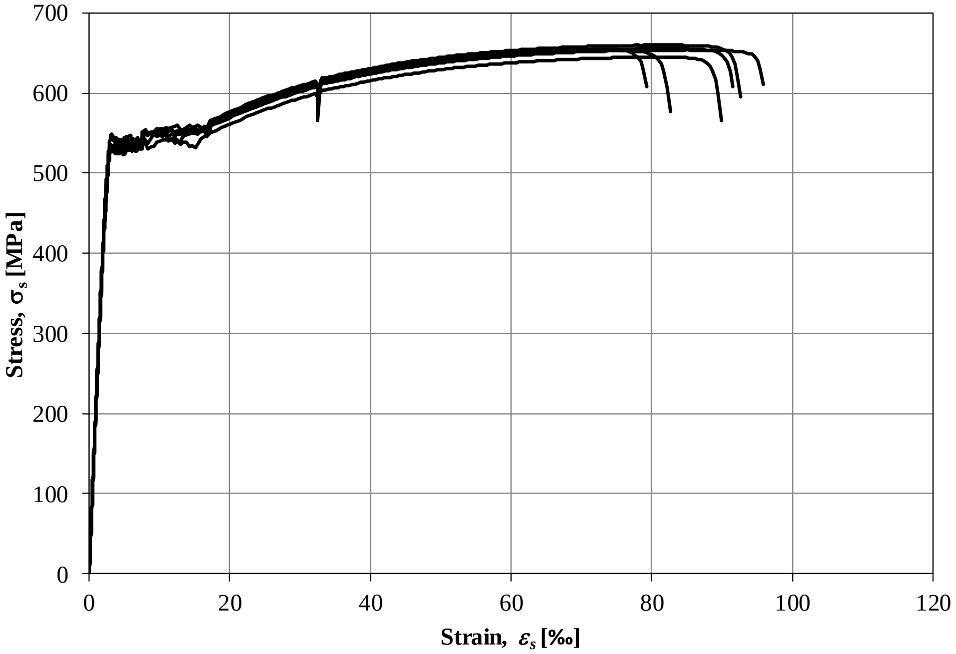

Figure B.5 Stress-strain curve for six ϕ10 steel reinforcement bars.

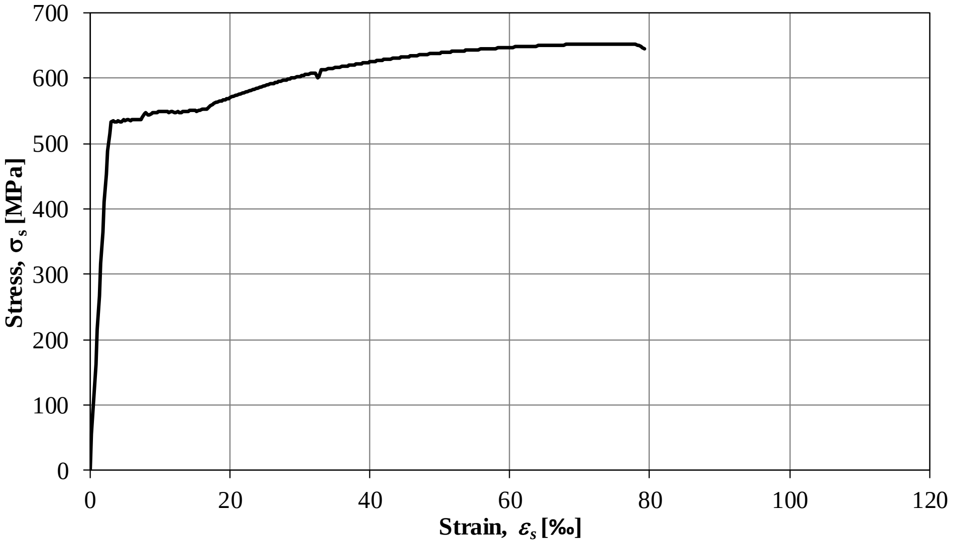

Figure B.6 Average stress-strain curve for six ϕ10 bars.

Appendix C Experiment Results

Results presented in this appendix provide force, average crack widths, number of cracks in the stabilized cracking stage, and total displacement for each prism. Each reinforced concrete prism has two figures: one presenting average crack widths for individual cracks, and one presenting total crack widths in relation to displacement.

C.1 Interpretation of results

Programmed to cease loading after an indication of a 2 % decrease in load, the MTS tensile testing machine may have led to lower strains than expected. For example, a hypothetically correct test would display a plateau in load with an increase in strain prior to unloading. A slow decrease in load after the plateau indicates some form of necking along the reinforcement bar within the prism and is a clear sign of failure, see Figure C.1. However, certain prisms had a clear steady increase in load and an abrupt stop resulting in an unsuccessful test, see Figure C.2.

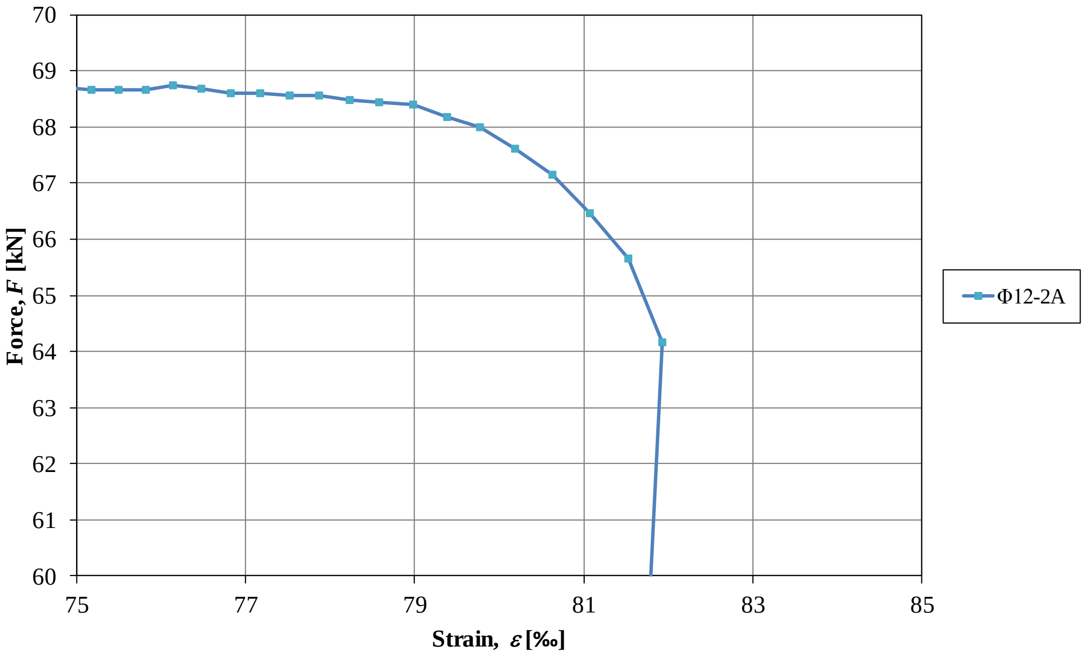

Figure C.1 Example of successful unloading in prism ϕ12-2A. A plateau in load is displayed prior to gradual unloading.

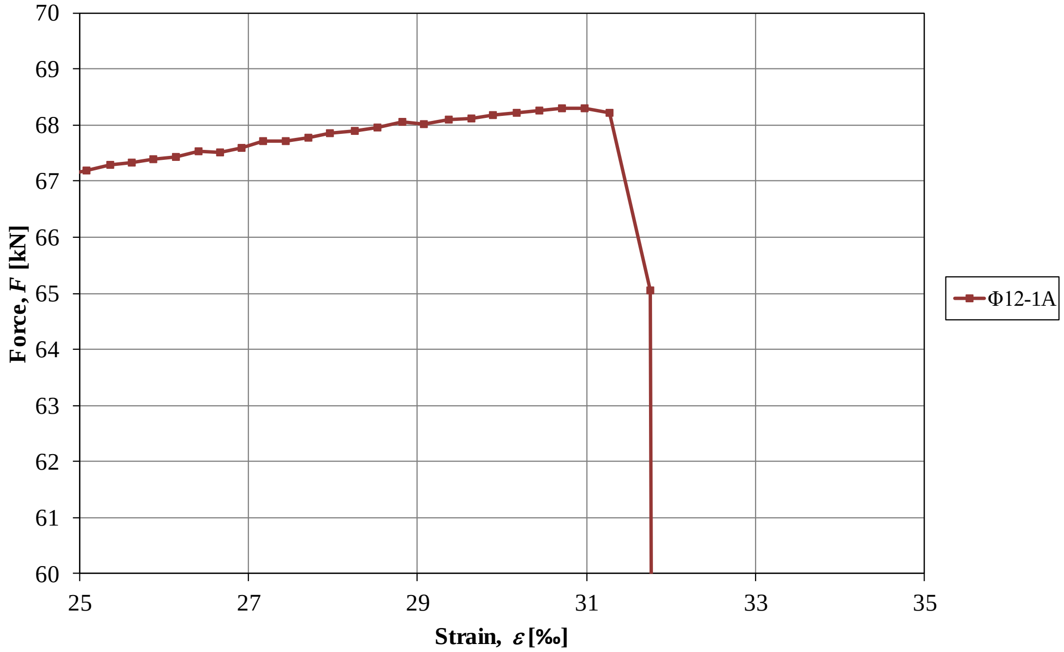

Figure C.2 Example of premature unloading in prism ϕ12-1A- A steady increase in load is displayed prior to abrupt unloading.

This indication of premature unloading resulted in lower strains than expected and an incomplete test. Determining which of the 18 prisms unloaded early and which successfully reached failure was an important step in the analysis process, see Table C.1. The reasons for this premature unloading are unclear as some prisms presented a 2 % loss in load yet station manager continued loading. Speculations and conclusions were made based on images in GOM Correlate and figures in Microsoft Excel.

Table C.1 Determination of premature unloading in all prisms.

Prism	Premature Unloading?
ϕ16-1	No [1)
ϕ16-2	No
ϕ16-3	No
ϕ12-1A	Yes [2)
ϕ12-2A	No
ϕ12-3A	No
ϕ12-4B	Yes [3)
ϕ12-5	No
ϕ12-6B	No

Prism	Premature Unloading?
ϕ12-7B	No
ϕ12-8C	No
ϕ12-9C	No
ϕ12-10C	No
ϕ12-11	No
ϕ12-12	No
ϕ10-1	No
ϕ10-2	No
ϕ10-3	No

1) Successful test with a clear plateau in load and no new crack in GOM Correlate.

2) New crack commenced premature unloading.

3) Concrete piece dislodges commencing premature unloading.

Judging images and the applied force in GOM Correlate showed the signs of premature unloading. For example, prism ϕ12-1A in Figure C.3 showed a constant increase in load and the sudden development of a crack at the point of unloading. This analysis was done for each individual prism to detect any signs of an unsuccessful test.

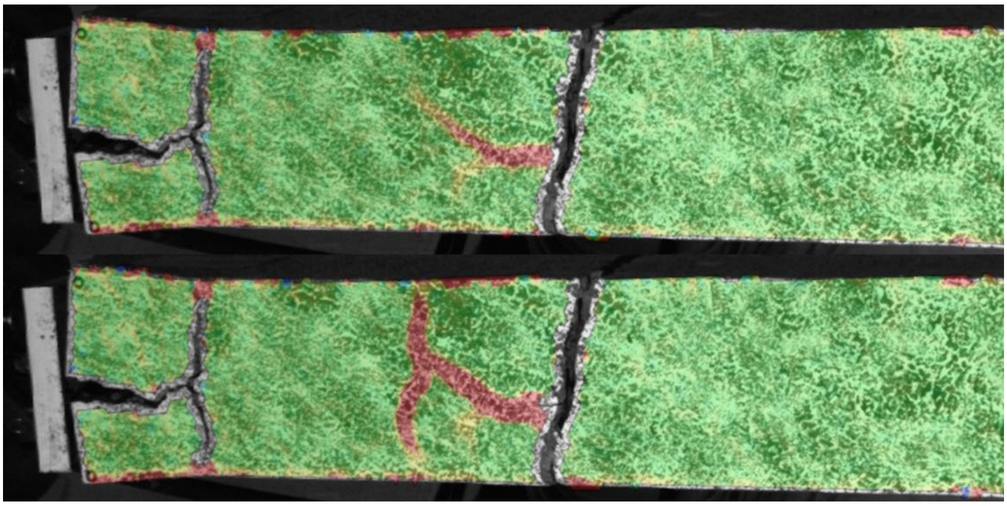

Figure C.3 Example of premature unloading in prism ϕ12-1A in GOM Correlate. A new crack developed resulting in premature unloading of the prism. This analysis of GOM Correlate images was conducted on all prisms.

Furthermore, many of the GOM Correlate 3D strain fields display a substantial crack and strain near the ends of the prisms. However, these are false cracks that indicate, in fact, the separation of the wooden block from the prism rather than an actual crack in the prism, see Appendix D. During the demolding process, the wooden blocks at the ends of the concrete forms cohered to the ends of the prisms. These false cracks were neither taken into consideration when counting total number of cracks nor when calculating crack widths.

C.2 ϕ16 prisms without PVC

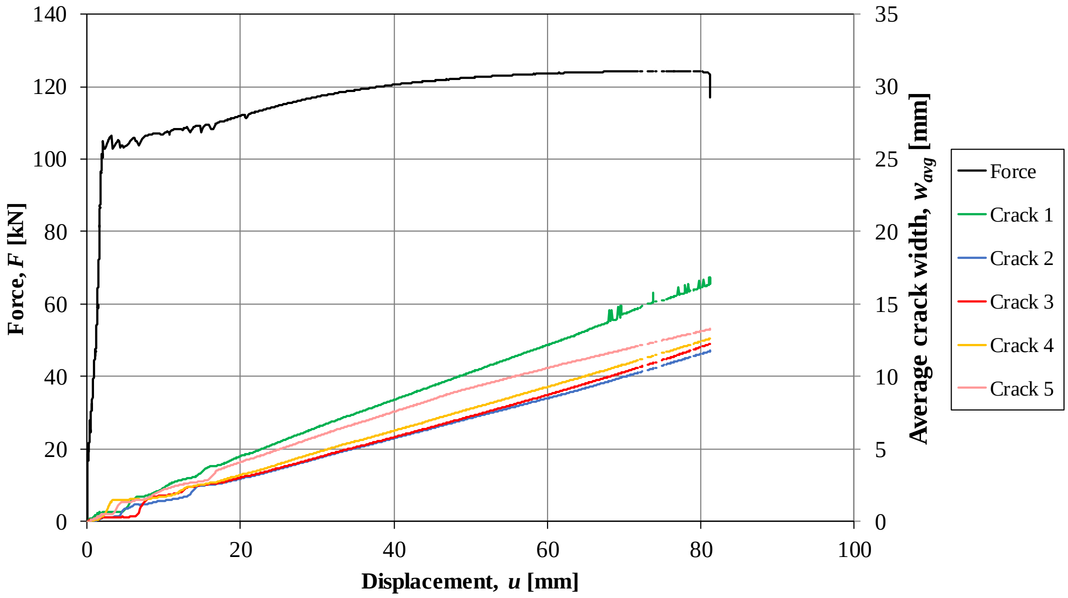

Figure C.4 *Force, average crack widths, and total displacement for prism ϕ16-1.*

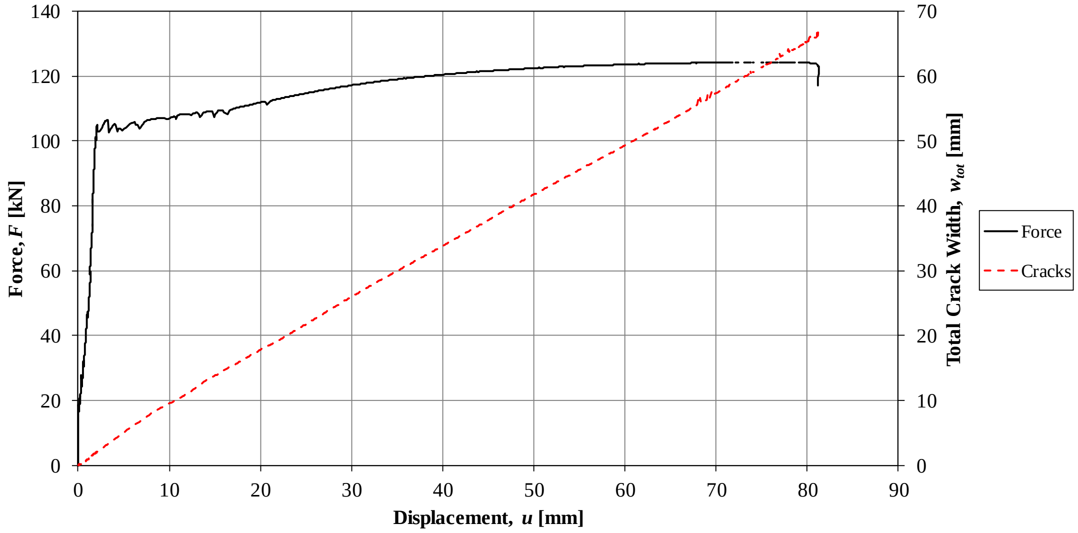

Figure C.5 *Total crack width and total displacement for prism ϕ16-1.*

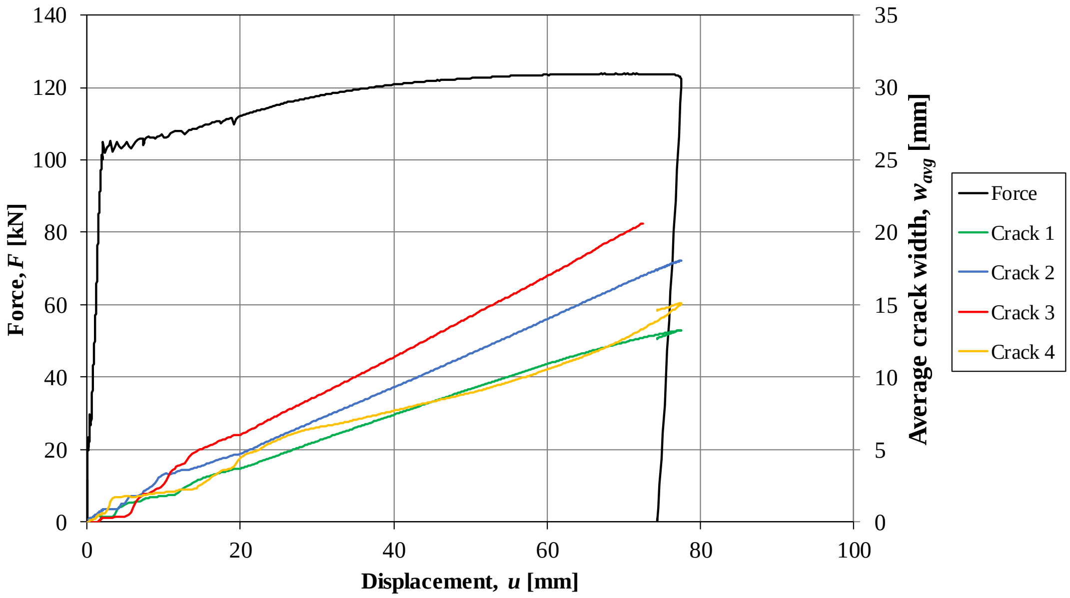

Figure C.6 Force, average crack widths, and total displacement for prism ϕ16-2.

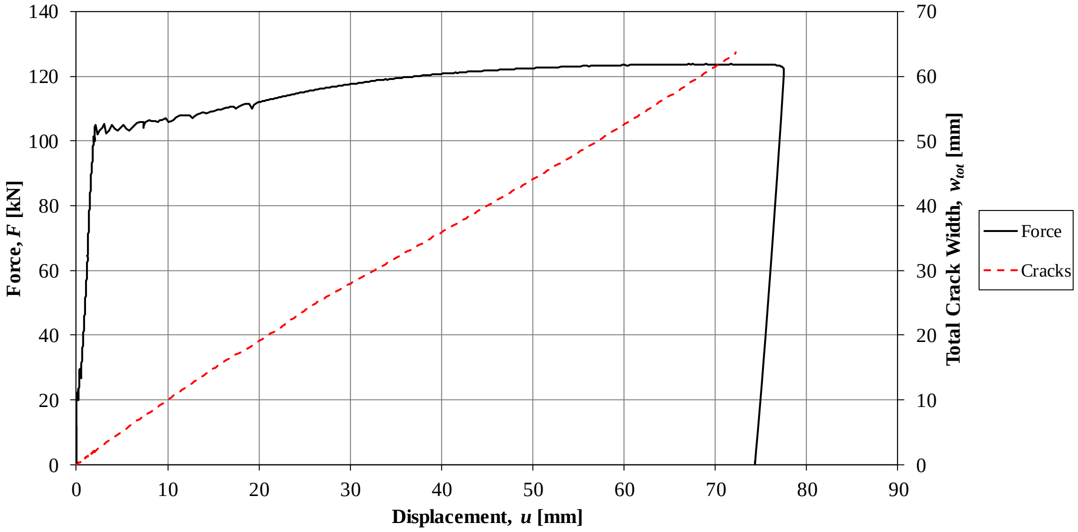

Figure C.7 Total crack width and total displacement for prism ϕ16-2.

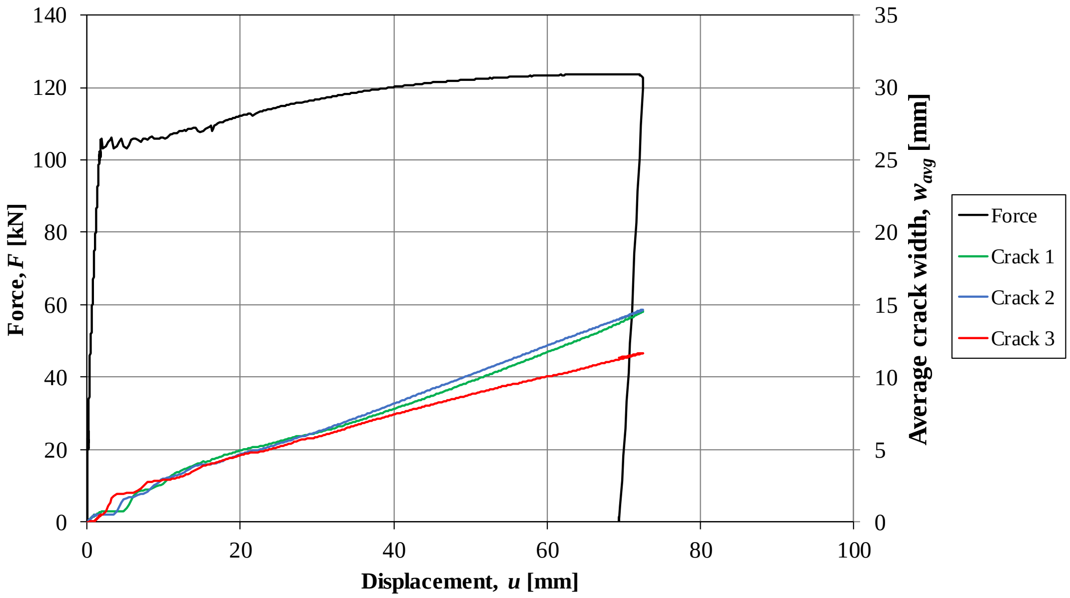

Figure C.8 Force, average crack widths, and total displacement for prism ϕ16-3.

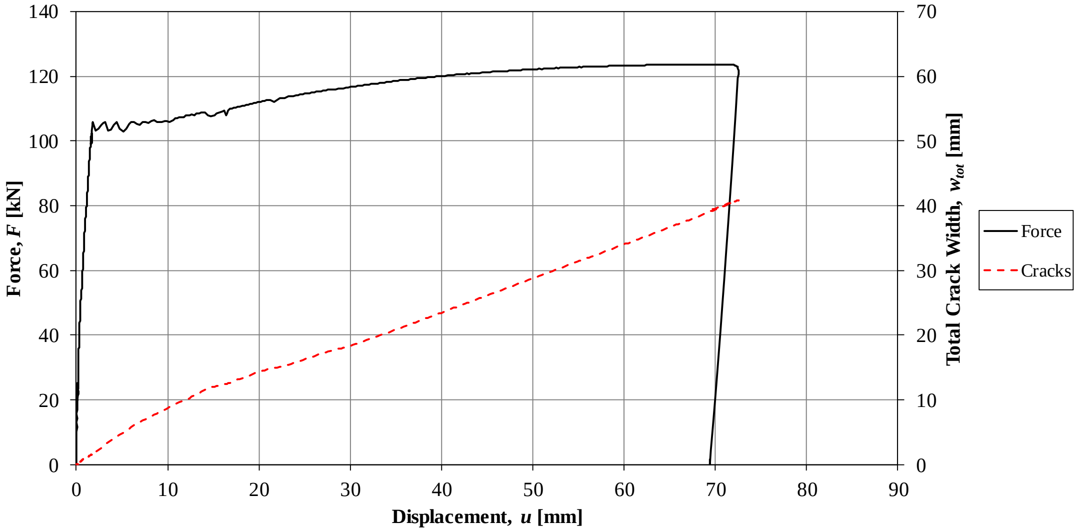

Figure C.9 Total crack width and total displacement for prism ϕ16-3.

C.3 ϕ12 prisms without PVC

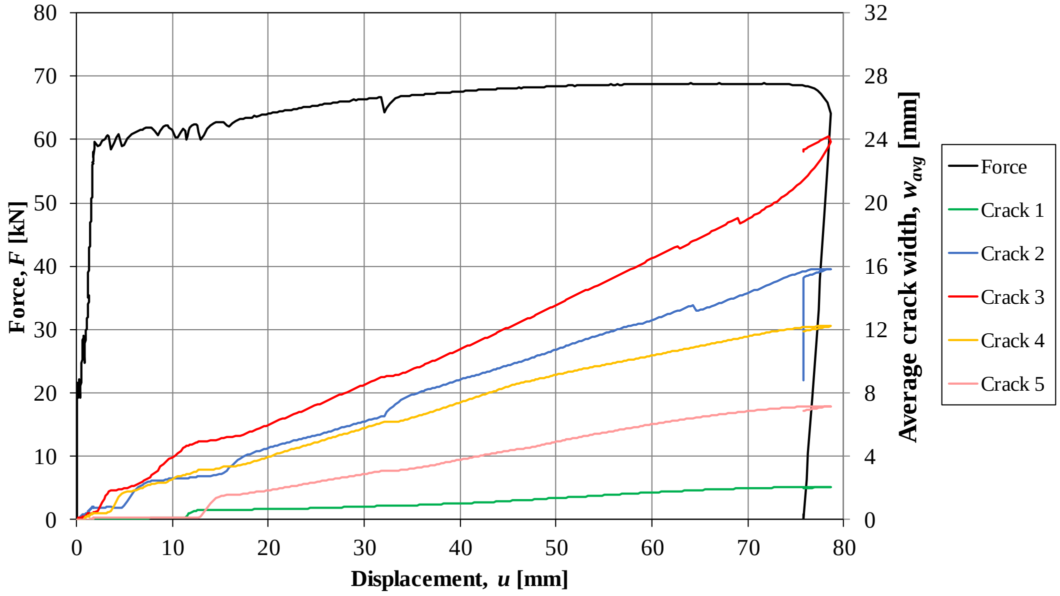

Figure C.10 Force, average crack widths, and total displacement for prism ϕ12-5.

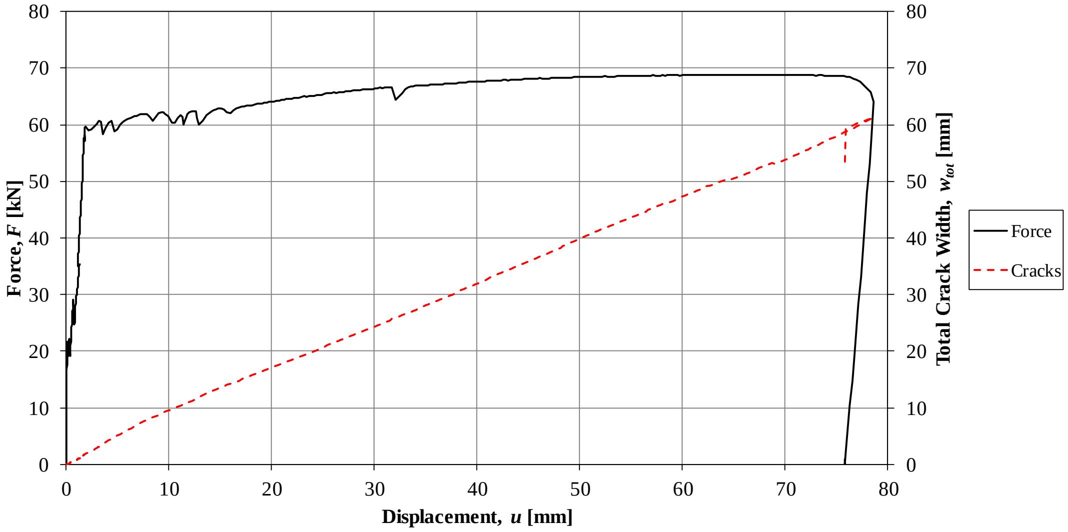

Figure C.11 Total crack width and total displacement for prism ϕ12-5.

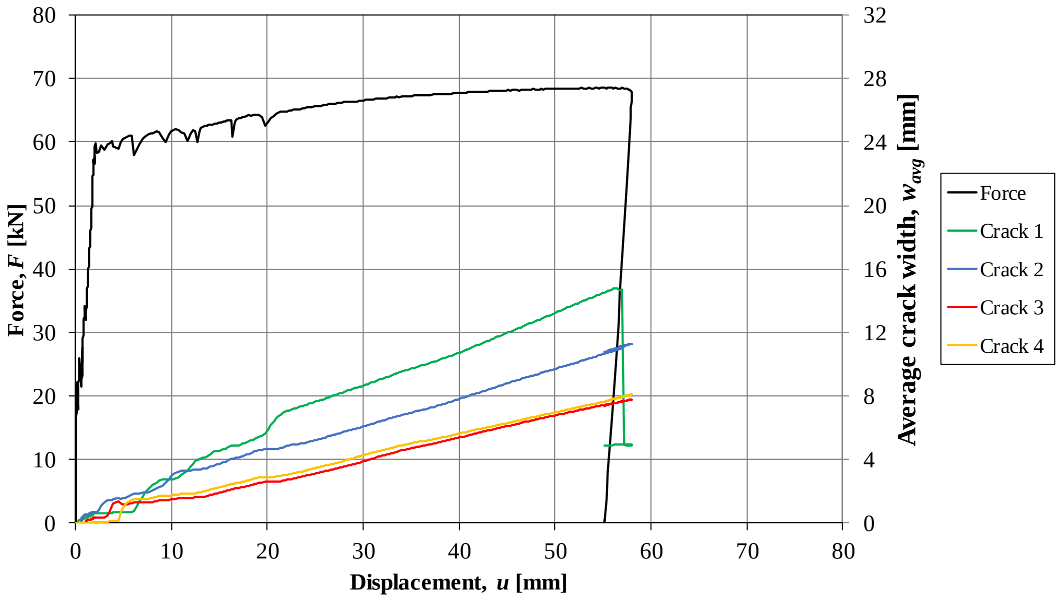

Figure C.12 Force, average crack widths, and total displacement for prism ϕ12-11.

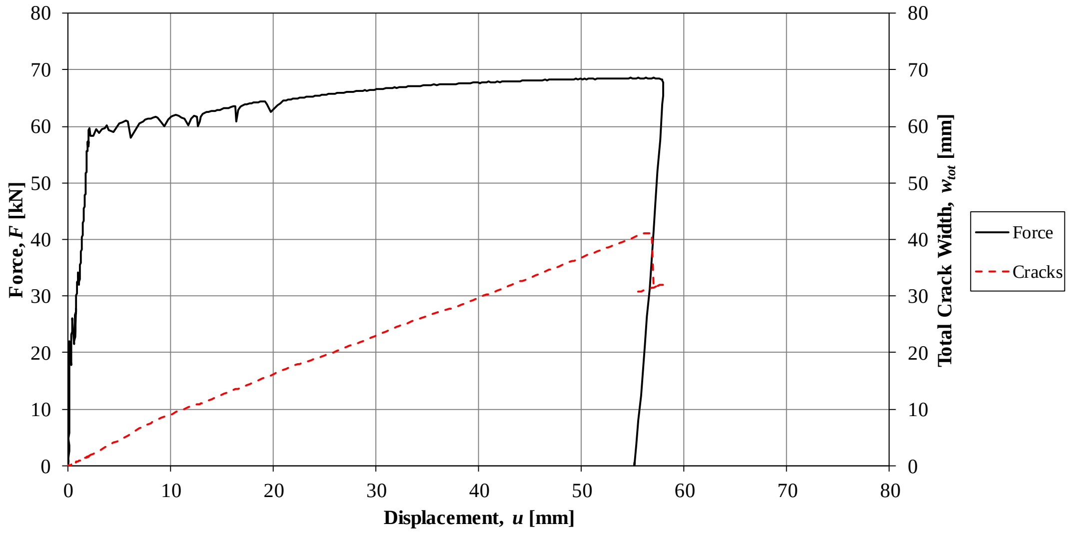

Figure C.13 Total crack width and total displacement for prism ϕ12-11.

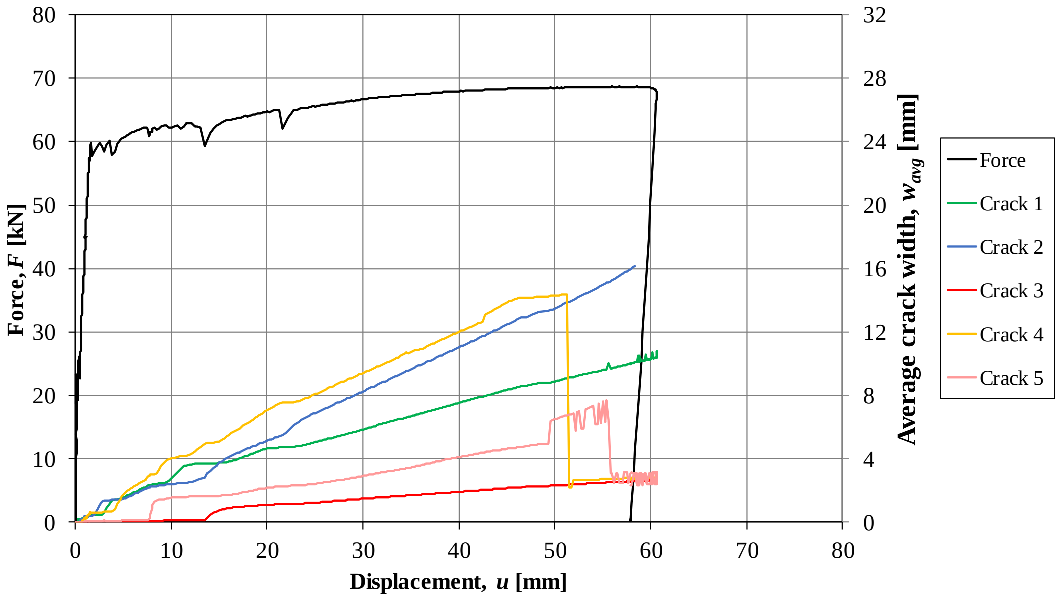

Figure C.14 Force, average crack widths, and total displacement for prism ϕ12-12.

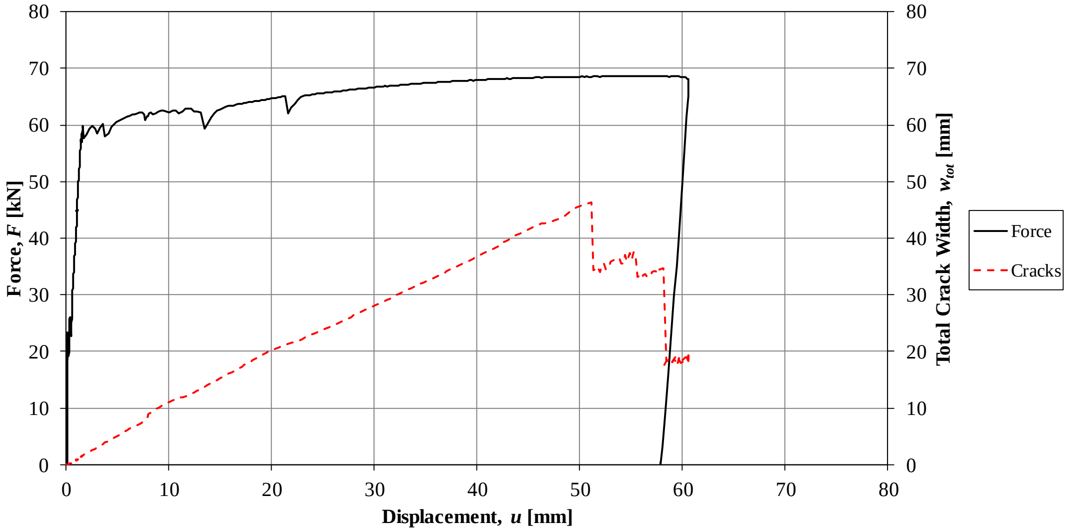

Figure C.15 Total crack width and total displacement for prism ϕ12-12.

C.4 ϕ12 prisms with 4x50 mm PVC

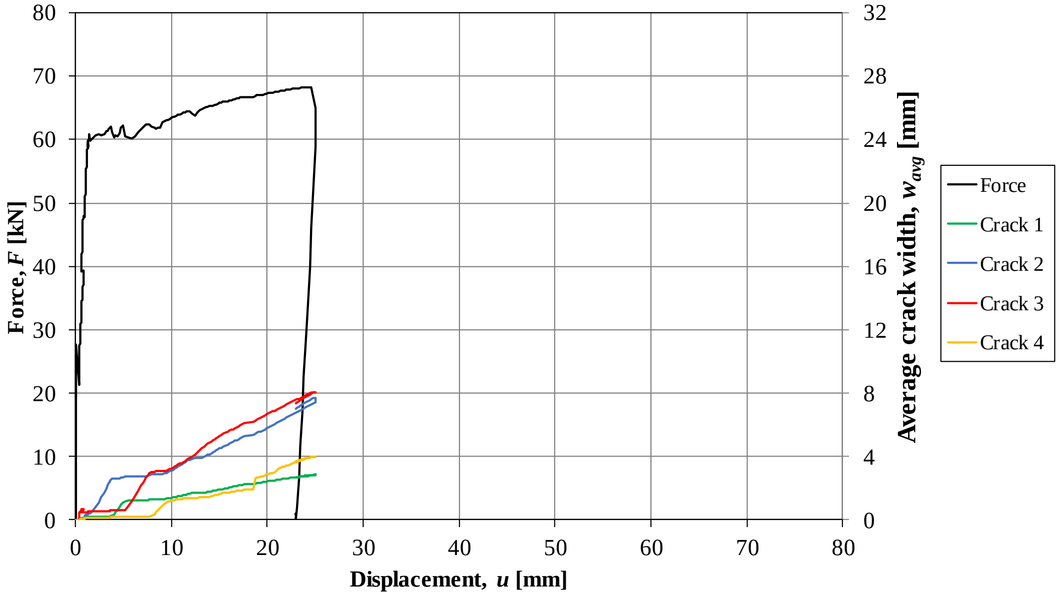

Figure C.16   Force, average crack widths, and total displacement for prism ϕ12-1A.

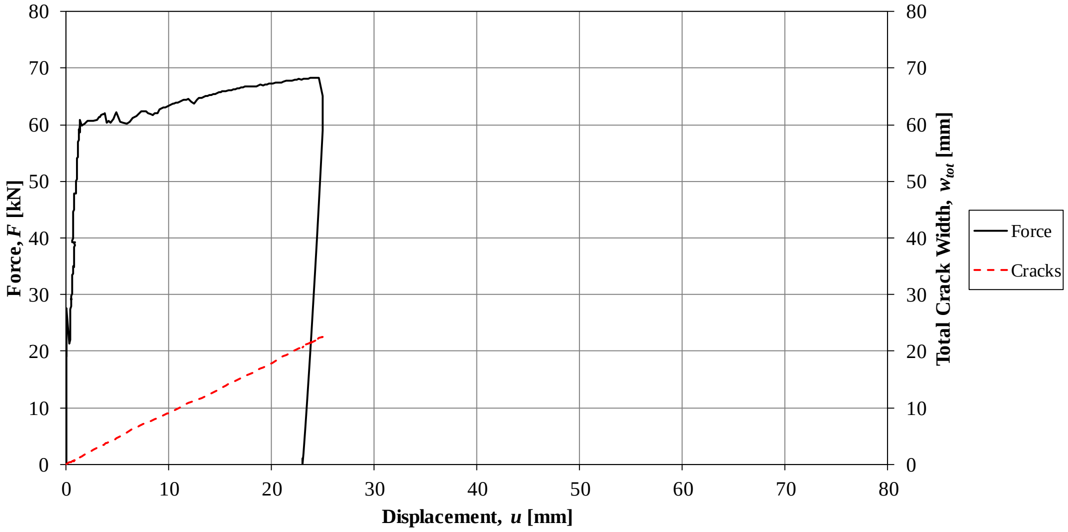

Figure C.17   Total crack width and total displacement for prism ϕ12-1A.

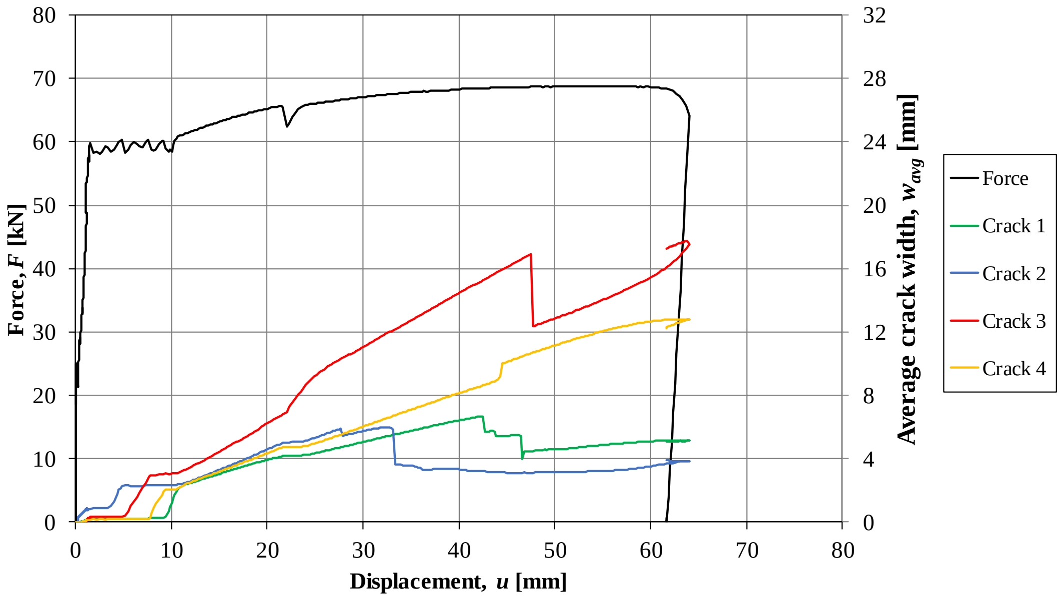

Figure C.18 Force, average crack widths, and total displacement for prism ϕ12-2A.

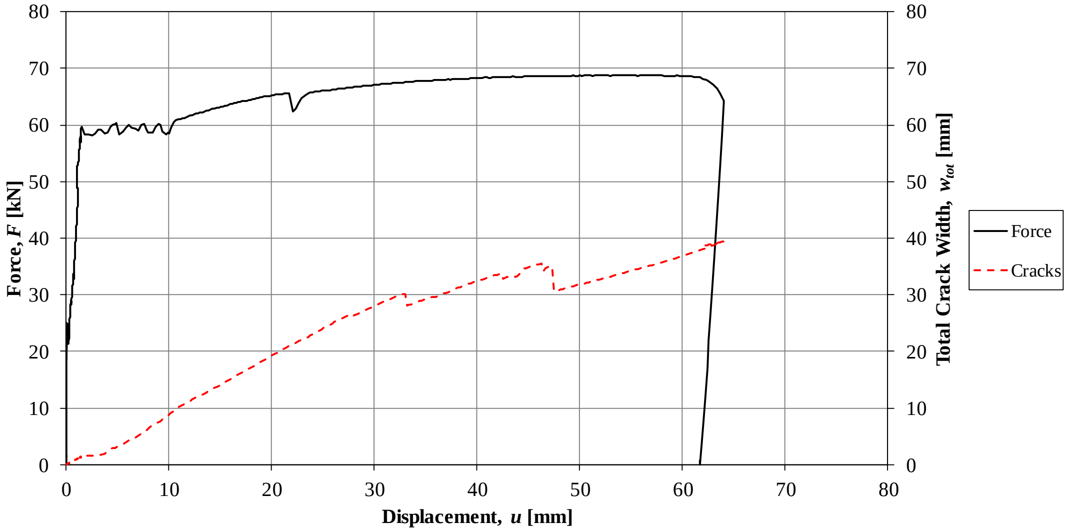

Figure C.19 Total crack width and total displacement for prism ϕ12-2A.

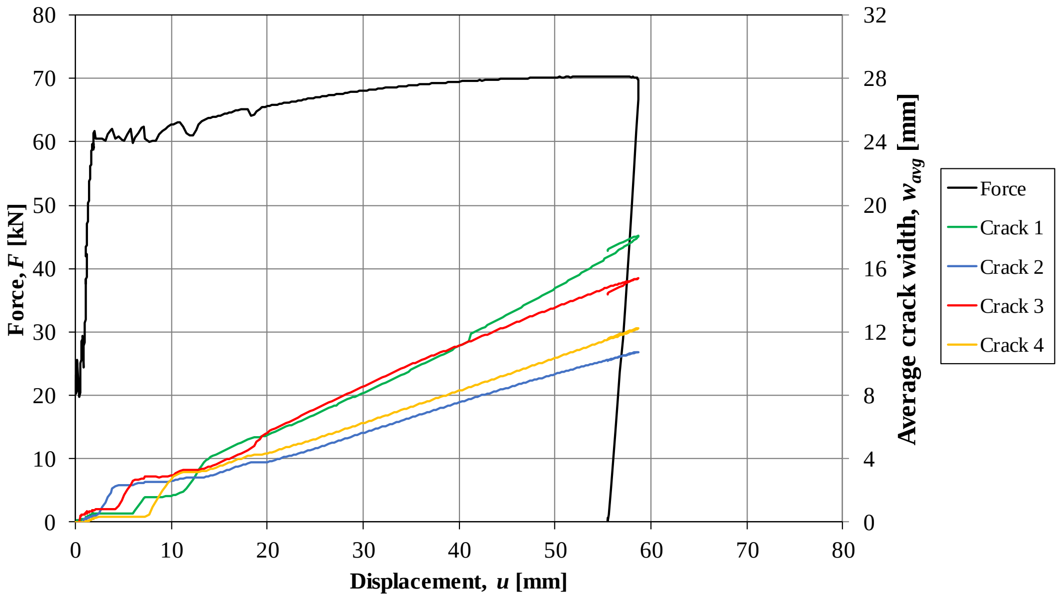

Figure C.20 Force, average crack widths, and total displacement for prism ϕ12-3A.

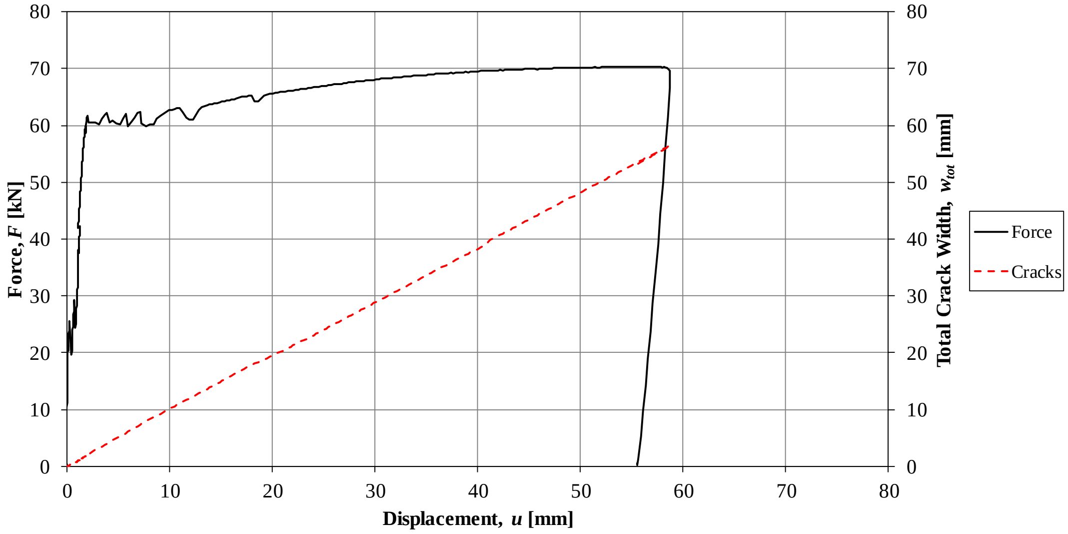

Figure C.21 Total crack width and total displacement for prism ϕ12-3A.

C.5 ϕ12 prisms with 8x50 mm PVC

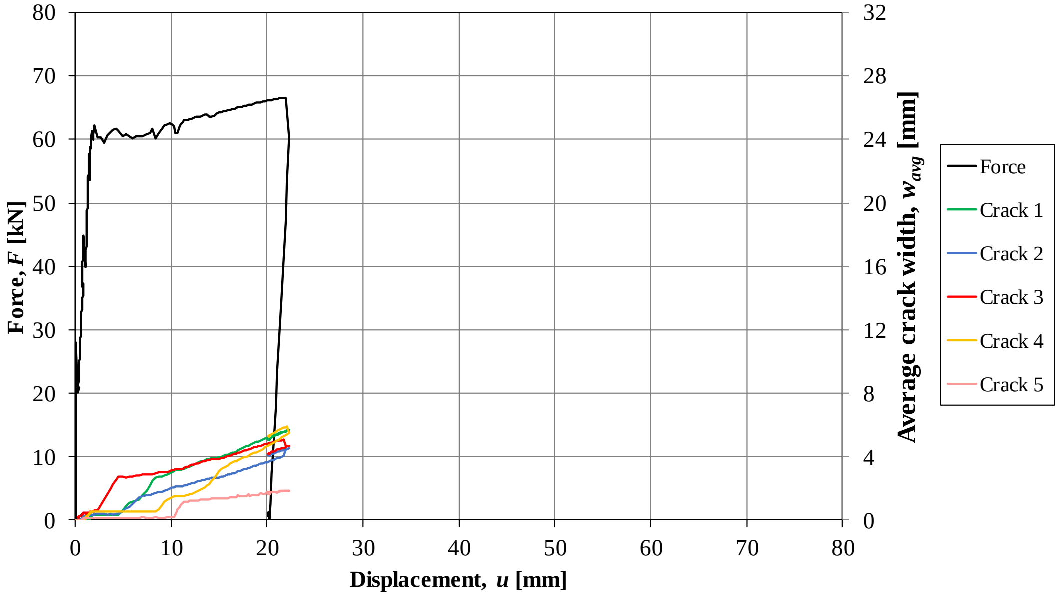

Figure C.22 Force, average crack widths, and total displacement for prism ϕ12-4B.

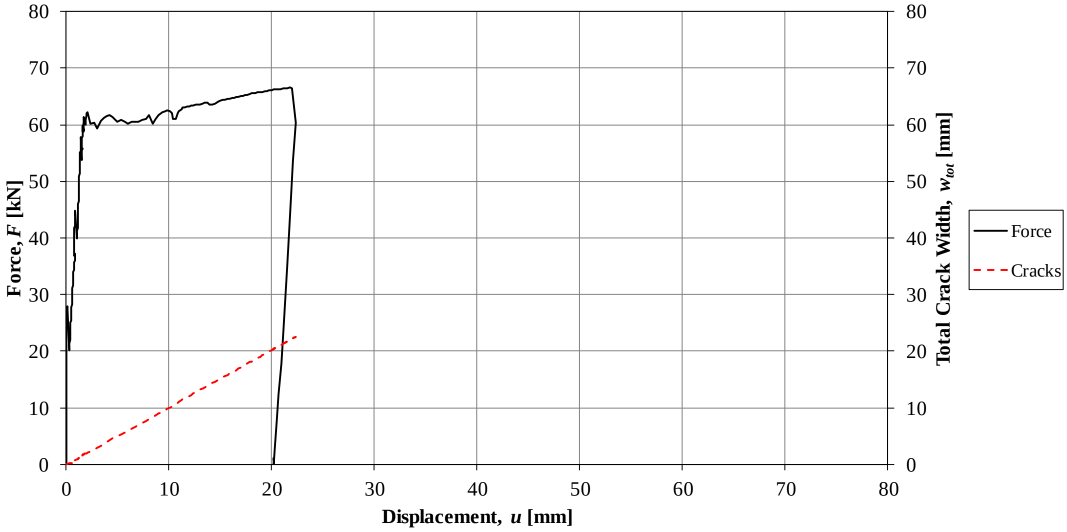

Figure C.23 Total crack width and total displacement for prism ϕ12-4B.

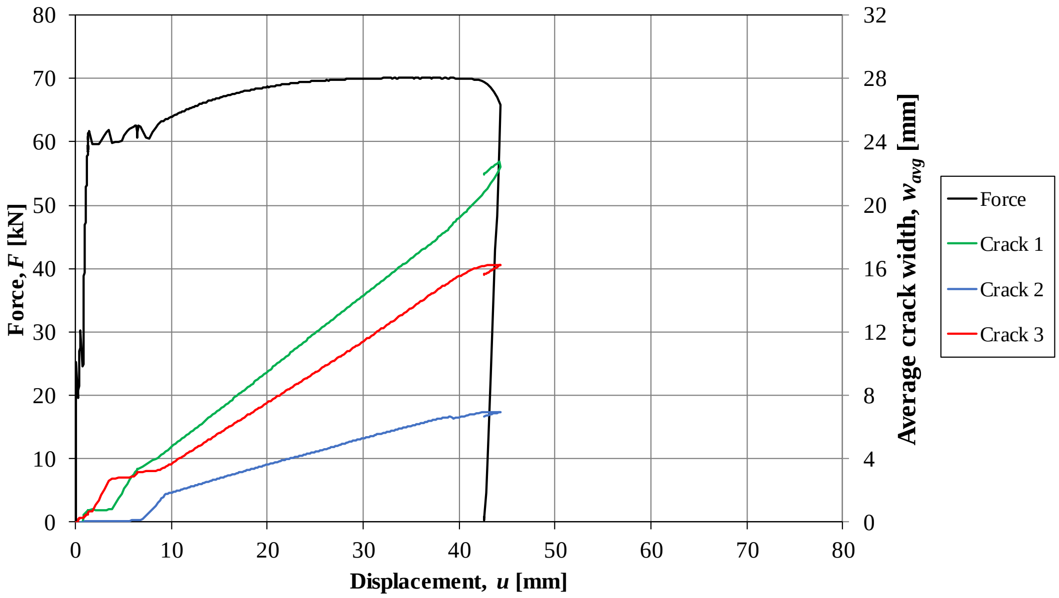

Figure C.24 Force, average crack widths, and total displacement for prism ϕ12-6B .

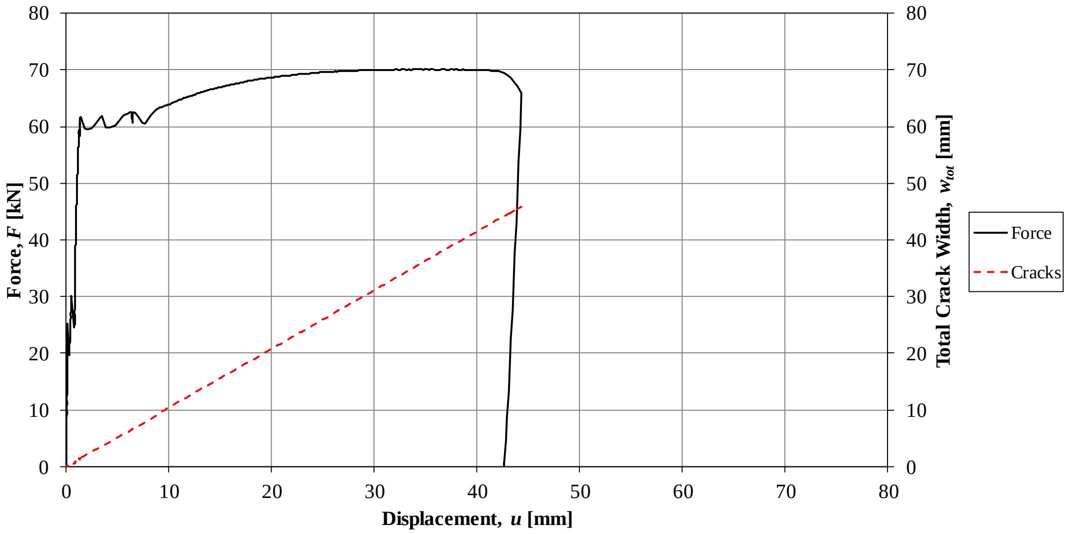

Figure C.25 Total crack width and total displacement for prism ϕ12-6B.

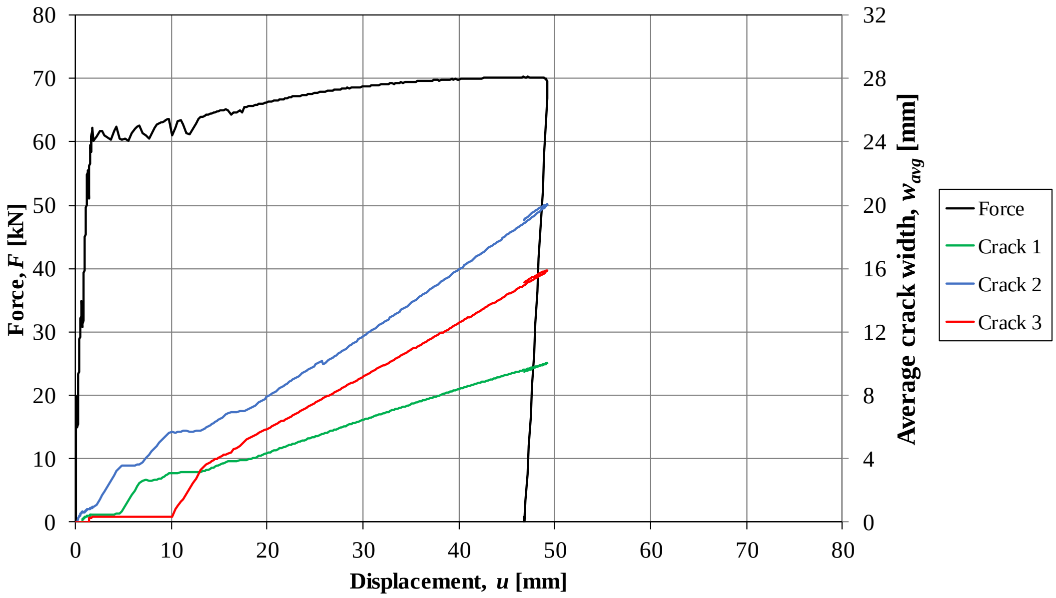

Figure C.26 Force, average crack widths, and total displacement for prism ϕ12-7B.

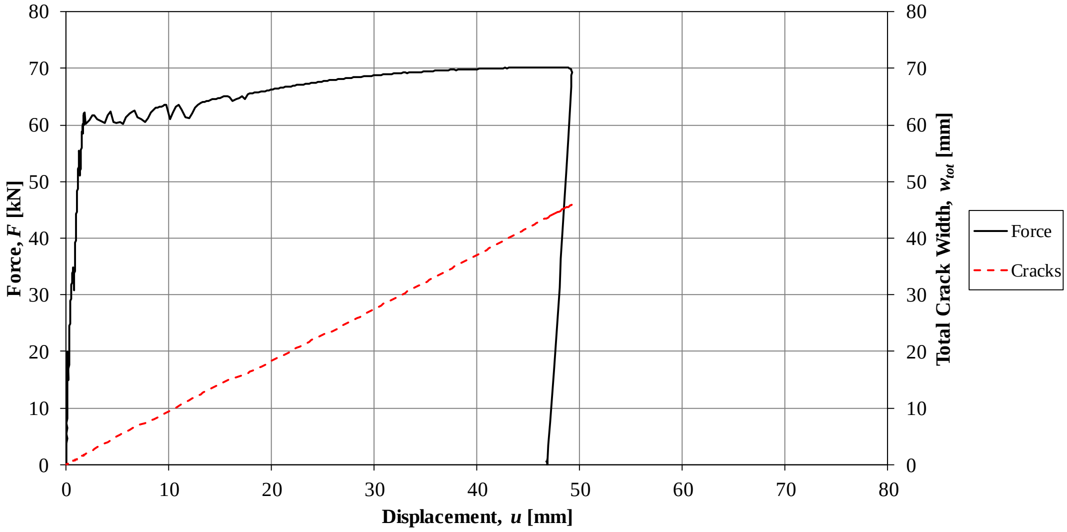

Figure C.27 Total crack width and total displacement for prism ϕ12-7B.

C.6 ϕ12 prisms with 4x100 mm PVC

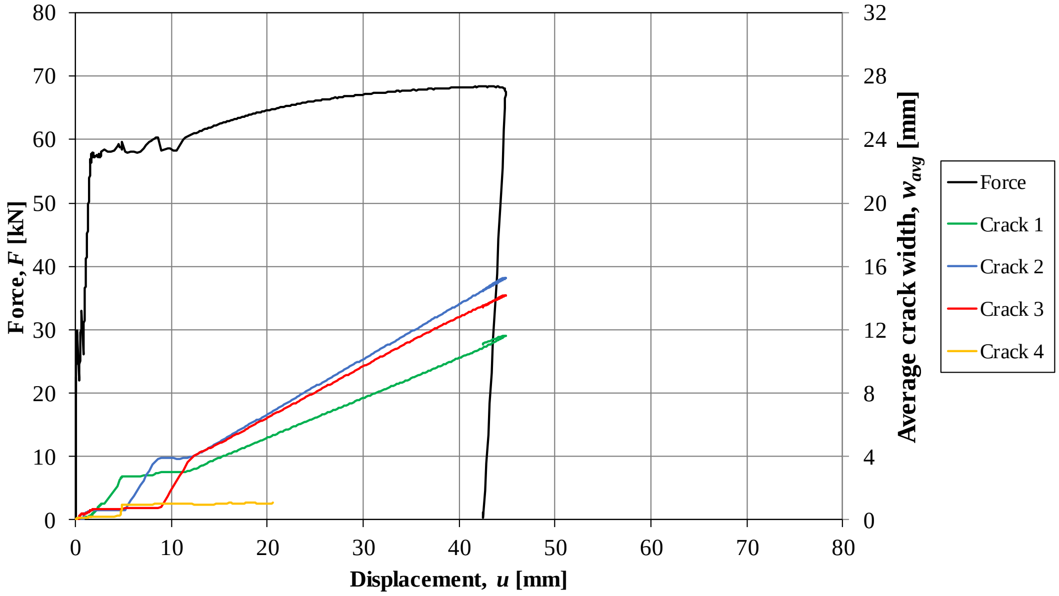

Figure C.28 Force, average crack widths, and total displacement for prism ϕ12-8C.

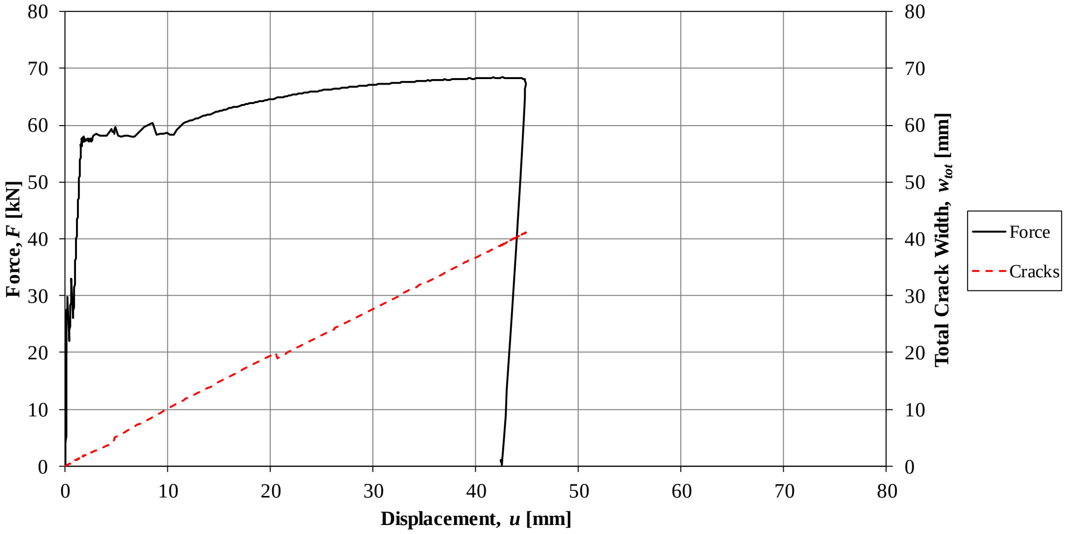

Figure C.29 Total crack width and total displacement for prism ϕ12-8C.

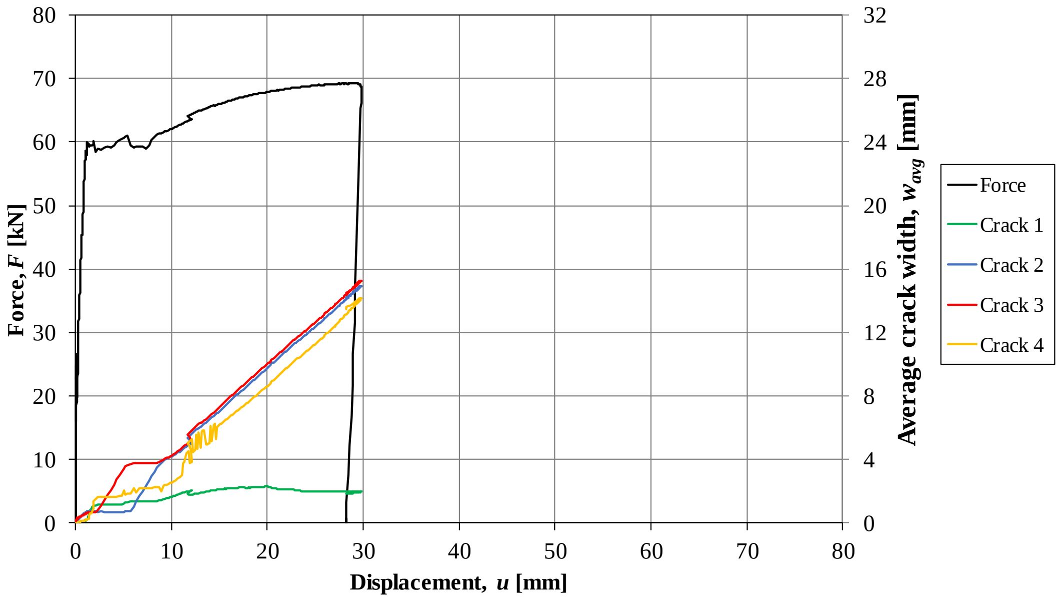

Figure C.30 Force, average crack widths, and total displacement for prism ϕ12-9C.

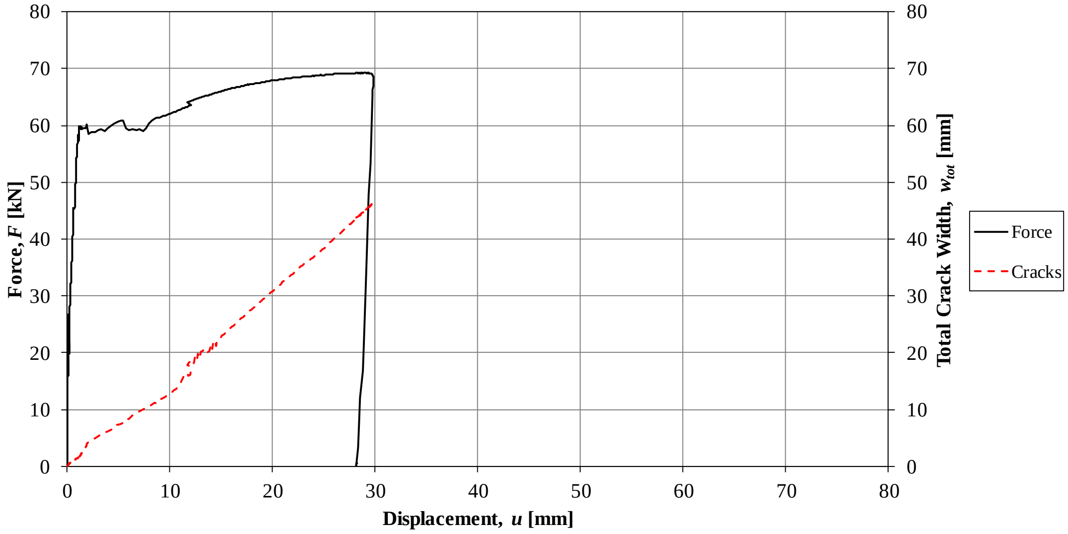

Figure C.31 Total crack width and total displacement for prism ϕ12-9C.

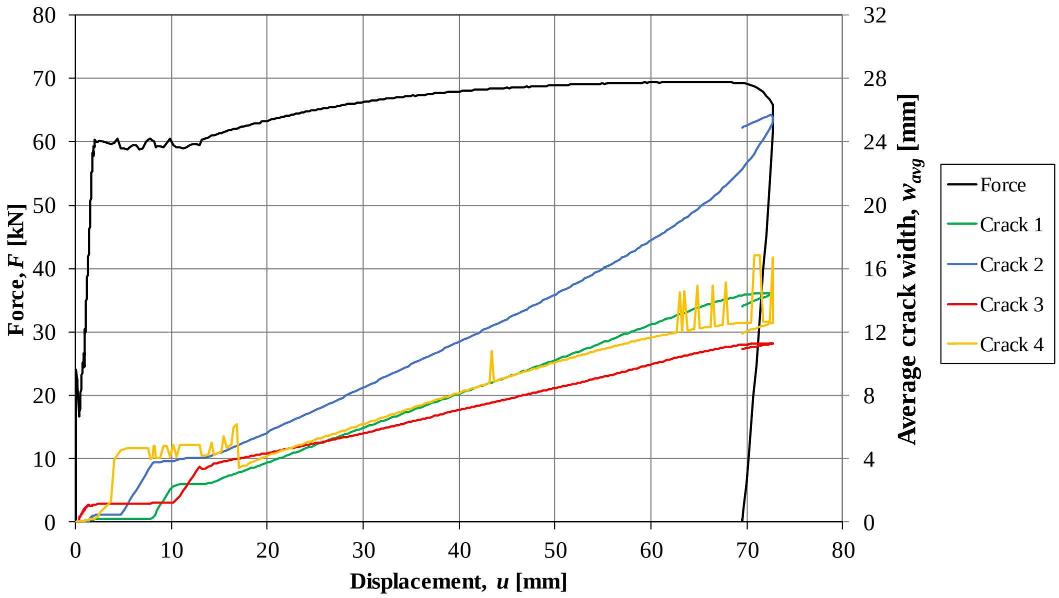

Figure C.32 Force, average crack widths, and total displacement for prism ϕ12-10C.

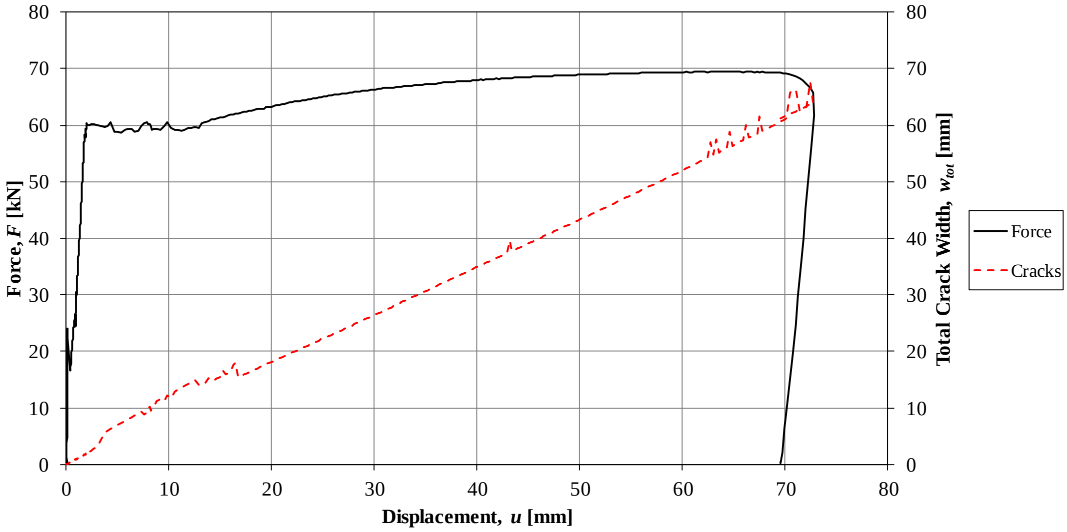

Figure C.33 Total crack width and total displacement for prism ϕ12-10C.

C.7 ϕ10 prisms without PVC

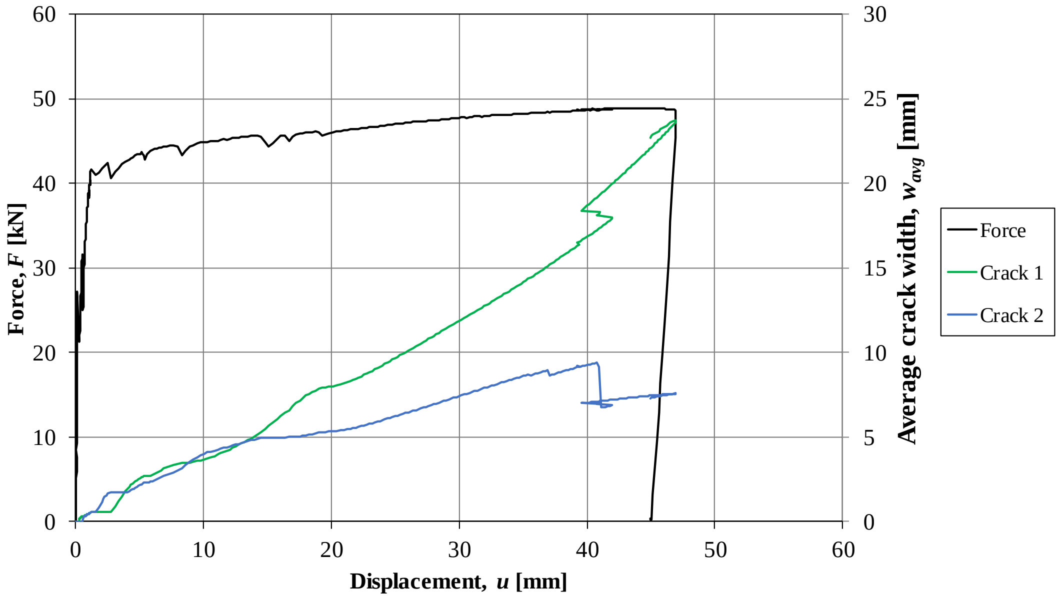

Figure C.34 Force, average crack widths, and total displacement for prism ϕ10-1.

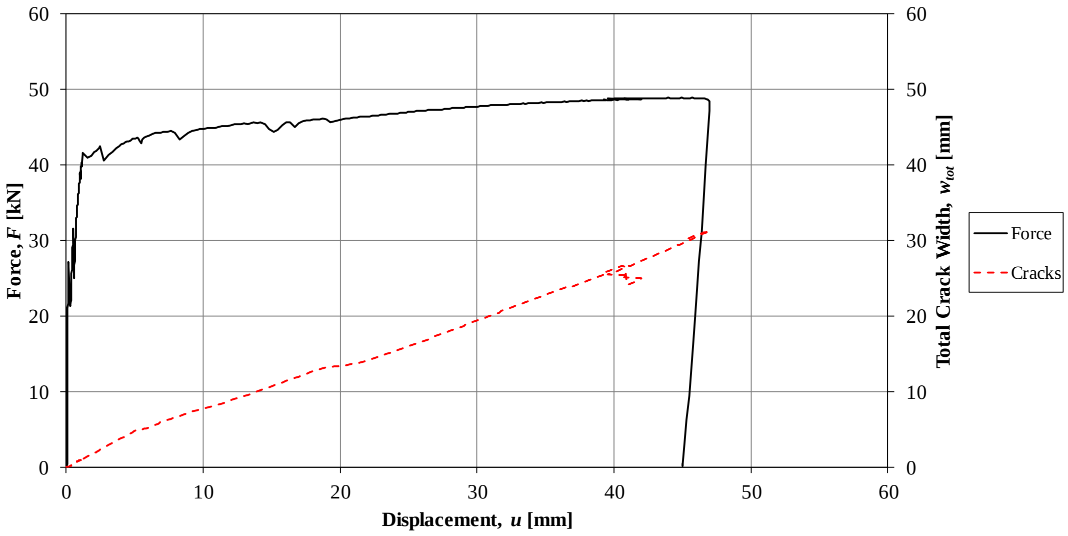

Figure C.35 Total crack width and total displacement for prism ϕ10-1.

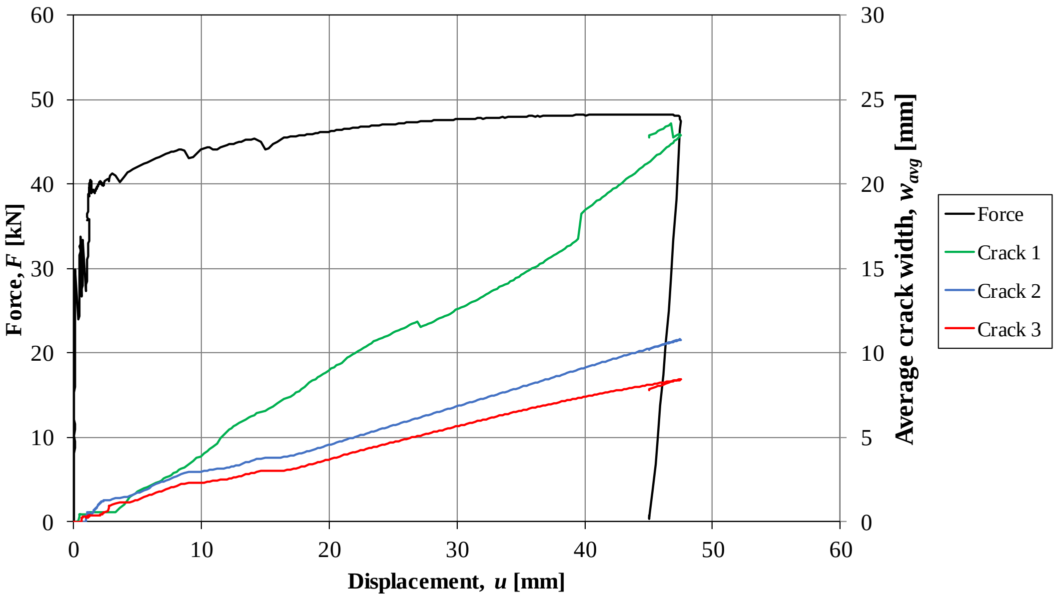

Figure C.36 Force, average crack widths, and total displacement for prism ϕ10-2.

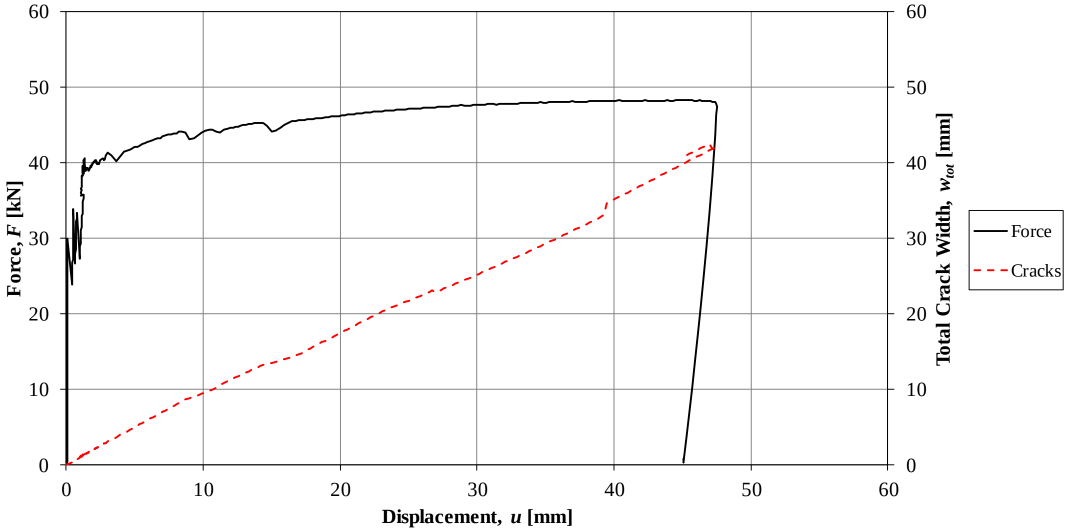

Figure C.37 Total crack width and total displacement for prism ϕ10-2.

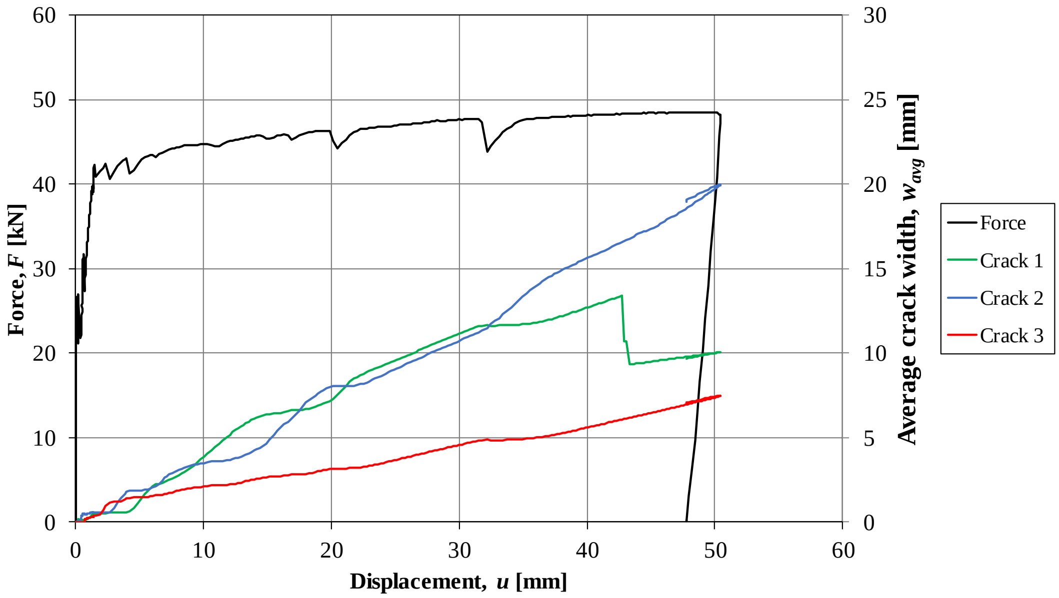

Figure C.38 Force, average crack widths, and total displacement for prism ϕ10-3.

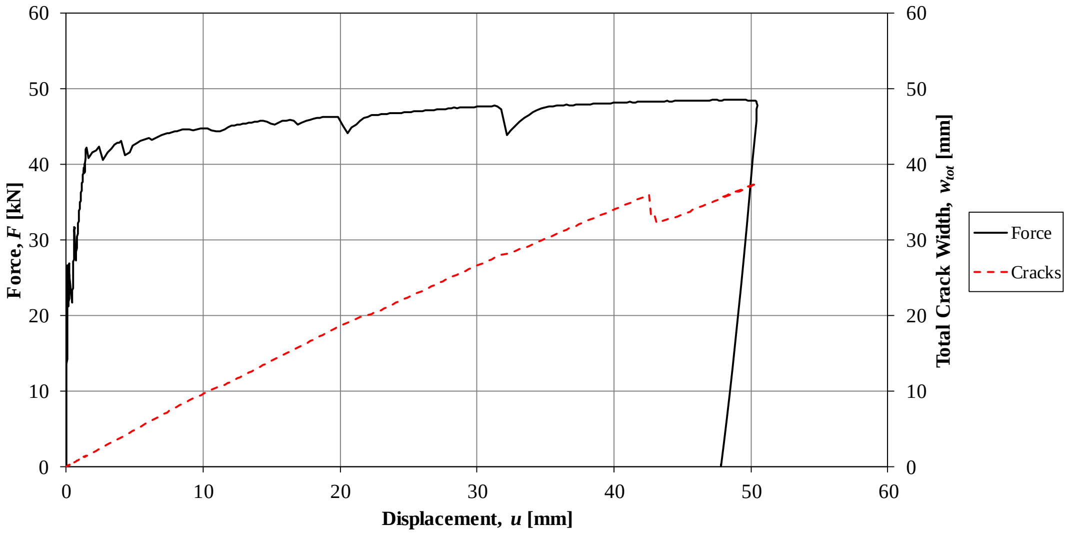

Figure C.39 Total crack width and total displacement for prism ϕ10-3.

C.8 All prisms

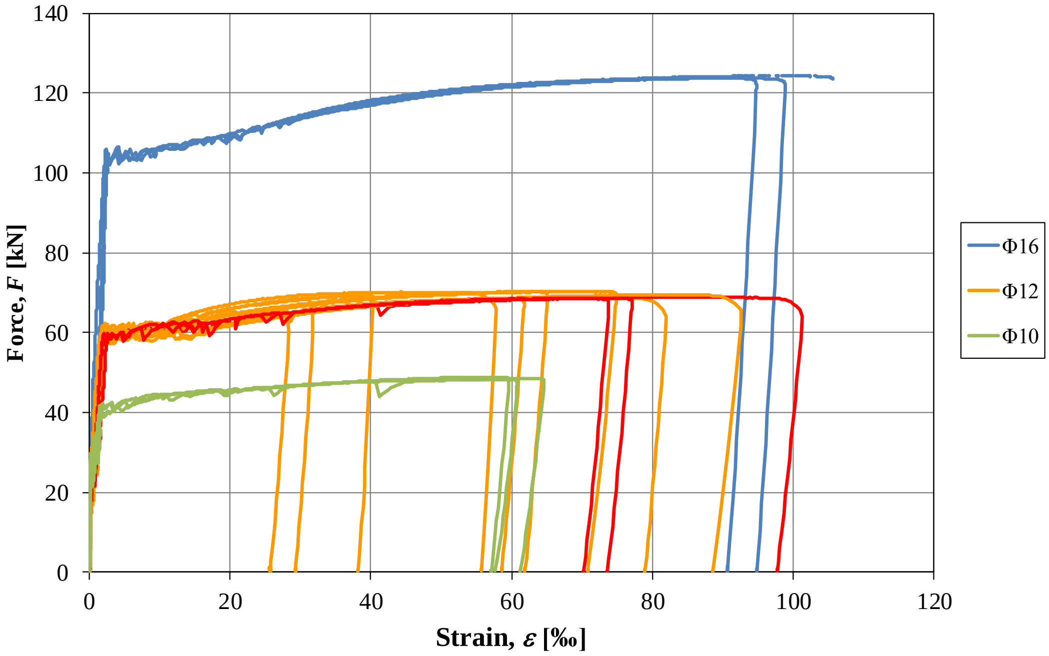

Figure C.40 Force-strain curves for all prisms. Red represent ϕ12 prisms without PVC and orange represents ϕ12 prisms with PVC.

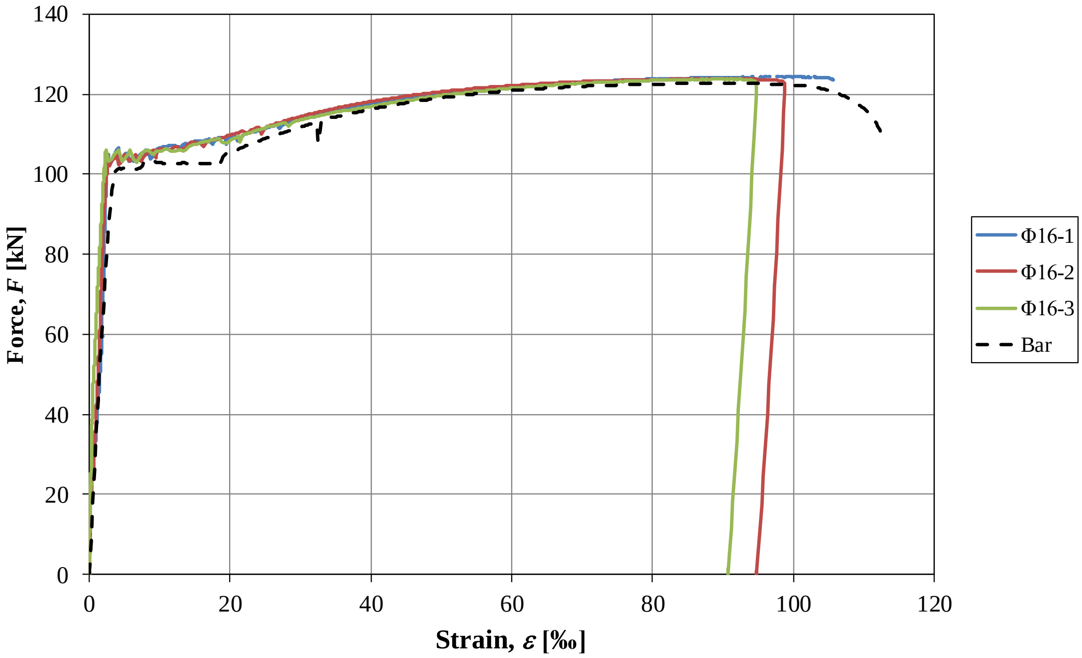

Figure C.41 Force-strain curves for ϕ16 prisms without PVC and the average ϕ16 material testing results (Bar).

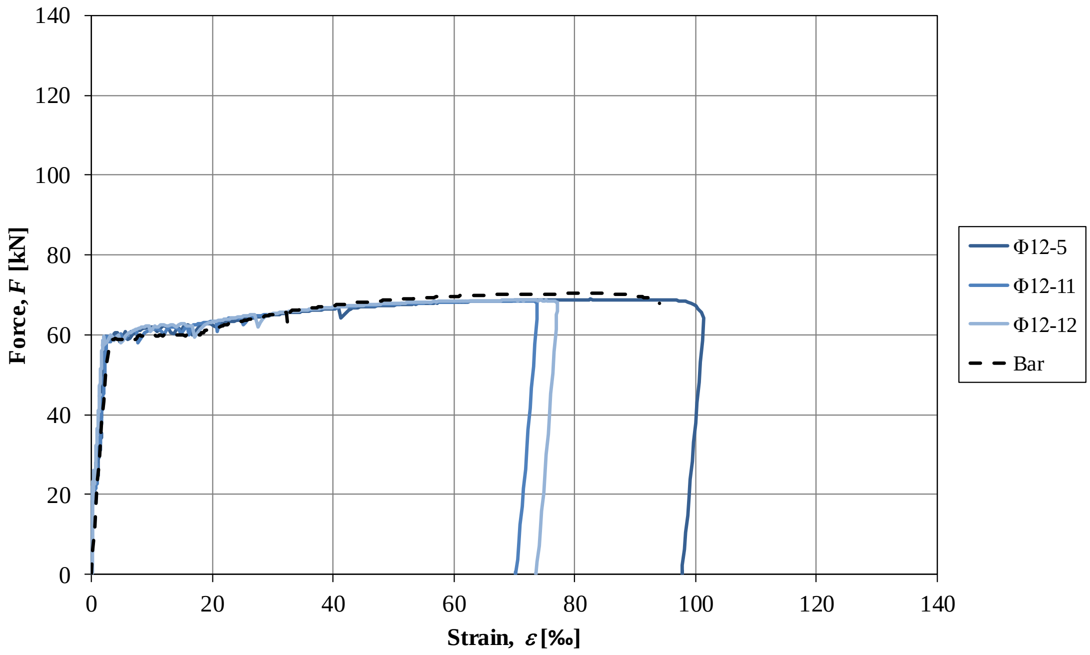

Figure C.42 Force-strain curves for ϕ12 prisms without PVC and the average ϕ12 material testing results (Bar).

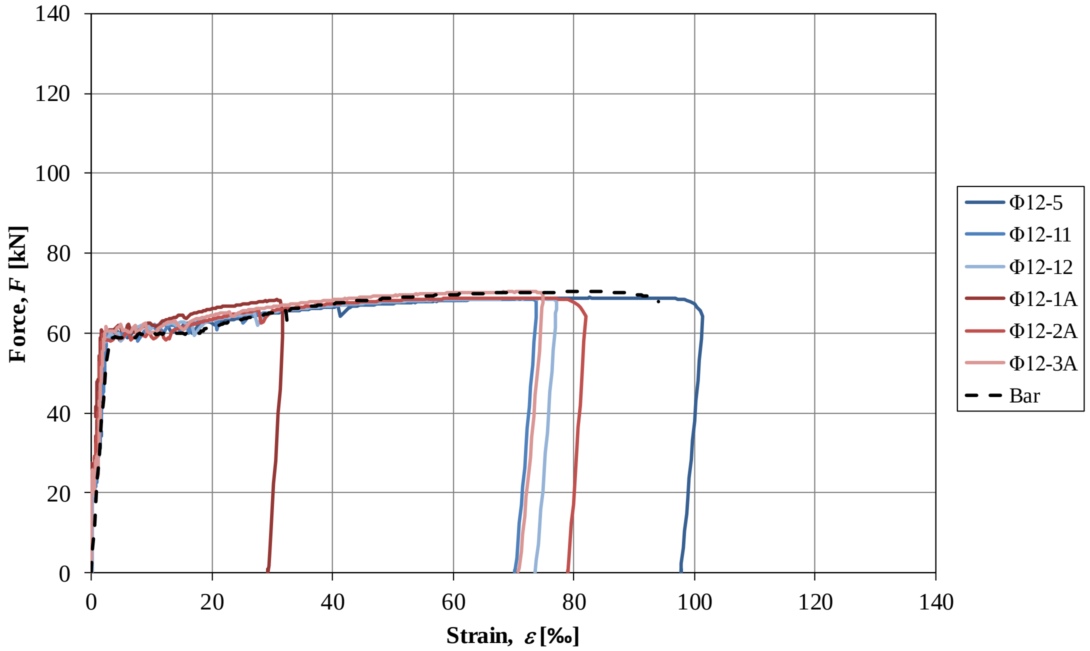

Figure C.43 Force-strain curves for ϕ12 prisms without PVC, prisms with 4x50 mm PVC, and the average ϕ12 material testing results (Bar).

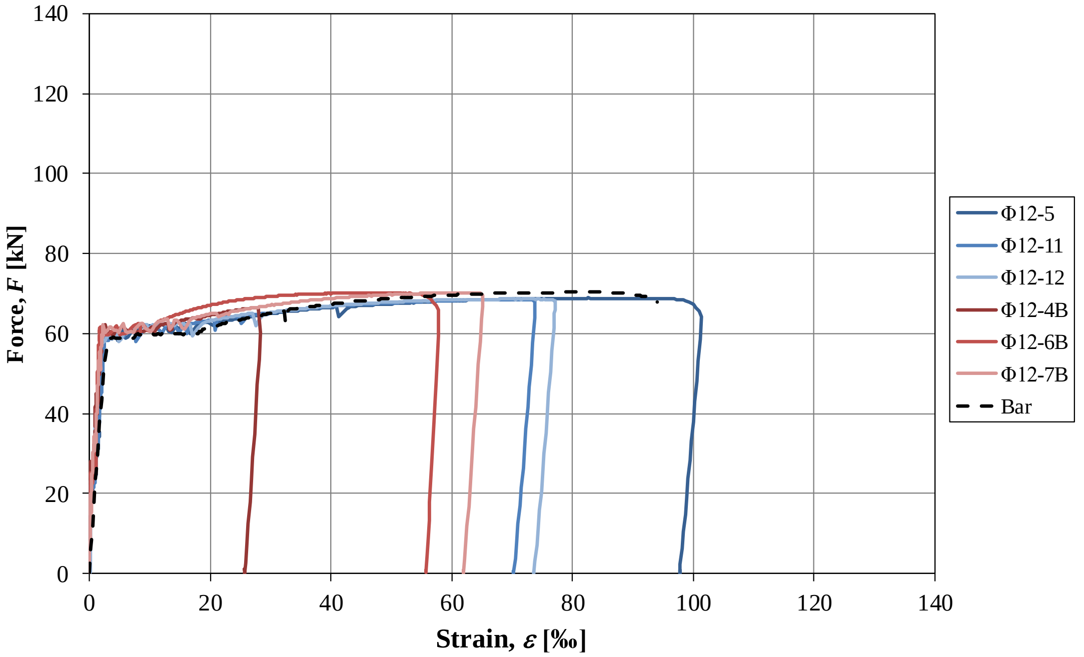

Figure C.44 Force-strain curves for ϕ12 prisms without PVC, prisms with 8x50 mm PVC, and the average ϕ12 material testing results (Bar).

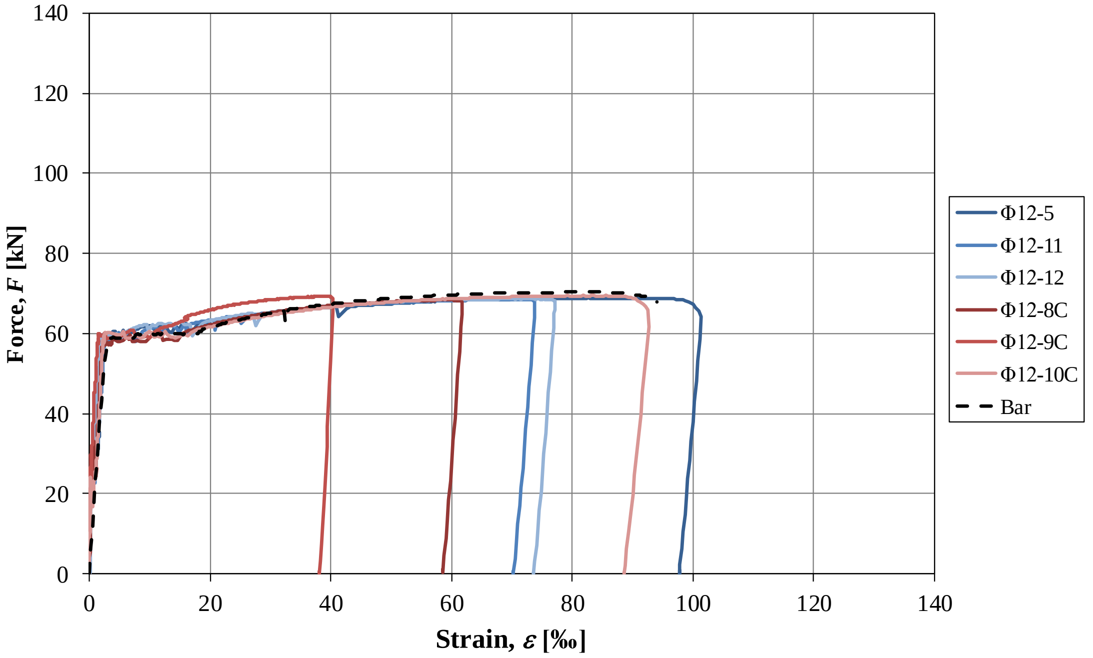

Figure C.45 Force-strain curves for ϕ12 prisms without PVC, prisms with 4x100 mm PVC, and the average ϕ12 material testing results (Bar).

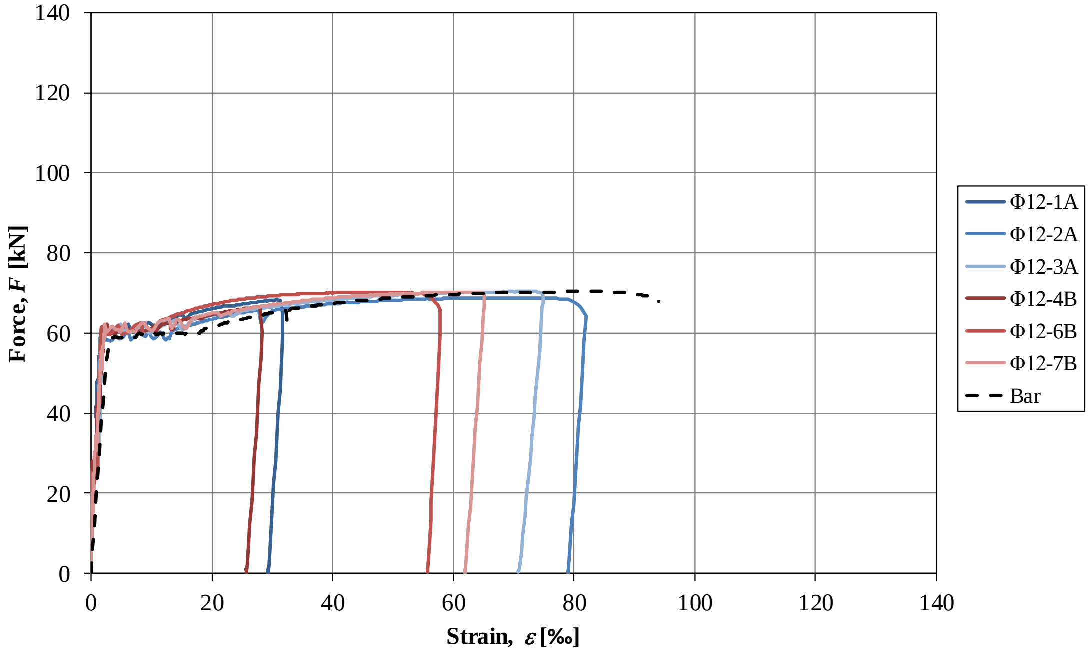

Figure C.46 Force-strain curves for ϕ12 prisms with 4x50 mm PVC, prisms with 8x50 mm PVC, and the average ϕ12 material testing results (Bar).

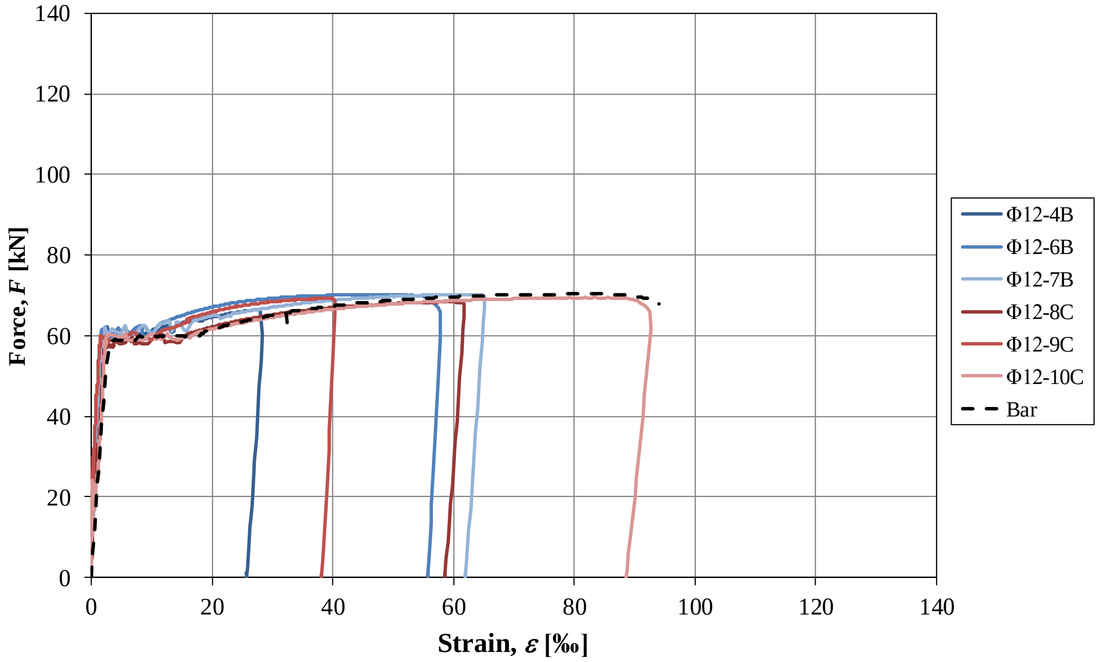

Figure C.47 Force-strain curves for ϕ12 prisms with 8x50 mm, prisms with 4x100 mm PVC, and the average ϕ12 material testing results (Bar).

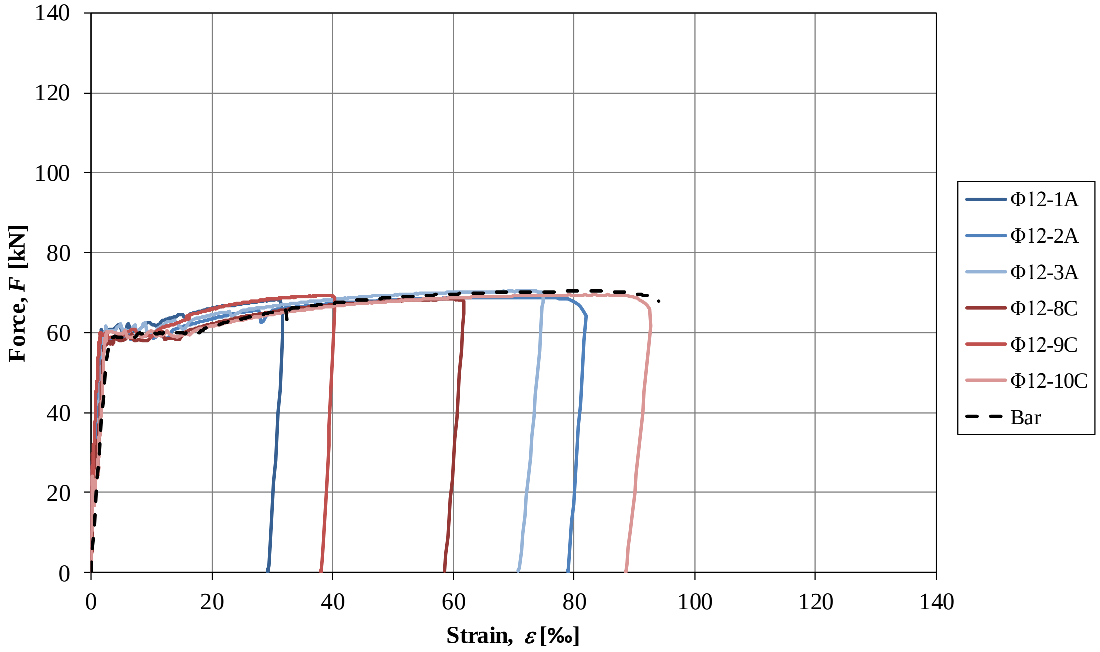

Figure C.48 Force-strain curves for $\phi12$ prisms with 4x50 mm, prisms with 4x100 mm PVC, and the average $\phi12$ material testing results (Bar).

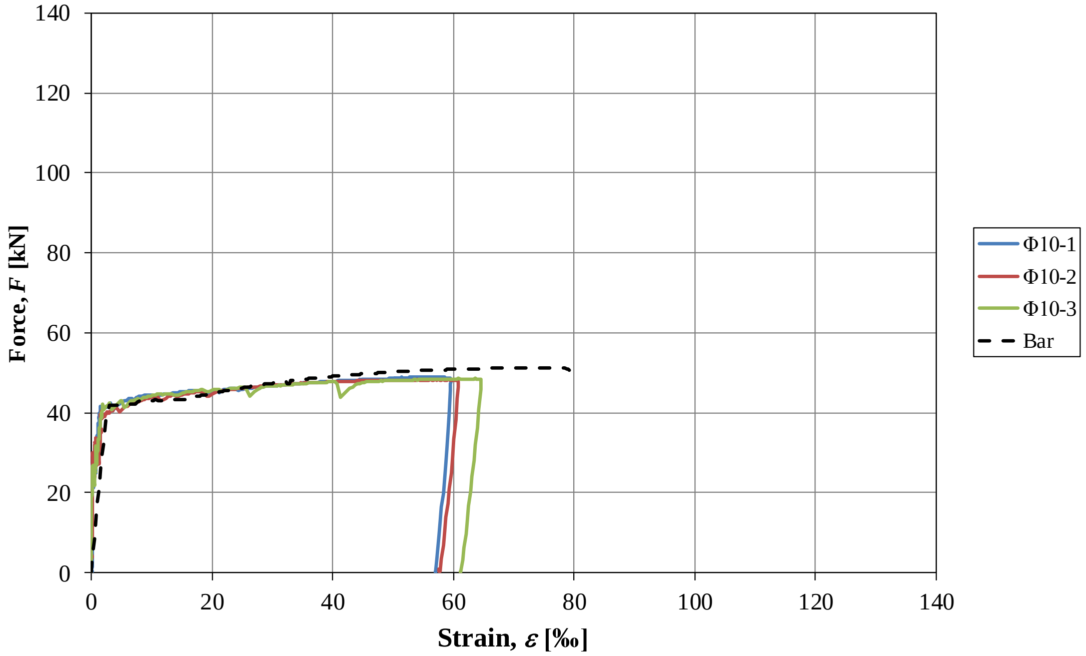

Figure C.49 Force-strain curves for $\phi10$ prisms and the average $\phi10$ material testing results (Bar).

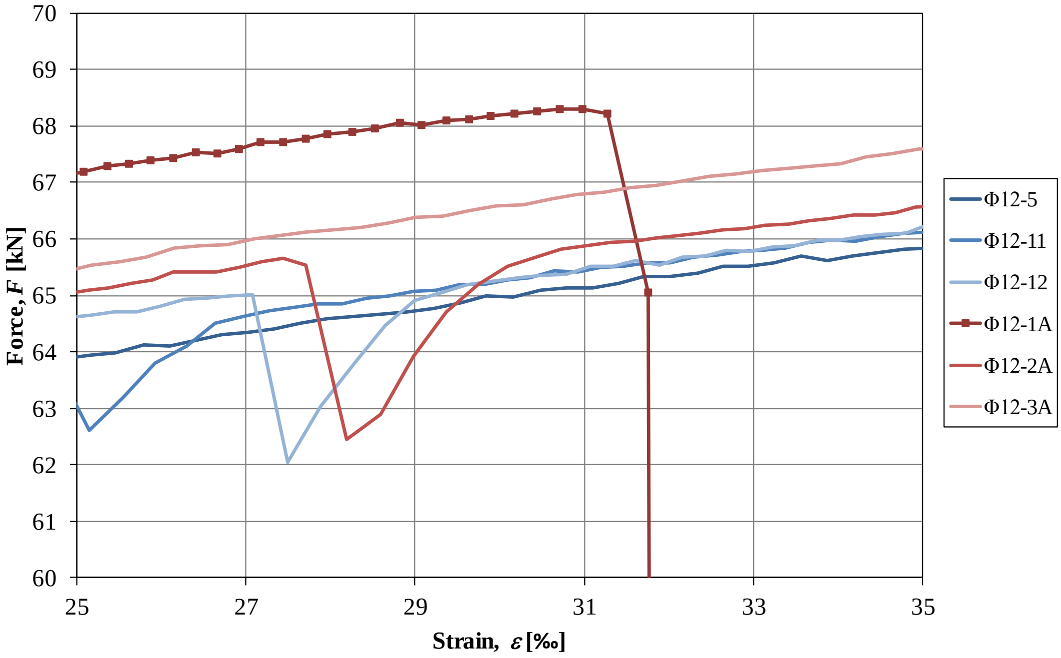

Figure C.50 Example of premature unloading in prism ϕ12-1A in comparison to various other prisms. A plateau in load is not achieved and unloading is abrupt.

Appendix D Strain Fields

GOM Correlate Professional 2018 was used to create 3D strain fields for each reinforced concrete prism. These strain fields highlight crack development and internal strains in each individual prism. Red indicates a strain of 1 % and green represents 0 % strain. Note the false crack at the ends due to separation of the wooden block from the concrete.

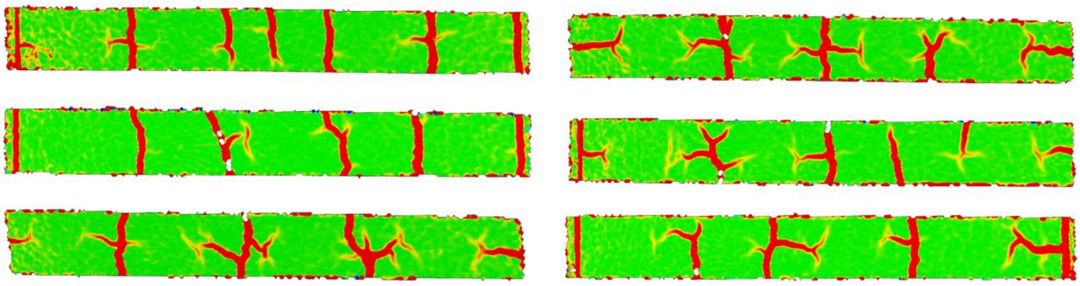

Figure D.1 Strain fields for ϕ16 prisms without PVC (left) and ϕ12 prisms without PVC (right).

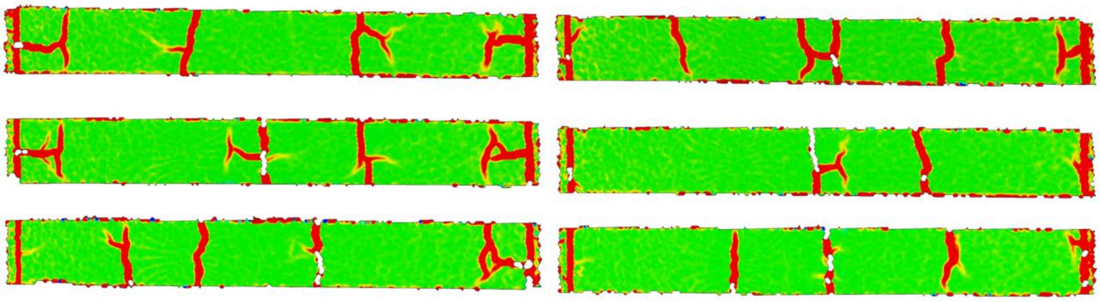

Figure D.2 Strain fields for ϕ12 prisms with 4x50 mm PVC (left) and ϕ12 prisms with 8x50 mm PVC (right).

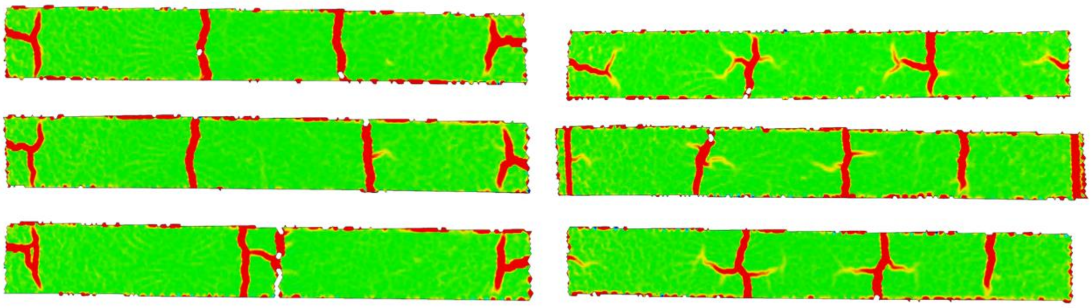

Figure D.3 Strain fields for ϕ12 prisms with 4x100 mm PVC (left) and ϕ10 prisms without PVC (right).

Appendix E GOM Correlate Reports

E.1 ϕ16 prisms without PVC

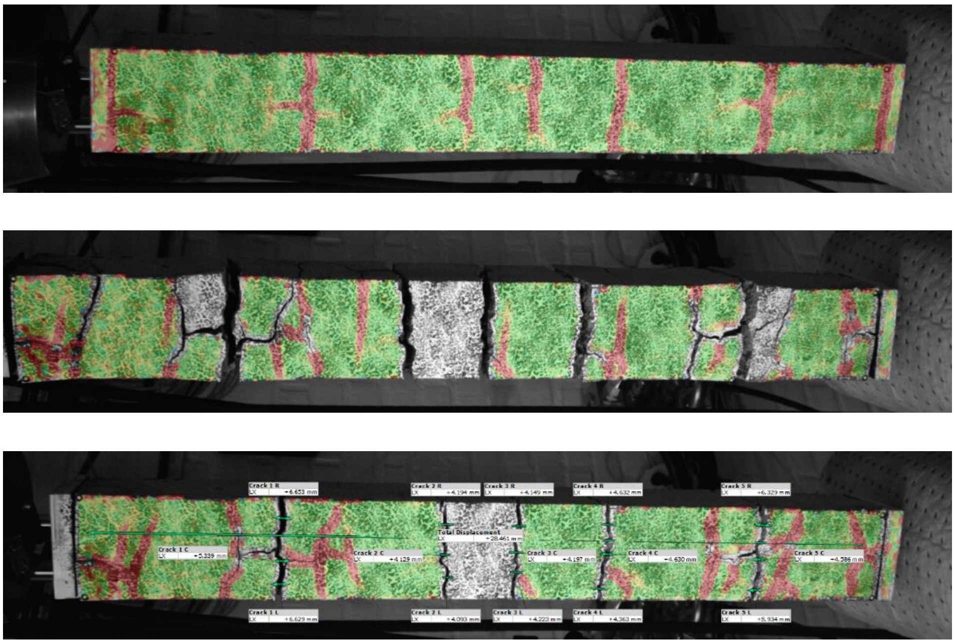

Figure E.1 Stabilized cracking stage, maximum load, and GOM calculation example for prism ϕ16-1.

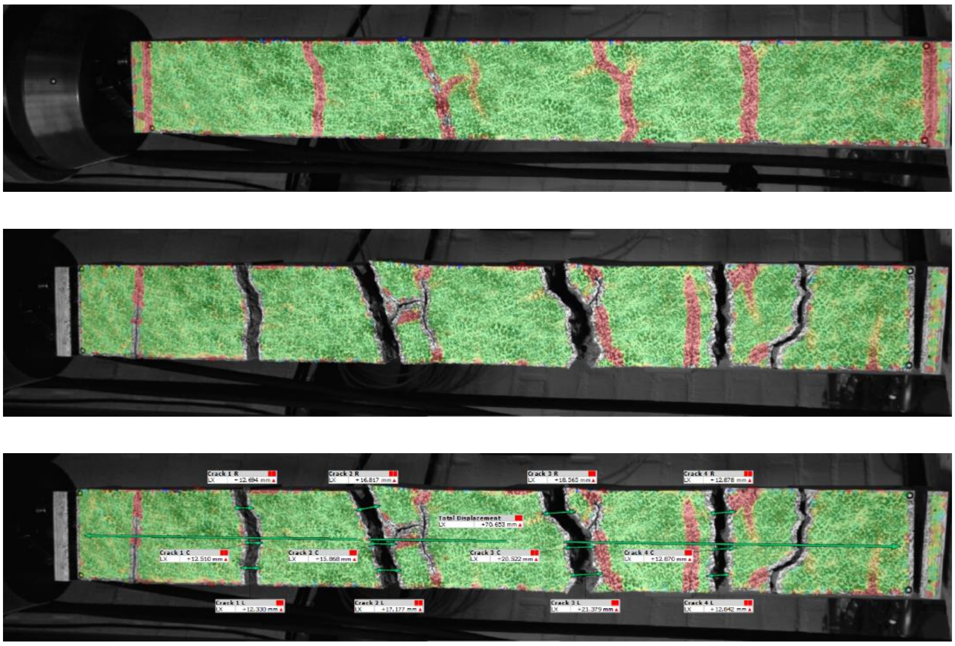

Figure E.2 Stabilized cracking stage, maximum load, and GOM calculation example for prism ϕ16-2.

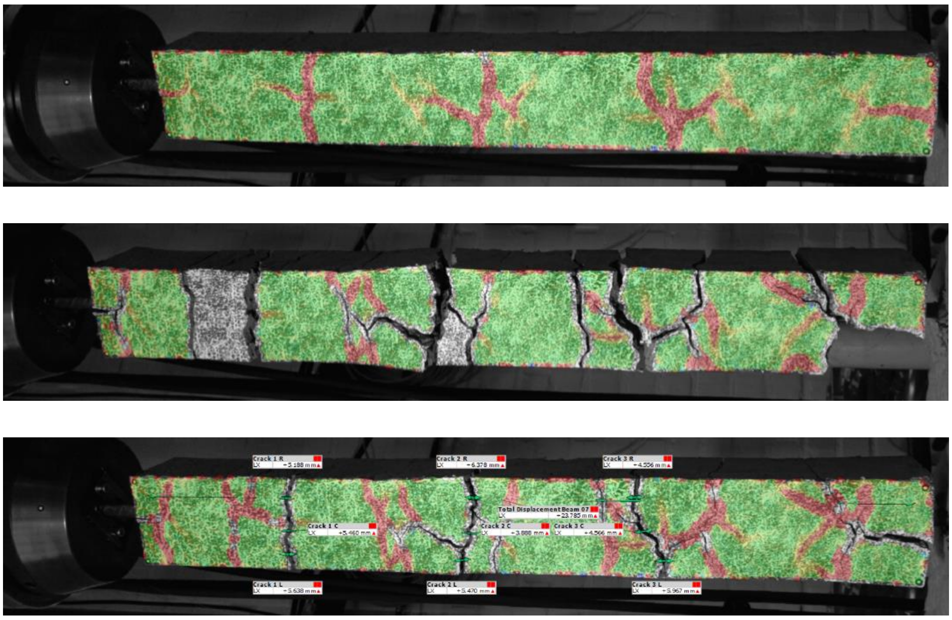

Figure E.3 Stabilized cracking stage, maximum load, and GOM calculation example for prism ϕ16-3.

E.2 ϕ12 prisms without PVC

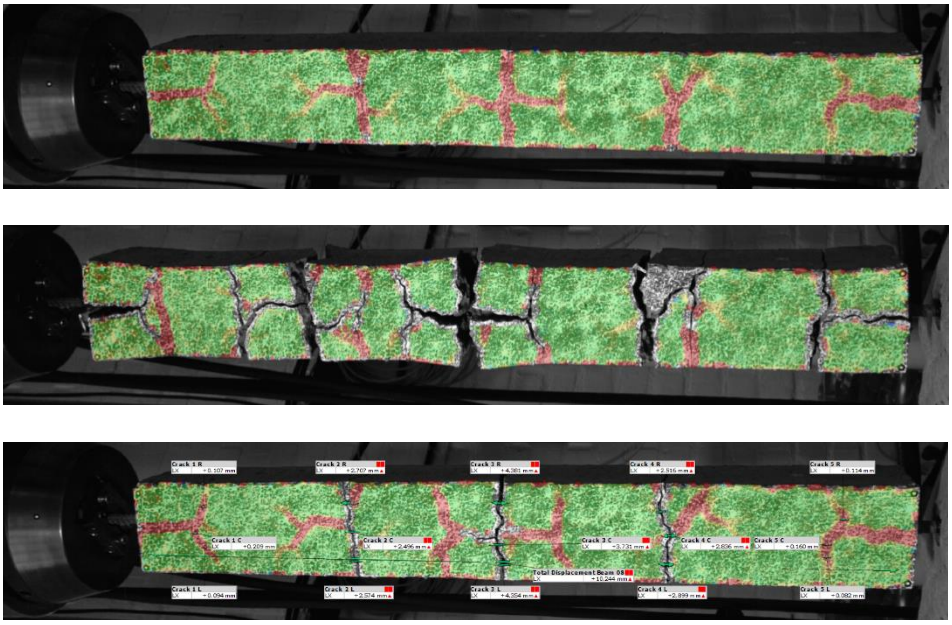

Figure E.4 Stabilized cracking stage, maximum load, and GOM calculation example for prism ϕ12-5.

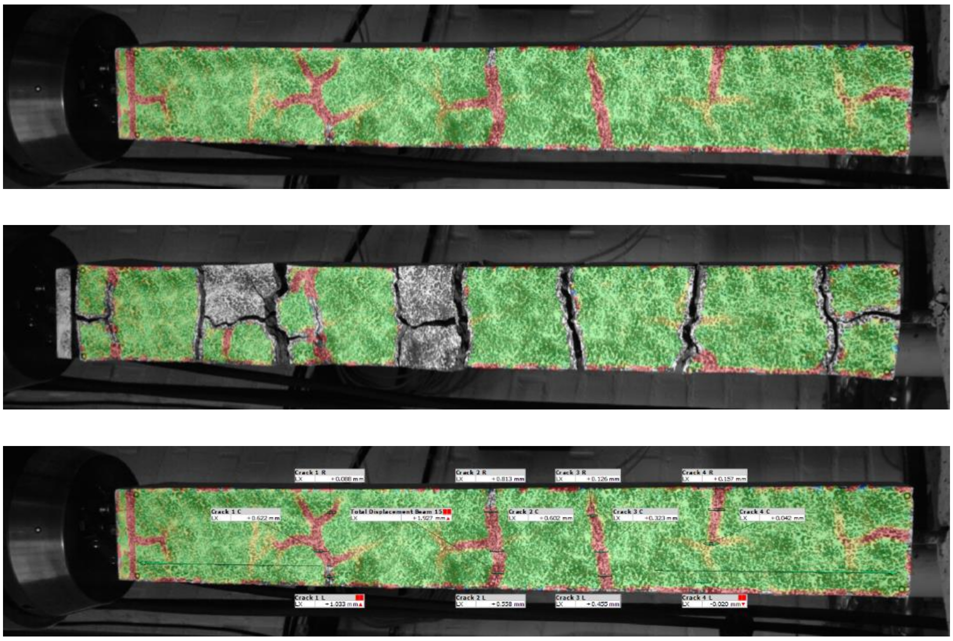

Figure E.5 Stabilized cracking stage, maximum load, and GOM calculation example for prism ϕ12-11.

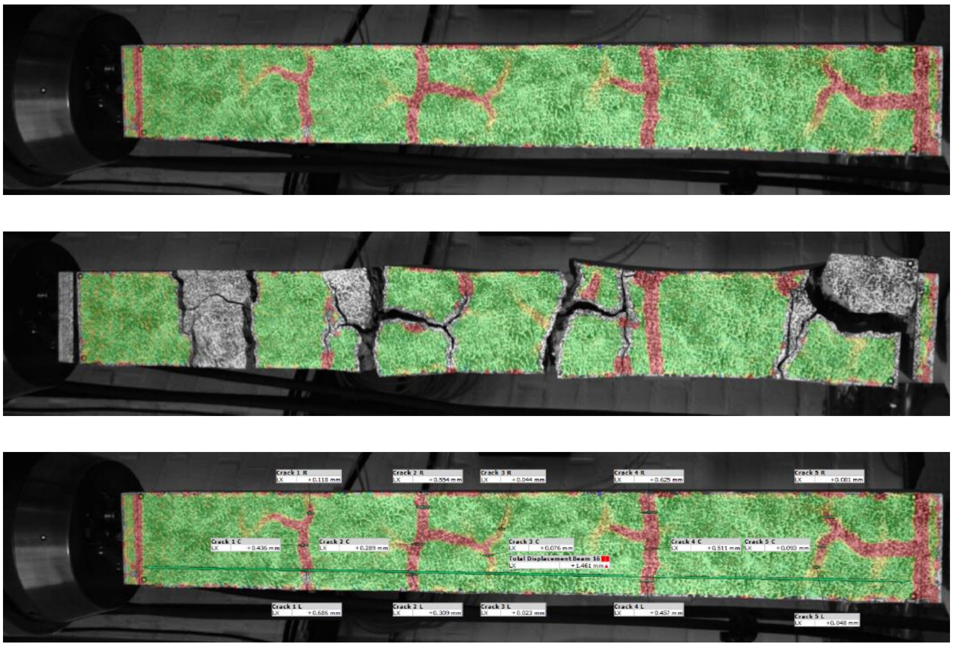

Figure E.6 Stabilized cracking stage, maximum load, and GOM calculation example for prism ϕ12-12.

E.3 ϕ12 prisms with 4x50 mm PVC

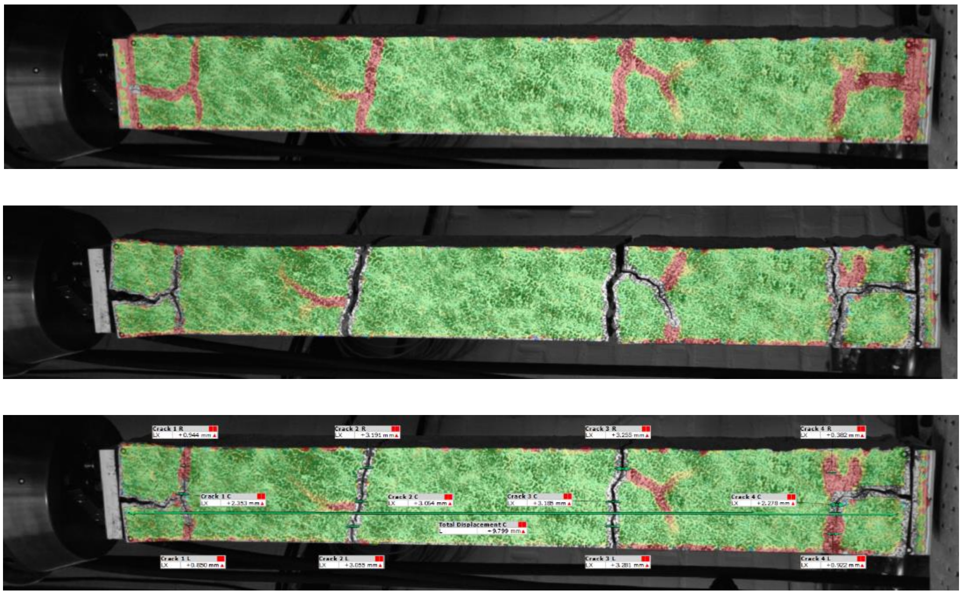

Figure E.7 Stabilized cracking stage, maximum load, and GOM calculation example for prism ϕ12-1A.

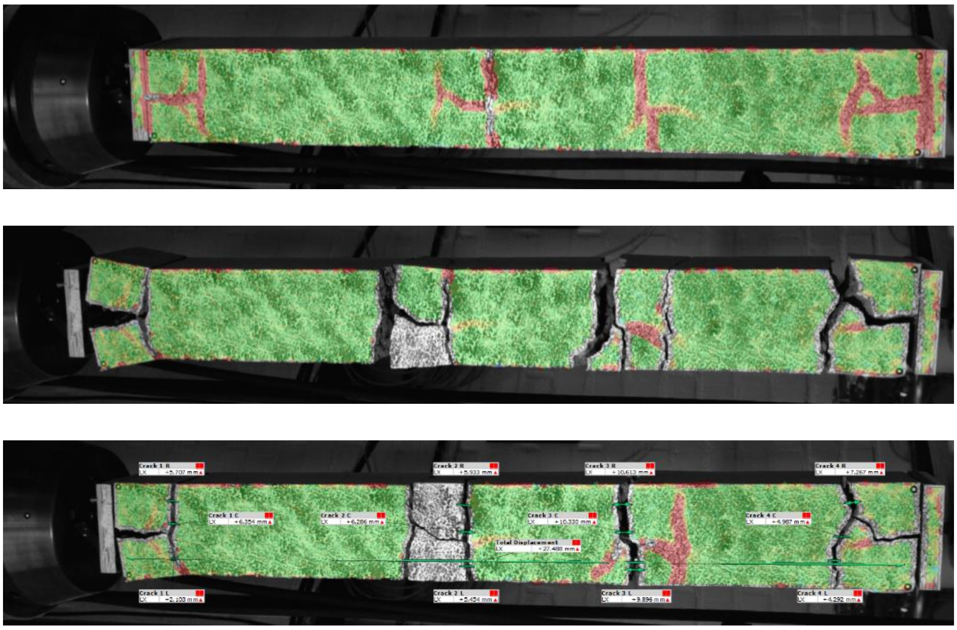

Figure E.8 Stabilized cracking stage, maximum load, and GOM calculation example for prism ϕ12-2A.

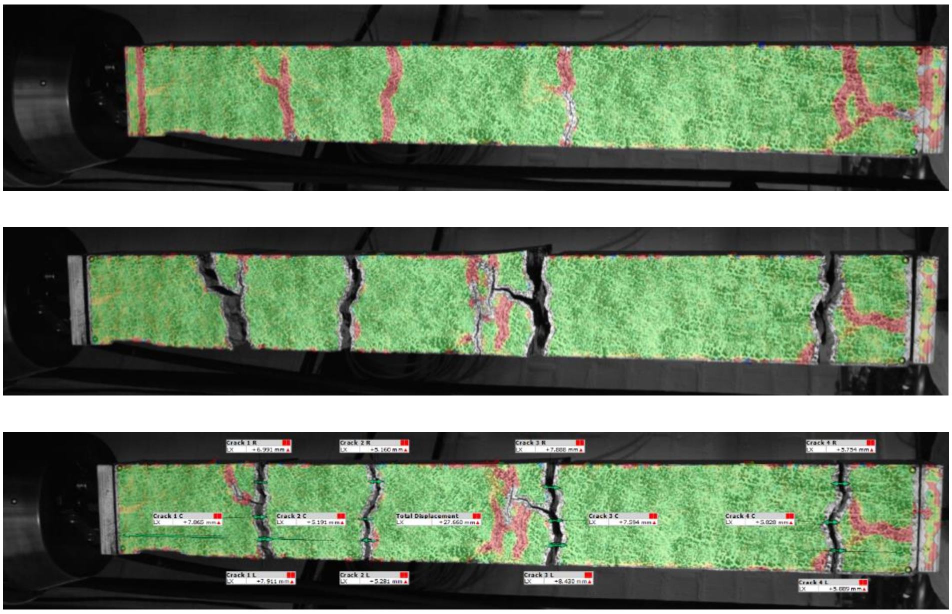

Figure E.9 *Stabilized cracking stage, maximum load, and GOM calculation example for prism ϕ12-3A.*

E.4 ϕ12 prisms with 8x50 mm PVC

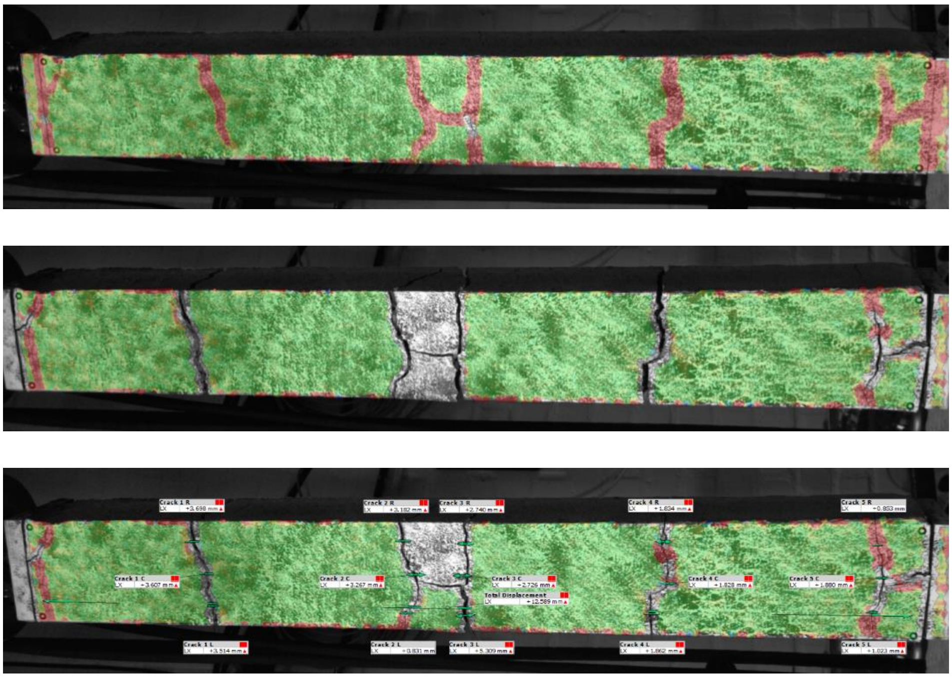

Figure E.10 *Stabilized cracking stage, maximum load, and GOM calculation example for prism ϕ12-4B.*

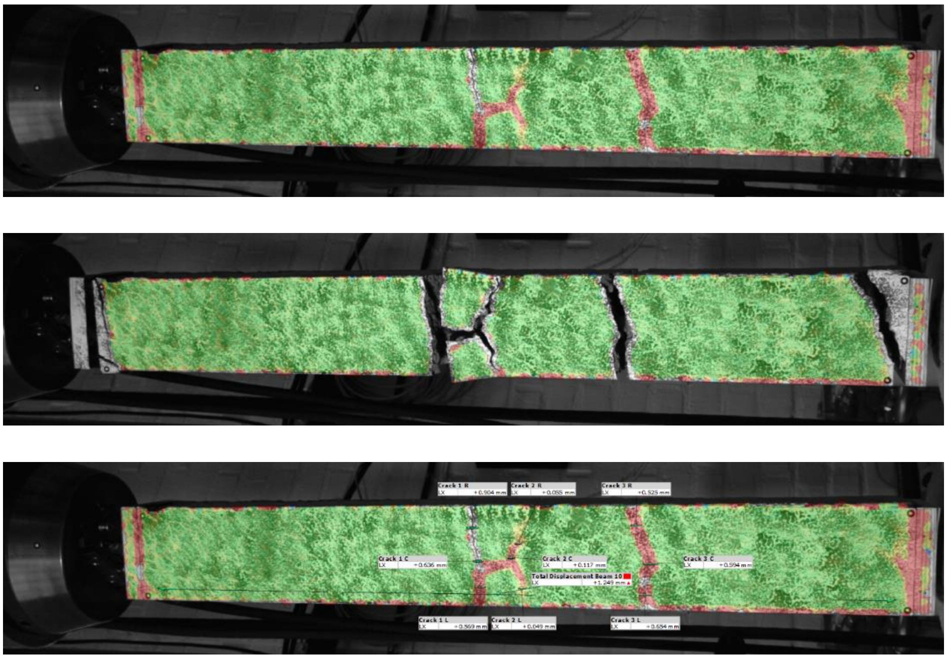

Figure E.11 Stabilized cracking stage, maximum load, and GOM calculation example for prism ϕ12-6B.

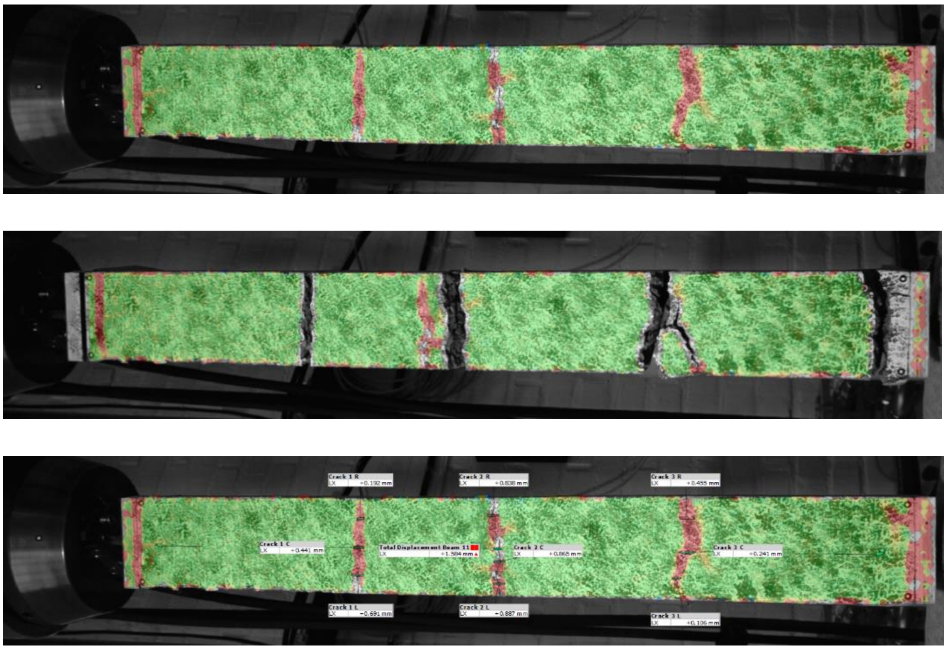

Figure E.12 Stabilized cracking stage, maximum load, and GOM calculation example for prism ϕ12-7B.

E.5 ϕ12 prisms with 4x100 mm PVC

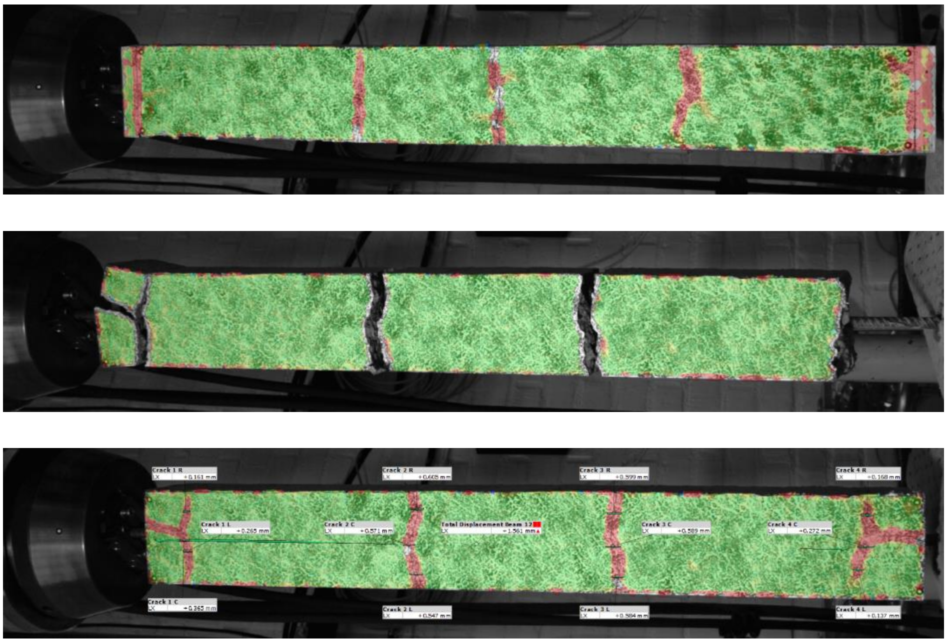

Figure E.13 Stabilized cracking stage, maximum load, and GOM calculation example for prism ϕ12-8C.

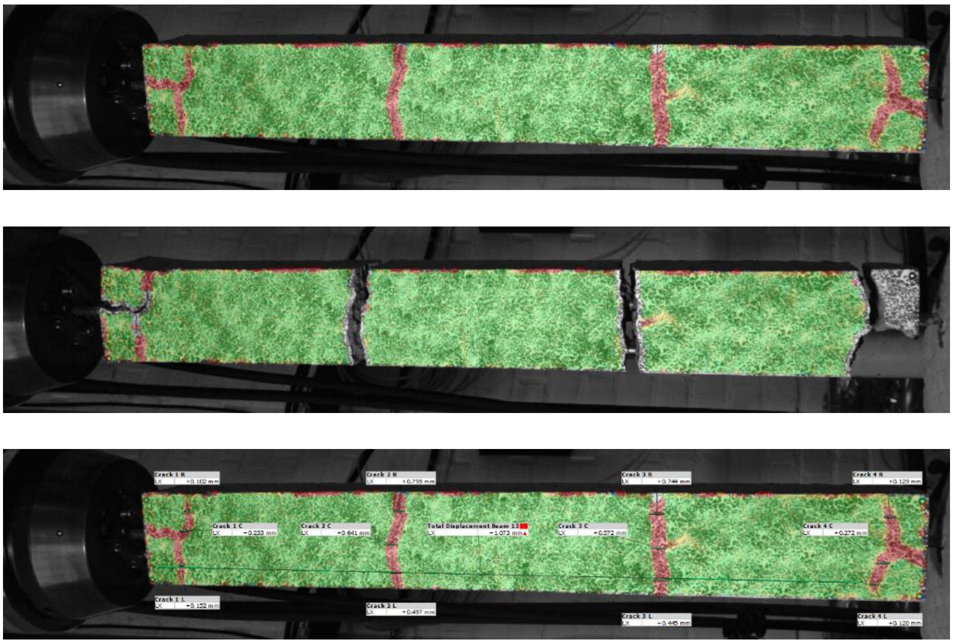

Figure E.14 Stabilized cracking stage, maximum load, and GOM calculation example for prism ϕ12-9C.

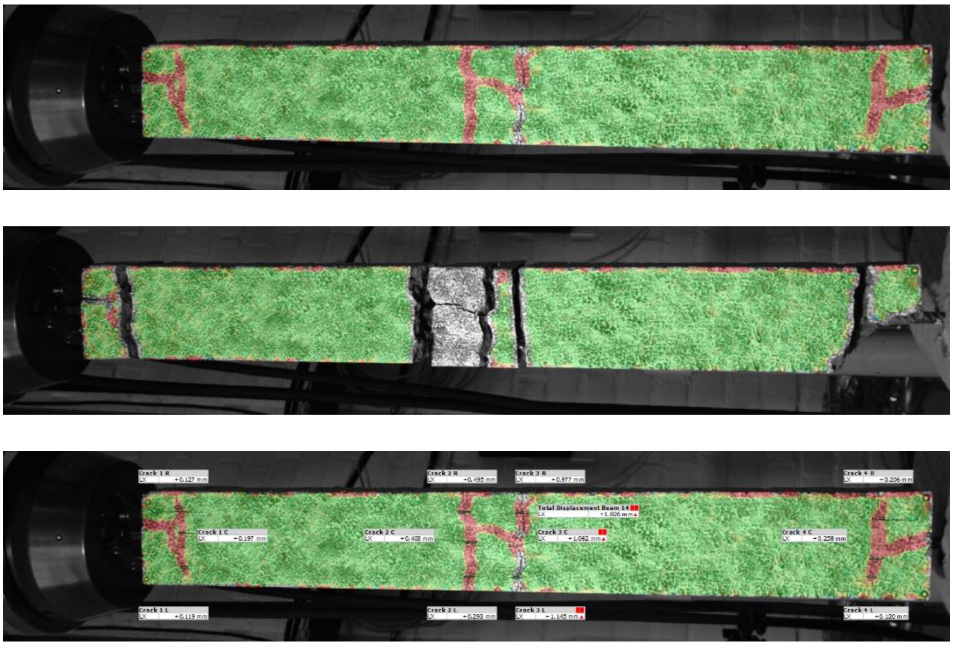

Figure E.15 Stabilized cracking stage, maximum load, and GOM calculation example for prism ϕ12-10C.

E.6 ϕ10 Prisms without PVC

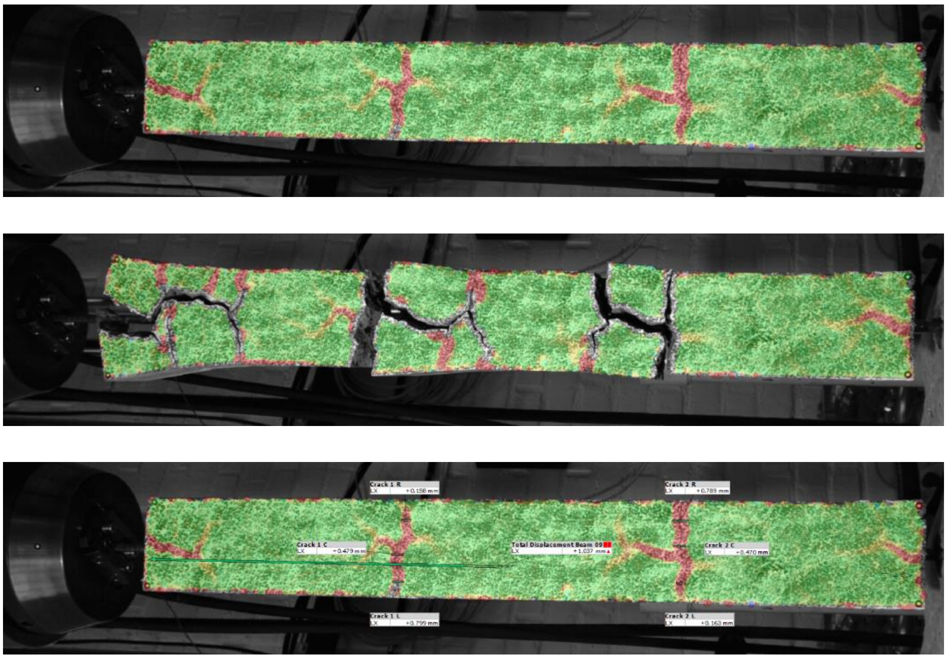

Figure E.16 Stabilized cracking stage, maximum load, and GOM calculation example for prism ϕ10-1.

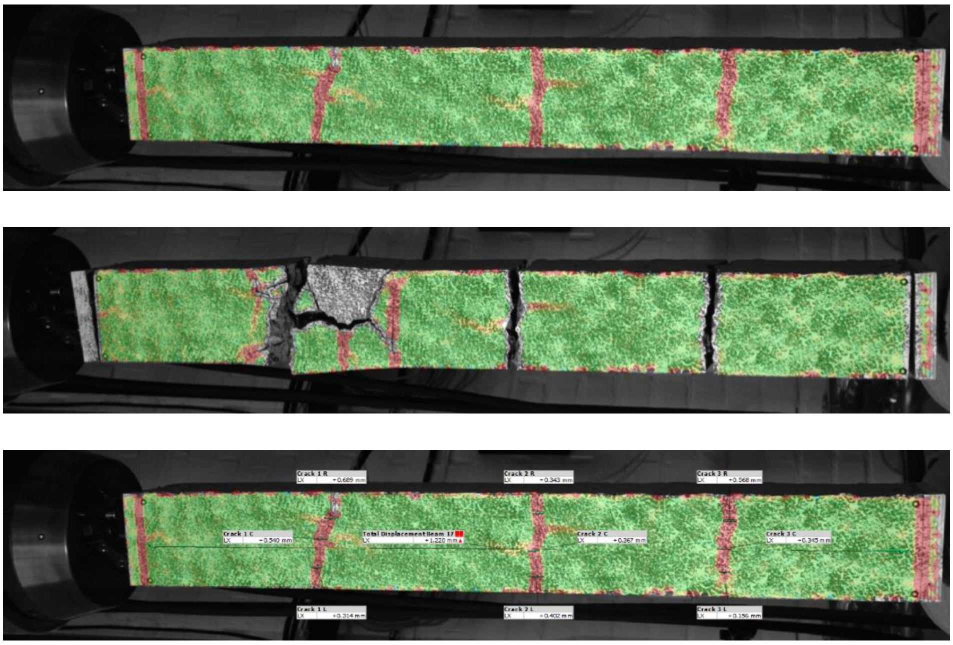

Figure E.17 Stabilized cracking stage, maximum load, and GOM calculation example for prism ϕ10-2.

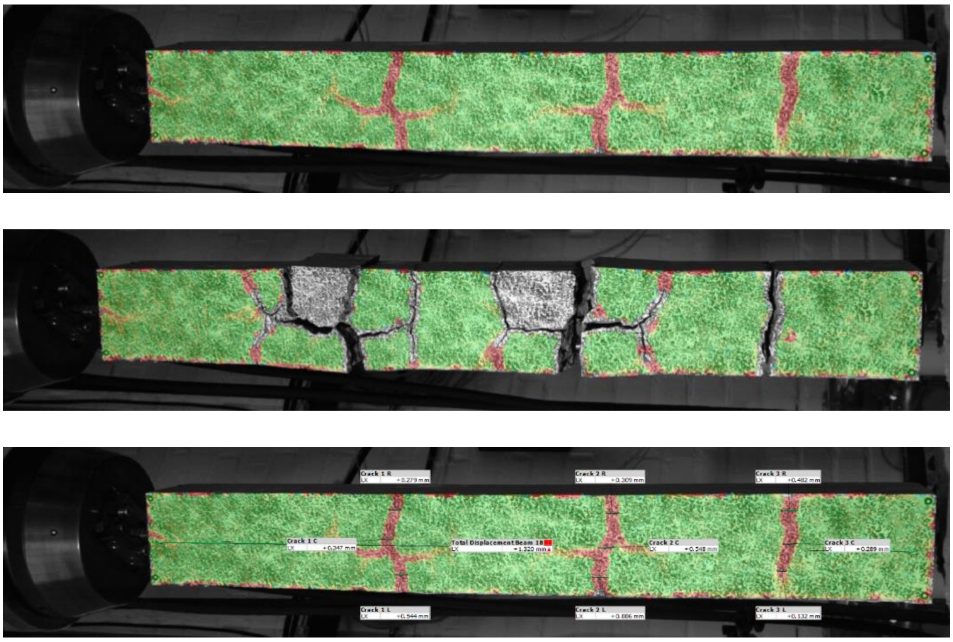

Figure E.18 Stabilized cracking stage, maximum load, and GOM calculation example for prism ϕ10-3.

Appendix F Prisms Post-testing

F.1 ϕ16 prisms without PVC

Figure F.1 Prism ϕ16-1(left) and ϕ16-2 (right) post-testing. Note that an image of prism ϕ16-3 was not taken and is therefore not included.

F.2 ϕ12 prisms without PVC

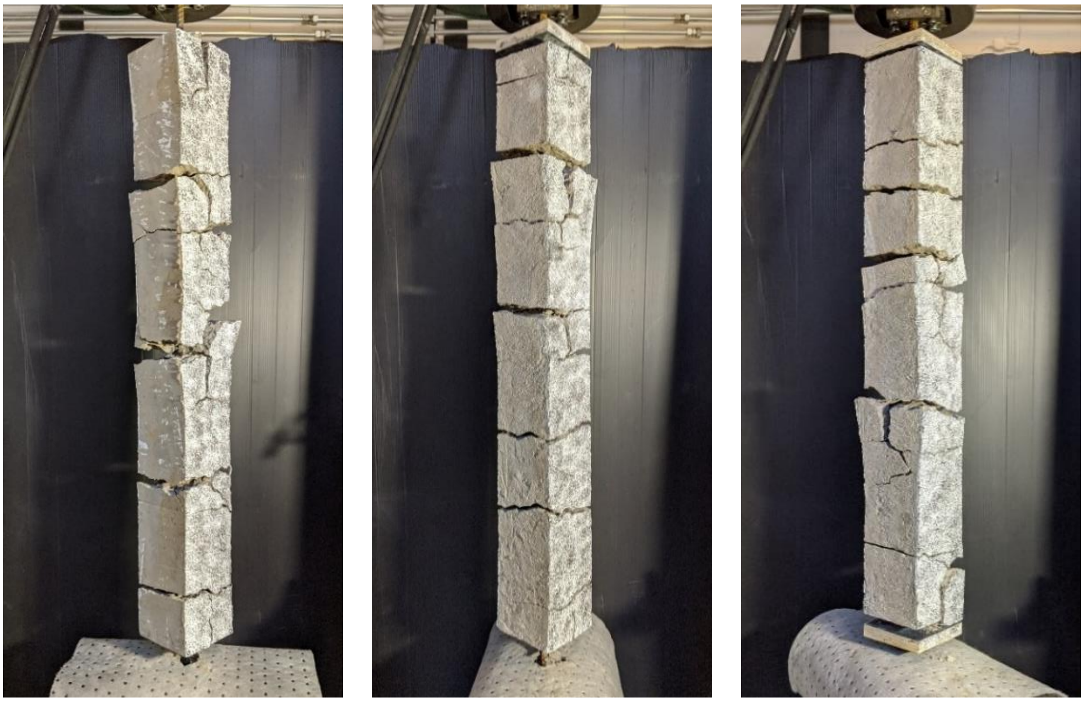

Figure F.2 Prism ϕ12-5 (left), ϕ12-11 (center), and ϕ12-12 (right) post-testing.

F.3 ϕ12 prisms with 4x50 mm PVC

Figure F.3 Prism ϕ12-1A (left), ϕ12-2A (center), and ϕ12-3A (right) post-testing.

F.4 ϕ12 prisms with 8x50 mm PVC

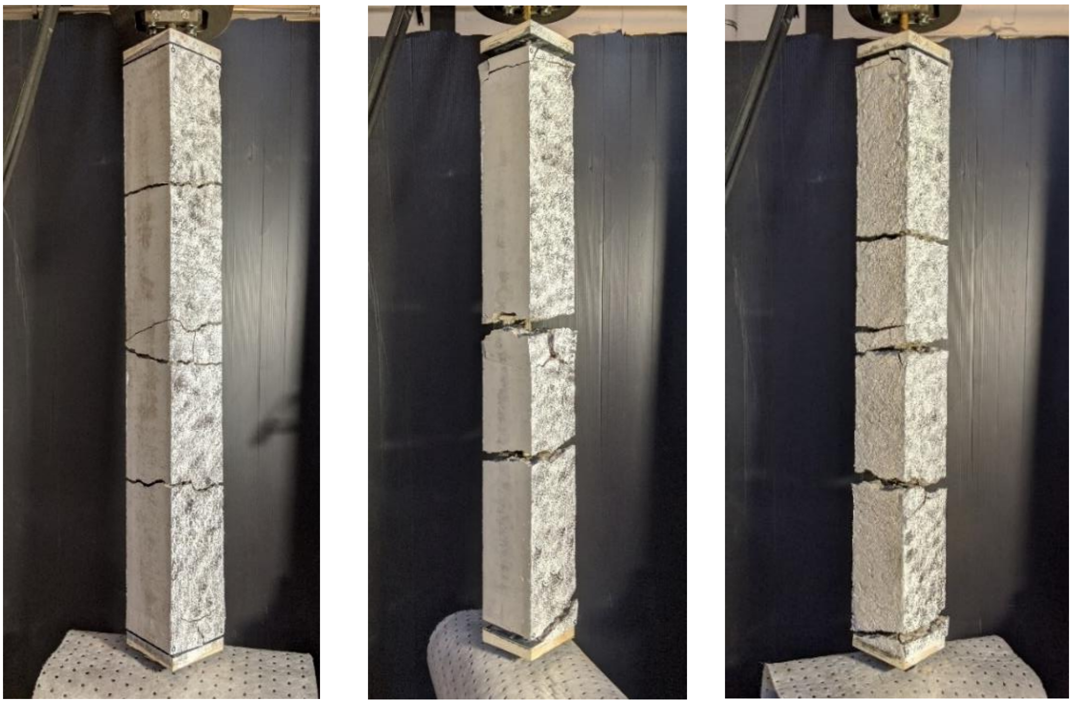

Figure F.4 Prism ϕ12-4B, ϕ12-6B (center), and ϕ12-7B (right) post-testing.

F.5 ϕ12 prisms with 4x100 mm PVC

Figure F.5 Prism ϕ12-8C (left), ϕ12-9C (center), and ϕ12-10C (right) post-testing.

F.6 ϕ10 prisms without PVC

Figure F.6 Prism ϕ10-1 (left), ϕ10-2 (center), and ϕ10-3 (right) post-testing.